ADDIS ABABA UNIVERSITY

SCHOOL OF GRADUATE STUDIES
SCHOOL OF EARTH AND PLANETARY SCIENCE
DEPARTMENT OF EARTH SCIENCES

HYDROGEOCHEMICAL AND ISOTOPE HYDROLOGY IN INVESTIGATING GROUNDWATER RECHARGE AND FLOW PROCESSES; BORENA LOWLANDS, SOUTHERN ETHIOPIA

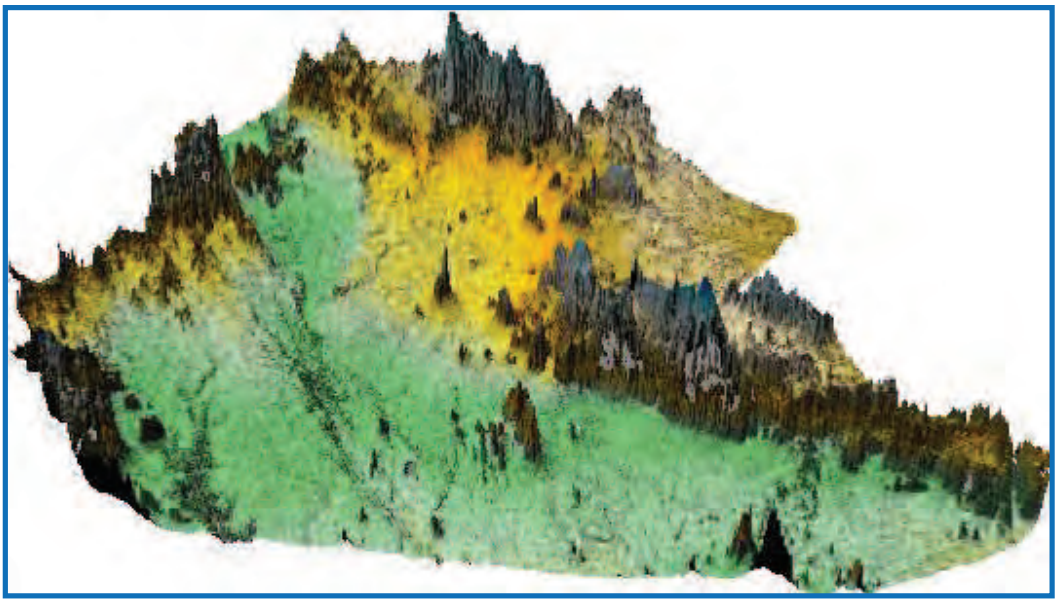

A THESIS SUBMITTED TO THE SCHOOL OF GRADUATE STUDIES OF ADDIS ABABA UNIVERISTY IN PARTIAL FULFILLMENT OF THE REQUIREMENTS FOR THE DEGREE OF MASTER OF SCIENCE IN HYDROGEOLOGY

BY: LIKISSA FANTA TASGARA

June, 2012
Addis Ababa

HYDROGEOCHEMICAL AND ISOTOPE HYDROLOGY IN INVESTIGATING GROUNDWATER RECHARGE AND FLOW PROCESSES; BORENA LOWLANDS, SOUTHERN ETHIOPIA.

A THESIS SUBMITTED TO THE SCHOOL OF GRADUATE STUDIES OF ADDIS ABABA UNIVERISTY IN PARTIAL FULFILLMENT OF THE REQUIREMENTS FOR THE DEGREE OF MASTER OF SCIENCE IN HYDROGEOLOGY

By: LIKISSA FANTA TASGARA

ADVISOR: SEIFU KEBEDE (PhD)

June, 2012
Addis Ababa

ADDIS ABABA UNIVERSITY
SCHOOL OF GRADUATE STUDIES
DEPARTMENT OF EARTH SCIENCES

HYDROGEOCHEMICAL AND ISOTOPE HYDROLOGY IN INVESTIGATING GROUNDWATER RECHARGE AND FLOW PROCESSES; BORENA LOWLANDS, SOUTHERN ETHIOPIA.

BY: **LIKISSA FANTA TASGARA**

APPROVED BY BOARD OF EXAMINERS:

Name	Signature	Date
Seifu Kebede (PhD): (Chairman)	_____	_____
Seifu Kebede (PhD): (Advisor)	_____	_____
Solomon Tadesse (Prof.): (Internal Examiner)	_____	_____
Tesfaye Tadesse: (External Examiner)	_____	_____

DECLARATION

I, the undersigned, declare that this is my original work and has not been submitted for any degree or examination in any university and that all sources of materials used for the thesis have been duly acknowledged.

Likissa Fanta Tasgara

Signature: _____

Date of submission: _____

The thesis has been submitted for examination with my approval as university advisor.

Seifu Kebede (PhD)

Signature: _____

Date of approval: _____

Place and Date of submission
Addis Ababa University School of Graduate Studies
June, 2012

DEDICATION

This work is dedicated to my Father Fanta Tasgara and my Mother Daditu Regassa who are the reasons for who I am!

ACKNOWLEDGMENT

First of all, I would like to thank 'Almighty God' who made everything possible, to begin and finish this work successfully.

I would like to thank Dr. Seifu Kebede, my advisor and instructor, for his wholehearted advice, encouragement and provision of all valuable reading materials that helped me to complete this work successfully.

My appreciation also goes to Prof. Tenalem Ayenew, my instructor, and all Earth Sciences Department instructors who supported me in gaining basic knowledge of Hydrogeology and related subjects. I am indebted to PhD students; Gadissa Deyassa, Tilahun Azagegn and Sileshi Mamo for their kind provision of reading materials and unreserved cooperation for the success of this work. My tank also goes to Ato Abebe Ketema for his valuable comment on my thesis and Ato Bekele Abahire who assisted me in giving unpublished hydrogeological reports of the area.

I am also very thankful to Oromia Water Works Design and Supervision Enterprise (OWWDSE), particularly to deputy general manager for Water resources studies and water supply works, Gezahegn Lemecha, for kind support and provision of all necessary secondary data without which completion of this thesis is impossible.

I have no words to express my feelings which I have for my brother Dereje Fanta and my sister Umera Fanta for their constant help and encouragement during my study. I am highly indebted to my father Fanta Tasgara, who taught me everything to lead my life. I would like to thank also Damashe Gudata, Bokashe Fanta, Nacho Fanta, Sanbata Fanta, and the whole family for their blessing, guidance, advice, encouragement and support.

I would like to convey my special thanks to my friends Addisu Deressa and Roba Edao for their constant encouragement and help. I cannot end also without acknowledging the support received from my fellow classmates. My gratitude also goes to Abdissa Doja, Shiferaw Diriba, Firezer Dendena, Itenesh Tesfaye, Tsehay Keneni, Dereje Merga and Abu Adam for their support and encouragement and many others whose name are not mentioned here in one way or the other.

At last but not least I am thankful to drivers Melese Geneti and Demis Tadesse for their kind cooperation during field work.

ABSTRACT

Hydrogeochemistry and isotope hydrology were used to investigate groundwater recharge and flow processes in Borena lowlands. The study area is characterized by semi-arid and arid climate. Surface water flows are intermittent. The available water resource, therefore, restricted to groundwater. Precambrian basement, Tertiary and Quaternary basalt, and recent alluvial and elluvial sediments are major geologic units. Fractured and weathered basalt is the principal aquifer.

The hydrochemical analysis shows that Borena groundwater varies in type over a wide range even within few kilometer intervals and broadly distributed rather than forming distinct clusters. However, three major water types can be distinguished depending on their position on a Piper diagram. These are Ca-Mg-HCO_3, Na-HCO_3 and Ca-Mg-SO_4-Cl/Na-Cl/SO_4 water types. In most cases Ca-Mg-HCO_3 type waters occur in areas of recharge and Na-Cl/Na-SO_4 type waters in rift/lower lying section. The intermediate water types are mixed and lay between these two end members. Ten subgroups were examined from the hierarchical cluster analysis in which distinct hydrgeochemical processes were clearly observed. The dissolution of minerals like olivine, pyroxenes, plagioclase, anhydrite, halite and CO_2 gases are deriving the observed natural groundwater chemistry, which are in most cases, balanced by the precipitation of calcite minerals and weathering/formation of clay minerals like Ca-montmorilonite, chalcedony, illite, and K-micas. Cation exchange reactions, particularly in Sarite lower plains, were also controlling chemical composition of the groundwater.

The isotopic composition of $\delta^{18}O$ and $\delta^{2}H$ in groundwater varies from -5.08$^0/_{00}$ to 0.08$^0/_{00}$ and from -29$^0/_{00}$ to -2.4$^0/_{00}$ respectively. In this work the altitude effect on $\delta^{18}O$ composition shows a depletion of -0.1$^0/_{00}$ per 100m elevation rise. Three recharge mechanisms; direct precipitation, regional groundwater and/or fast selective and flash floods recharge mechanisms were known from the groundwater isotope interpretation. The hydrogeochemical and environmental isotope analysis result clearly indicates regional groundwater flows from elevated sections for instance; Elwaya, Yabello, Utalo, Gololcha via the middle Gelchet plains to main Ririba fault. A flow from Mega and Megado escarpments to megado/Biloko lowlands is also identified.

For the sub basin recharge rate was estimated using chloride mass balance method and is 28mm/yr. The recharge rate shows variations mainly with topography, groundwater chloride content and annual rainfall amounts. The northwestern (Mermero), northeastern (Yabello) and eastern (Mega) parts receives highest recharge where as the southwestern and southern sectors get the lowest groundwater recharge rates.

Keywords: *hydrogeochemistry, environmental isotopes, groundwater recharge, semi-arid, Borena lowlands*

TABLE OF CONTENTS

Pages

LIST OF FIGURES

LIST OF TABLES

LIST OF ANNEXES

ACRONYMS

AAU	Addis Ababa University
BHE	Borehole in Escarpments and highland plains
BHM	Borehole in Middle plains
BHR	Borehole in Rift and lowland plains
BGPAP	Borena Ground Water Potential Assessment Project
DEM	Digital Elevation Model
EC	Electrical Conductivity
EGS	Ethiopian Geological Survey
GDMP	Genale Dawa Master Plan project
GIS	Geographic Information Systems
GMWL	Global Meteoric Water Line
HCA	Hierarchical Cluster Analysis
HDWE	Hand Dug Well in Escarpments and highland plains
HDWM	Hand Dug Well in Middle plains
HDWR	Hand Dug Well in Rift and lowland plains
IAEA	International Atomic Energy Agency
ITCZ	Inter-Tropical Convergence Zone
LMWL	Local Meteoric Water Line
m.a.s.l	Meter above sea level
mm/yr	Millimeter per year
MWoR	Ministry of Water, Energy Resources
NGO	Non Governmental Organization
OWRB	Oromia Water Resources Bureau
OWWDSE	Oromia Water Works Design and Supervision Enterprise
pH	the negative logarithm of hydrogen ion
RA	Residual Alkalinity
SI	Saturation Index
SPE	Spring in Escarpments and highland plains
SPM	Spring in Middle plains
SMOW	Standard Mean Ocean Water
SPR	Spring in Rift and lowland plains
TDS	Total Dissolved Solids
UTM	Universal Transverse Mercator
WWDSE	Water Works Design and Supervision Enterprise
WHO	World Health Organization

1. INTRODUCTION

1.1. BACKGROUND

The research area is located in Borena zone which is characterized by hot and semi-arid climate. It is one of the drought prone areas in Oromia region, where there is scarce rainfall and no perennial surface water body. Surface water flows are usually limited to flash floods due to short duration, high intensity rainfall events with very infrequent recurrences, which have little potential as a source of water. The available water resource in the study area is, therefore, restricted to groundwater. Consequently, the local communities and cattle living in the area are entirely dependent on groundwater utilization through drilled wells.

The availability of reliable, safe water supplies is becoming increasingly important to the livelihood of communities throughout the world, particularly in semiarid and arid environment. In such an environment similar to the current research area, where groundwater is the only source of water, the basic knowledge of groundwater recharge received by aquifers is far more critical to the sustainable use of water than it is in humid regions. Reliable recharge estimation and quantification of the groundwater resources in all climatic zone in general and in semi-arid and arid zone in particular always remains the most difficult part of the hydrogeological studies. Hence, for better results, detail understanding of the source of recharge and its mechanism is very essential.

Hydrogeochemistry and environmental isotope techniques have found a wide spectrum of applications for hydrological problems encountered in water resources development and management. They offer unique methodologies for many of the problems involved in arid and semiarid zone hydrology. Proven isotope methodologies are already an integral part of the hydrogeological exploratory investigations related to water resources. Thus, this research uses both hydrogeochemical and isotope hydrology techniques to investigate groundwater recharge and flow processes in Borena lowlands.

1.2. PROBLEM STATEMENT

In Borena lowlands the Oromia Regional State has paid much attention in assessment and development of groundwater potentials. Many test wells were drilled and satisfactory result is obtained regarding groundwater potential. In parallel to the investigation, construction of big water supply structures and distribution systems are under way to solve the existing acute water supply problems in the area. This has increased groundwater exploitation in the area. It is obvious that the increased groundwater extraction than the prevailing environmental balance will cause significant changes in the potentiometric surfaces of the aquifers in such semiarid areas.

Although developing groundwater is the only means to alleviate the shortage of domestic water supply in the area, it needs consideration of different scientific approaches to know the source and mechanisms of recharges. Moreover, reliable recharge estimation and quantification of the groundwater resources always remains the most difficult part of the hydrogeological studies, and for better results, detail understanding of the source of recharge and its mechanism is very essential. Therefore, this research use the principles and methodologies of integrated hydrogeochemistry and isotope hydrology, which is very influential in investigating groundwater recharge and flow processes in semi-arid and arid environments.

1.3. OBJECTIVE

1.3.1. General objective

The general objective of the research is to investigate and refine the understanding of groundwater recharge and flow processes using hydrogeochemistry and isotope hydrology in Borena lowlands of south and southwest Yabello town.

1.3.2. Specific Objectives

- Identify the isotopic composition of groundwater and rainwater and see their variations
- Determine the recharge sources and mechanisms
- Identify regional, intermediate and local groundwater flow systems
- Model and determine the hydrogeochemical processes that derive the natural groundwater chemistry and identify source of water quality problems
- Estimate recharges rates

1.4. RELEVANCE OF THE RESEARCH

Depending on the groundwater exploratory result obtained in the area, other than domestic water supply currently there is an increasing demand to start developing groundwater resource for irrigation too. This could increase stresses on naturally limited groundwater resources in this semi-arid areas. Therefore, this research helps to know the recharge processes, which is the major source of groundwater, and helps to exploit and effectively utilize this limited and precious resource. In such highly water demanding environments, the research has also far-reaching practical use for future development and handling of this scant water resource in a proper manageable way.

1.5. STUDY DESIGN

1.5.1. Approach

Office and field works are the approaches followed to investigate groundwater recharge and flow processes of the study area.

During office work different literatures and reports directly or indirectly related to this work were collected from OWWDSE, EGS, and National Metrological Agency (NMA). Most of the secondary physico-chemical and environmental isotope data were acquired from OWWDSE.

Field work has been conducted to measure in-situ parameters like EC, Temperature, pH, TDS, and to collect primary data for environmental isotope (Deuterium and Oxygen-18) and physico-chemical analyses.

After the primary data was collected, some major cations (Na, K, Ca, and Mg) and anions (HCO_3, Cl, SO_4, and NO_3) had been determined in OWWDSE and WWDSE laboratory. Environmental isotopes (Deuterium and Oxygen-18) had been determined in AAU water isotope laboratory.

1.5.2. Material and Data Inputs

The materials used during the investigation were geological map, hydrogeological map, DEM, GARMIN GPS-72, EC meter, pH meter and Bottles for sampling representative water. The main Computer software's used were Global mapper-11, ArcGIS-9.3, Aquachem-4, STATISTICA-8, and PHREEQC interactive-2.8. Secondary physico-chemical and environmental isotope data were also used in line with the primary data.

1.5.3. Previous Investigations

Many groundwater investigations were carried out in the area by different organizations to develop groundwater resources for rural and urban domestic water supply. OWRB and NGO's operating in the area conducted most of these works. The results of previous works are briefly outlined below.

OWWDSE (2011): Groundwater potential assessment in south and southwest of Yabello town. This investigation consists of three phases and at present only the first and second

phase's work is accomplished. The study indicates that the groundwater bearing aquifer is highly weathered and fractured basalt laying in most of the nearly flatlands and is moderate to high yielding. Poor and good water quality is seen side by side in one similar geologic and geomorphologic feature, for example, in Sarite locality. The groundwater flow direction is from north, west, and east toward Ririba valley and finally flows towards south, the Kenya's border. The groundwater source is from modern age precipitation. This work estimated recharge rate using different methods and the average annual value derived is 55mm/yr.

MAB Consult – Consulting Hydrogeologist and Engineers (2009): Delineating groundwater potential areas using remote sensing, field studies, Digital Elevation Models (DEM) and Geographic Information Systems (GIS) in Yabelo, Arero and Teltele woredas (Moyale-Teletele Sub Basin). It covers the northern part of this research area. This work mapped the most possible promising area and had recommended subsurface data to verify the work.

EGS (2004, 1999 and 1994). Geology of Yabello (NB37-14), Sololo (NB37-2) and Hagermariam (NB37-10) at 1:250,000 scale. According to these work, the vast plains of the area is covered by Bulal basalt which is affected by different faulting systems. The report on the geological mapping of Yabello sheet recommends further groundwater investigation in the volcanic plains of the research area.

MoWR (2005): Genale-Dawa river basin integrated resources development master plan study; final report part II sector Studies, Vol.II.2.A. Hydrology and climate, Vol.II.2.B. Geology, Vol.II.2.D. Hydrogeology. This study covers nearly 95% of the research area. The study indicated that extensive fracturing that occurred in the past geologic time during the development of the present rift system controls the ground water system in the basin. It briefly described the hydrogeological and geological characteristics of different geologic units at regional level.

EGS (2000): Hydrogeological and isotope hydrological investigation in part of Genale-Dawa basin. This work used both conventional hydrogeological and isotope hydrology to explore the mechanisms and source of groundwater recharge. According to this work, the

^{3}H age shows modern age groundwater in most of the results obtained from shallow wells. The recharge rate also estimated to be between 10 and 40mm/yr using well-mixed model (aquifer porosity and saturated aquifer thickness). However most of the data are outside of present study boundary.

Coppock (1994): Synthesis of pastoral research, development and change in the Borena plateau of southern Ethiopia. This covers some part of the current research area. The research composed of an inter-disciplinary study, but focused on rangeland and land use investigations. It states that water resource is the fundamental feature that has shaped the Borena society. Deep wells in particular are a focal point for social organization.

In summary, except OWWDSE and EGS, none of these previous works have dealt with recharge processes. Instead recommends further groundwater investigation in this particular Bulal basalt. In view of this OWRB had initiated to undertake groundwater potential assessment in this specified area and hired OWWDSE for the consultancy service. And thus OWWDSE had attempted to explore the potentiality of this basalt using different conventional hydrogeological investigation techniques. The water chemistry data obtained from OWWDSE have been used in hydrochemical analysis of the present work. The hydrogeological report and map prepared by OWWDSE had also been used as a main reference.

1.5.4. Research Frame Work

Natural groundwater recharges could occur from precipitation, rivers, canals and lakes. Hence to achieve the objectives of the research, groundwater recharge and flow processes investigation method has to be selected depending on data sets available. Hydrogeochemical and isotope data can give insight understanding on groundwater recharge and flow processes in combination with geomorpholgical, geological, structural, hydrological, and hydrogeological knowledge in particular site. The general outline of this research process is illustrated in Figure 1.1

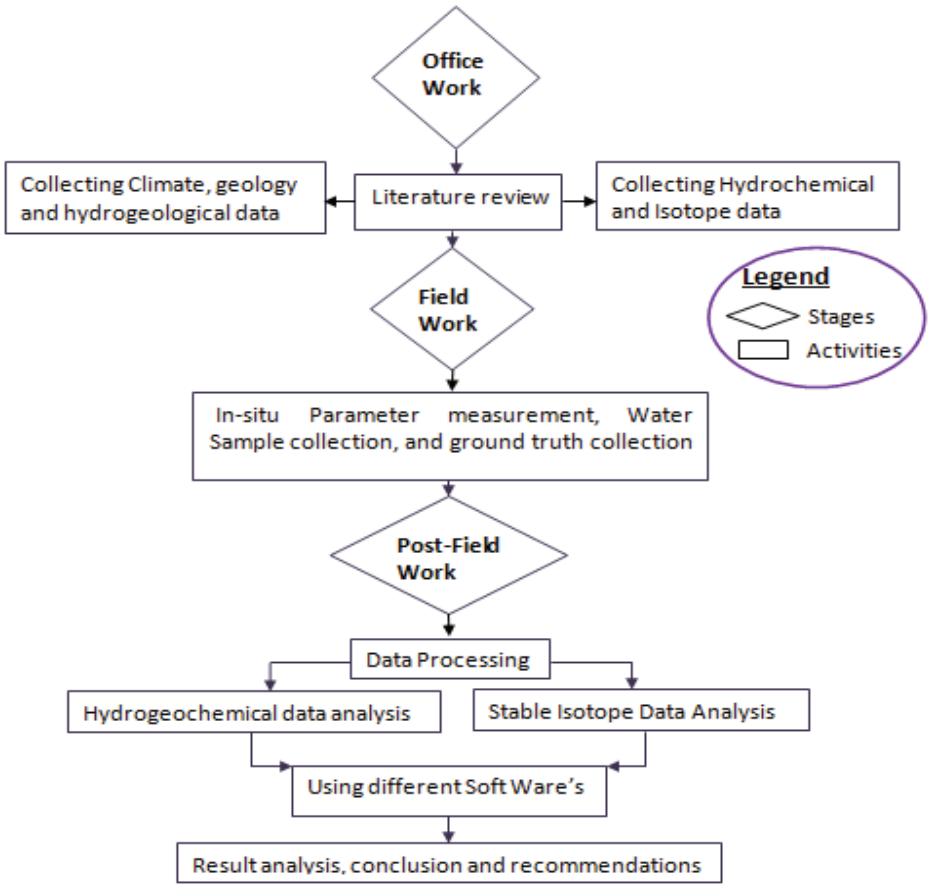

Figure 1-1: *major research outlines*

1.5.5. Research Outlines

The content of this research is categorized in to seven chapters. **Chapter 1** *deals with* the general introduction of the research, problem statement, objectives, relevance of the research and previous investigations. **Chapter 2** describes the methodology and principles employed to investigate groundwater recharge and groundwater flow processes. **Chapter 3** discusses briefly the research area. **Chapter 4 and 5** discusses the hydrogeochemical and isotope data analysis and interpretations. **Chapter 6** deals with the result of the research using evidences of hydrogeochemical and isotope data analysis result for groundwater recharge and flow process. **Chapter 7:** This chapter briefly summarizes and gives conclusions on the thesis output. It also recommends some further necessary works on unattainable problems and matters in this thesis.

2. METHODOLOGY

2.1. SAMPLING METHODS

Thirty two water samples were collected in September-October, 2011, for major and minor ion analysis (see Annex 3). 27samples were collected from wells, springs and hand-dug wells within fractured volcanic and basement aquifers. The other 4 samples were from rainfall of the area and 1 was from runoff water collected at the lower part of the catchment. Three open bucket having gate valve at their bottom side were used to collect the rainwater. One liter paraffin oil was added in each bucket to protect evaporation of water from the bucket. Water samples were analyzed to determine the isotopic composition of oxygen-18 and deuterium per mill with respect to the standards. The samples were analyzed in AAU water isotope laboratory. Concentration in mg/l of major ions (SO_4^{2-},Cl^-, HCO_3^-, CO_3^{2-}, Na^+, K^+, Ca^{2+} and Mg^{2+}) have been determined for 17 water samples; 4 samples in WWDSE laboratory and 13 samples in OWWDSE laboratory. Water temperature, pH, and EC and TDS are measured in-situ as well as in laboratory.

2.2. HYDROGEOCHEMISTRY

2.2.1. Hydrogeochemical Facies Concept

According to Chebotarev (1955) and Back (1960, 1966), variation in water composition evolves along groundwater flow direction even in a homogeneous aquifers due to chemical reactions and water-rock contact time. The groundwater flow direction is assumed to be perpendicular to iso-concentration contour of the reacting minerals (Plumer *et al*. 2005). Different water facies along the flow lines from recharge to discharge area and/or from shallow to deep groundwater circulation can tell us the distinct feature of water evolved from source to sink. The iso-concentration contours of reacting dissolved constituents that vary in water composition evolving in the direction of flow can also indicate different water type mixing points along its pass.

2.2.2. Residual Alkalinity

This is also used to identify the recharge-discharge area of groundwater system of a given aquifer. This method can show clear groundwater flow direction particularly in Alluvial deposit where Ca and Mg dominate near mountain foot and get decreased as flowing far distance from the mount foot along the alluvial fan. It was employed by computing the Residual Alkalinity (RA = $[HCO_3^-]$ meq/l – ($[Ca^{2+}]$ meq/l + $[Mg^{2+}]$ meq/l)) that shows variations along the groundwater flow path. Spatial variation in elemental ratios (Ca/Mg and Ca/Na) and individual constituents (SO_4^{2-} and $\delta^{18}O$) were also mapped to identify the recharge source and flow directions.

2.2.3. Equilibrium Conditions of Groundwater

The hydrochemical equilibrium conditions of groundwater and mineral phases of the aquifer rocks can be evaluated using saturation indices. The equilibrium state of the water with respect to a mineral phase can be determined by calculating saturation index (SI) using analytical data. Variation in the groundwater chemistries is mainly a function of the interaction between the groundwater and the mineral composition of the aquifer materials through which it moves (Nwankwoala and Udom, 2011).The saturation index ($SI_{mineral}$) of a certain mineral is defined as the (logarithmic) ratio of the ion activity product (IAP) to the equilibrium constant (K) that is $SI_{mineral}$ = log(IAP/K). When a mineral is in equilibrium with respect to a solution, the SI is zero. Undersaturation is indicated by a negative SI and supersaturation by a positive SI (Appelo *et al*. 2005). Hence, SI is used to evaluate the extent of water chemistry dissociation along the flow path. Saturation indices for calcite (SI_{cal}), dolomite (SI_{dol}), halite (SI_{hal}) and gypsum (SI_{gyp}) were computed using Phreeqc computer code, version 2.8.

2.2.4. Linear Correlation

This is used to see the trend and correlation of major and total dissolved ions along flow path. It can depict whether different major cations and anions have the same source or not. High positive ion correlations are assumed to have the same sources while high negative correlation shows different origin of minerals in the water. This also gives

highlight on recharge-discharge relations. As one moves from recharge to discharge area the negatively corellable variable highly vary in magnitude.

2.2.5. Hierarchical Cluster Analysis (HCA)

This was used to classify waters of large numbers of samples in to objective groups with similar physical and chemical properties. Statistical classification of geochemical data by Q-mode hierarchical cluster analysis (HCA) has been proven to provide a suitable basis for objective classification of water composition into hydrochemical facies (Meng and Maynard, 2001; Güler *et al*., 2002, Güler and Thyne, 2003; Kebede *et al*., 2005). Before using the HCA, the raw collected chemical data were log-transformed and standardized to restrict the biases caused by the variables that have the greatest or smallest variance or magnitude of clustering results. It helps to conduct geochemical modeling for different facies and to interpret the hydrochemical evolution along a flow path by grouping similar physical and chemical properties of different water samples. In this investigation, STATISTICA data analysis software version 8.0 (Stat Soft Inc. 1984-2007), commercial software package was used for HCA, descriptive statistics and linear correlations.

2.2.6. Inverse Geochemical Modeling

This method was used to identify the chemical evolution of groundwater in the study area. Using this method the type and amount of minerals in moles that can dissolve or precipitate along a groundwater flow path will be determined provided that the flow path can be selected depending on available general hydrogeological information. It gives an insight understanding on how much minerals is dissolving in water or precipitating from water that can add or remove total dissolved solids respectively in particular pumping water well. It also indicates types of geochemical processes controlling the chemical compositions of groundwater. The PHREEQC Interactive version 2.8 computer code was used to simulate the modeling.

2.3. ENVIRONMENTAL ISOTOPES ($\delta^{18}O$ and $\delta^{2}H$)

This method was used to know the recharge source, recharge mechanisms and sources of water quality problems by using fractionation principles. Deuterium and Oxygen–18 will fractionate during the process of evaporation and condensation.They are relatively

enriched in liquid phase and depleted in vapor phase. Hence, it helps to identify different sources of recharge and identify the variations in isotopic composition of groundwater and rainwater. The fractionation of stable isotope (heavy/lighter isotopes) depends on different effects such as altitude, temperature, distances from the source and rainfall season and amount. Isotopic composition is expressed in terms of $^{2}H/^{1}H$ and $^{18}O/^{16}O$ ratios, represented by δ values signifying the deviation in parts per thousand($^{0}/_{00}$) from a designated standard. Values will be cited with respect to SMOW (Standard Mean Ocean Water), such that

$$\delta_{sample} = \left(\frac{R_{sample}}{R_{SMOW}} - 1\right) X\ 1000$$

where R = $^{2}H/^{1}H$ or $^{18}O/^{16}O$ ratio measured in sample and standard (Fritz and Fontes, 1980; cited in Gibson *et al.*, 1993).

The stable isotope composition of water is also useful and clearly shows the source of salinity. Saline water due to evaporation will be more enriched in Oxygen-18 than the source water, whereas water that is saline due to salt dissolution or addition or transpiration will not change in isotopic composition.

2.4. CHLORIDE MASS BALANCE METHOD (CMB)

This will be employed to determine groundwater recharge rate. Chloride, one of the most common elements in groundwater, which only precipitates at very high concentrations, has been recognized as an ideal conservative tracer of water-cycle processes (Huang, 2010). It is a conservative tracer, which indicates evaporation. This method is based on the fact that precipitation contains chloride from sea salt aerosol. During evaporation the concentration increases, and the increase is a measure of the evaporation. Hence, the total recharge to groundwater will be estimated using the following equation.

$$R = \frac{P * Cl_{p} - RO*Cl_{RO}}{Cl_{gw}}$$

Where, R is the recharge to groundwater in mm/yr, P is the mean precipitation amount in mm/yr, Cl_P is the chloride content in precipitation in mg/l, RO is mean annual surface runoff in mm/yr, Cl_{RO} is chloride in surface runoff in mg/l, and Cl_{gw} is chloride in groundwater in mg/l. However, as most of runoff cannot go out of the target area, the chloride content washed-out from the area with runoff is assumed to be negligible and so that the amount of Chloride in runoff taken as zero in this investigation.

3. DESCRIPTION OF THE STUDY AREA

3.1. LOCATION AND ACCESSIBILITY

The research area is found in the Southern Ethiopia, Oromia Region, Borena zone. It is located between 3° 31' 41" and 5° 09' 31" latitude and 37° 01' 13" and 38° 32' 59" longitude within 650 - 750km radius from Addis Ababa (Figure 3.1). It is bounded by Ethio-Kenyan border in the south and southwest, by Rift valley lakes basin in the north and northwest, and by Dawa sub-basin in the east. It covers an area of about 16,495 km^2, which is nearly about half of the Lega-Wata/Lega-Sure sub-basin; one of the sub-basins in Genale-Dawa Basin.

The site can be accessed by Asphalt road from Addis Ababa to the border town of Moyale that passes via towns of Yaballo and Mega. All weather roads, secondary and tertiary roads connect different part of the study area.

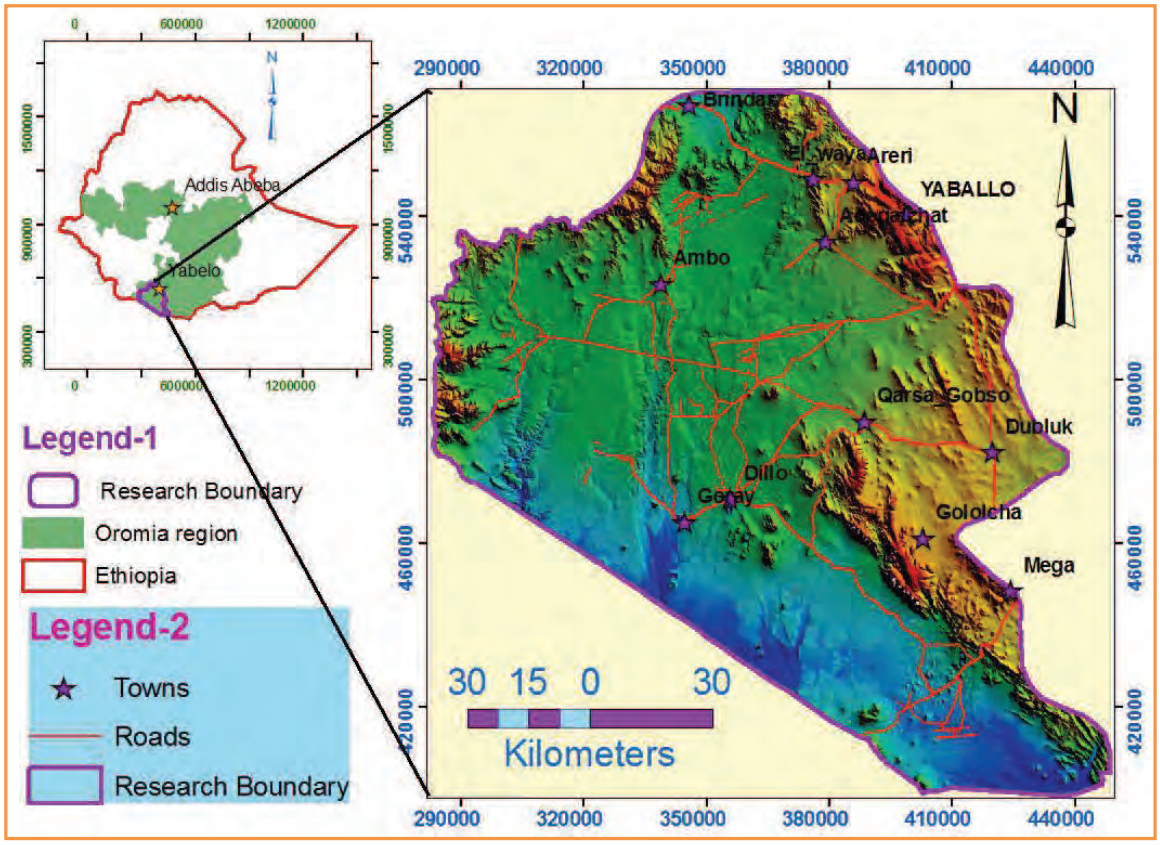

Figure 3-1: *Location Map*

3.2. GEOMORPHOLOGY AND DRAINAGE

The general elevation of the area declines from north to south following the streams converging to the Ririba main fault. However, the mountain ranges near Yabello and Mega towns, where step faults uplifted crystalline rocks more than 1000 meters, gave rise to the highest known elevation in the area. The lowest and highest elevations are 740 and 2484 meters above sea level, respectively. The most upland parts to northeast, east and southeast is covered with Precambrian basement formations whereas the low laying area is dominated by volcanic rocks. Some volcanic domes and remnant basement mountains in the low lying plains are the exceptions. The northwestern mountains and plains of the area are volcanic rocks.

The study area sub-basin is categorized under dry basins where only ephemeral streams are available. There are many ephemeral streams draining to lowland plain areas. These emerges from highly rugged topography of northern, eastern and western highlands and flow to the low lying flat topography to join the main Ririba valley which finally crosses the adjoining Ethio- Kenya border.

In general the geomorphology of the area is grouped in to basement hills and upland plains, Mega rift escarpment, recent volcanic landforms, Ririba fault zones, volcanic mountains and highland plateau and volcanic plains and lowland plains (OWWDSE, 2006) (Figure 3.2A). According to the tectonic structure, geomorphologic units and topographic rise above sea level the area has also been delineated in to escarpments and highland plains (≥1500m), middle plains (1000–1500m) and lowland plains and rift (≤1000m) sections (Figure 3.2B). In this work, the hydrochemical data analysis and interpretation for groundwater recharge and flow processes were treated based on these topographic subdivisions.

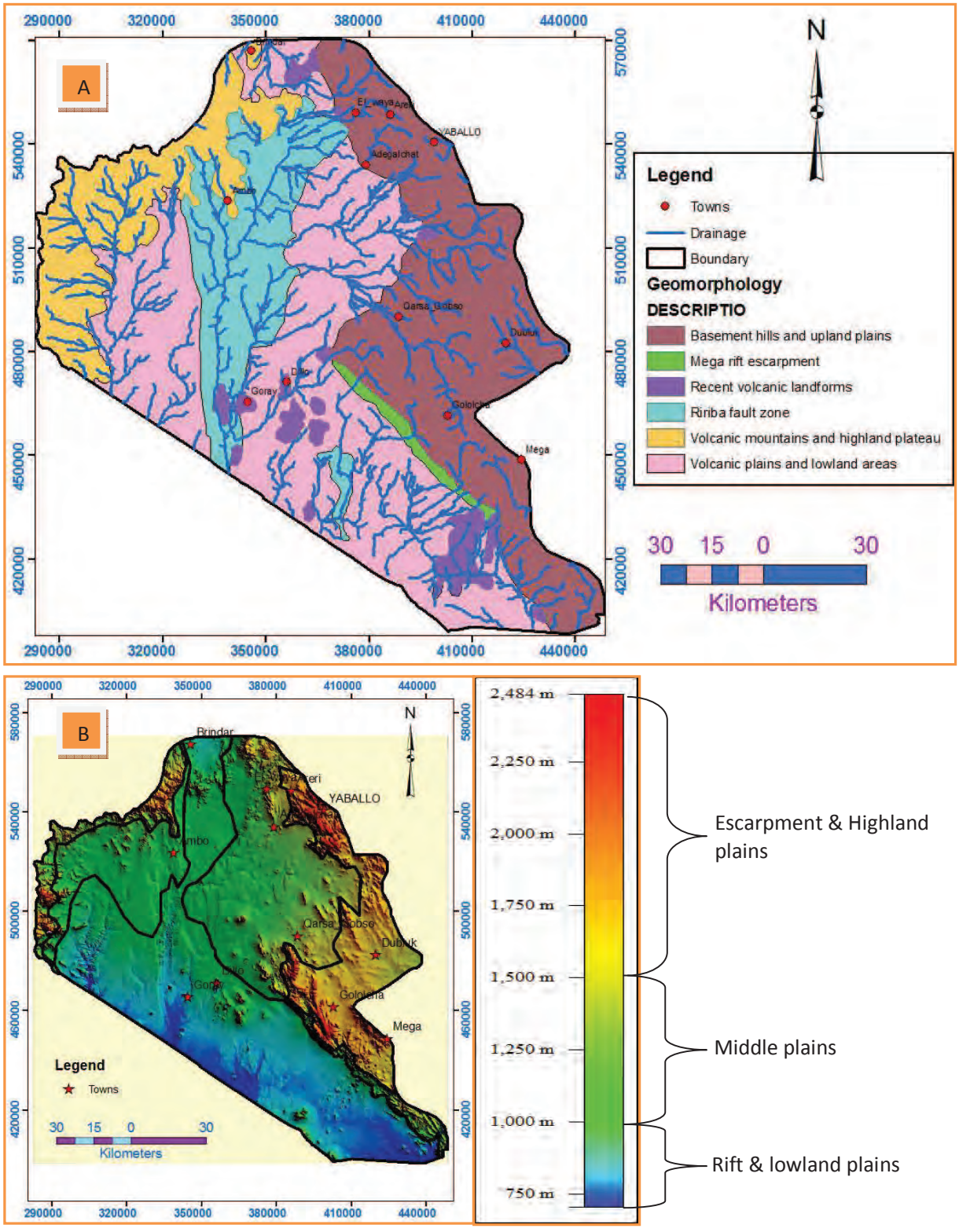

Figure 3-2: ***A)*** *Geomorphologic and Drainage map (Source OWWDSE, 2011);* ***B)*** *Topographic setup divided into escarpment, middle and rift sector.*

3.3. *CLIMATE*

The area is characterized by hot semi-arid climate experiencing high-temperature, low rainfall and high evapotranspiration. This climatic condition is favorable to sustain grasses and acacia trees (Zenaw *et al.*, 2000). The main cause of the rainfall in this region is the southward migrating Inter-Tropical Convergence Zone (ITCZ) and westward propagating disturbance from the Indian Ocean. Two rainy seasons have been experienced; the main rainy season often extending from mid of March through to end of May and the small rainy season from mid of September to November. The rest of the months are generally dry. The distribution of rainfall is unreliable in all of the study area. It increases with altitude. However, as Yabello occur in a rain shadow of the central mountain range (Billé, 1983); the average rainfall at Yabello is lower than at Teltele and Moyale where the elevation is lower. Furthermore, higher average rainfalls occur at Moyale as its position on the escarpment with northern Kenyan desert subjects it to a higher rainfall (Coppock, 1980). In this work, the mean annual rainfall depth was estimated by isohyetal method and is about 590.8mm.

The climate is typical of equatorial region and modified by altitude. Air temperature in the area increases with decreases in altitude. The highest mean air temperature rises above 30^0c in the low lands below 1000m elevation. The mean annual potential evapotranspiration estimated according to Thornthwaite method for Moyale, Yabelo, and Mega stations are 1048mm, 1302.5mm, and 1048mm respectively that exceed the mean annual rainfall of the same stations, 644mm, 689.5mm, and 689mm respectively (EGS, 2000). Therefore, the study area is characterized by highest evapotranspiration exceeding average rainfall except few months throughout the year.

3.3.1. Arial Depth of Precipitation

There are only three meteorological stations located in the north, northeast and southeast of the study area; Teltele, Yabelo and Mega stations respectively. These are located only along the margins of the study area following main roads and are not evenly distributed. No stations are found in central and lowlands of the study area. Thus, to get a good estimate of mean areal rainfall depth three additional metrological data from Kenya was

downloaded from world metrological website (agromet@fao.org). These are Sabarie Police, Moyale-Sololo and North-Horr stations.

Even though dominated by flat topography, the study area consist various physiographic features ranging from 740-2484 m.a.s.l. Hence, the distribution of rainfall could be influenced by Orographic effect. In such areas, the best methods for determination of areal depth of precipitation are Theissen polygon and Isohyetal contour. In this study, the average areal depth of precipitation over the catchment has been determined using Arithmetic mean, Theissen polygon and Isohyetal contour methods and the results were compared. The mean monthly point rainfalls of the stations in and around the study area are shown in Annex 1.

3.3.1.1. Arithmetic Mean Method

Arithmetic mean method is the mean of all the rain gauges that are located on relatively flat topography and closely and evenly distributed. However, the gauges here are not evenly spaced and the topography also varies. Hence the value obtained from this method could not be as such reliable.

Six stations, three from Ethiopia and three from Kenya, were used to determine the areal depth of precipitation. Accordingly, the study area gets mean annual precipitation depth of **546.2mm** (Table 3.1.).

Table 3-1: *Areal mean annual rainfall depth determined by Arithmethic mean method*

No	Station Name	Rainfall(mm)
1	Yabello	583
2	Mega	688
3	Teltele	706
4	North Horr	180
5	Moyale Sololo	724
6	Sabarei police	396
	Total	**546.2**

3.3.1.2. *Thiessen Polygon Method*

Thiessen polygon method involves determining the area of influence for each station and convert point rainfall to represent areal rainfall. It considers the point rainfall data up to half way to the adjacent stations/gauges. The polygon was drawn using ArcGIS computer code and the area of influence is obtained for the four stations (Figure 3.3). The precipitation of each polygon was determined by multiplying the area weighing percentage and point precipitation enclosed in the polygon (Table 3.2) as in equation below. Thus the annual mean rainfall for the area is **613.5mm.**

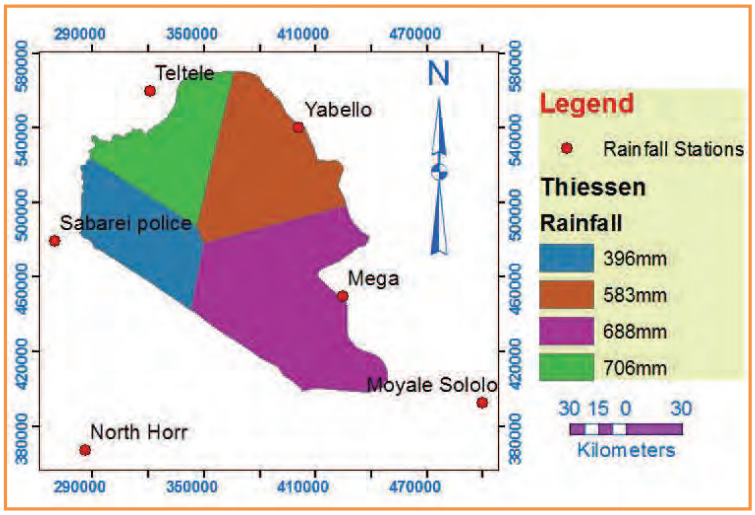

$$\overline{R} = \frac{1}{A}\sum_{i=1}^{n} a_i R_i$$

Where R_i are the rainfall measurements at n rain gauges, ai is area enclosed in polygon and A is the total area of the catchment

Figure 3-3: *Theissen Polygon map*

Table 3-2: *Areal mean depth of precipitation calculated using theissen polygon method*

Stations	Mean annual rainfall (mm)	Area of influence (km^2)	Weighted area (%)	Weighted rainfall (mm)
Yabello	583.0	4288.4	26.0	151.6
Mega	688.0	6319	38.3	263.6
Teltele	706.0	3031.8	18.4	129.8
Sabarei Police	396	2854.3	17.3	68.5
Total		16493.5	100.0	**613.5**

3.3.1.3. *Isohyetal Method*

Although most of the area under consideration is nearly flat, there is rugged and elevated landmass that can influence the distribution of rainfall by Orographic effect. In such areas, Isohyetal method is the best for determination of areal depth of precipitation. This approach provides good results, because it allows the influence of physiographic

parameters to be taken into account. These factors include elevation, slope and exposure to rain bearing winds (shaw, 1988). Hence, the average areal depth of precipitation over the catchment has been determined using Isohyetal methods and the results compared with the other methods. Contours of equal rainfall are drawn from available rainfall gauges in the area (Figure 3.4). Average weighted rainfall is equal to the weighted area between each contour and the median depth of rainfalls between the contours (Table 3.3). Thus the annual mean rainfall for the area is **590.8mm.**

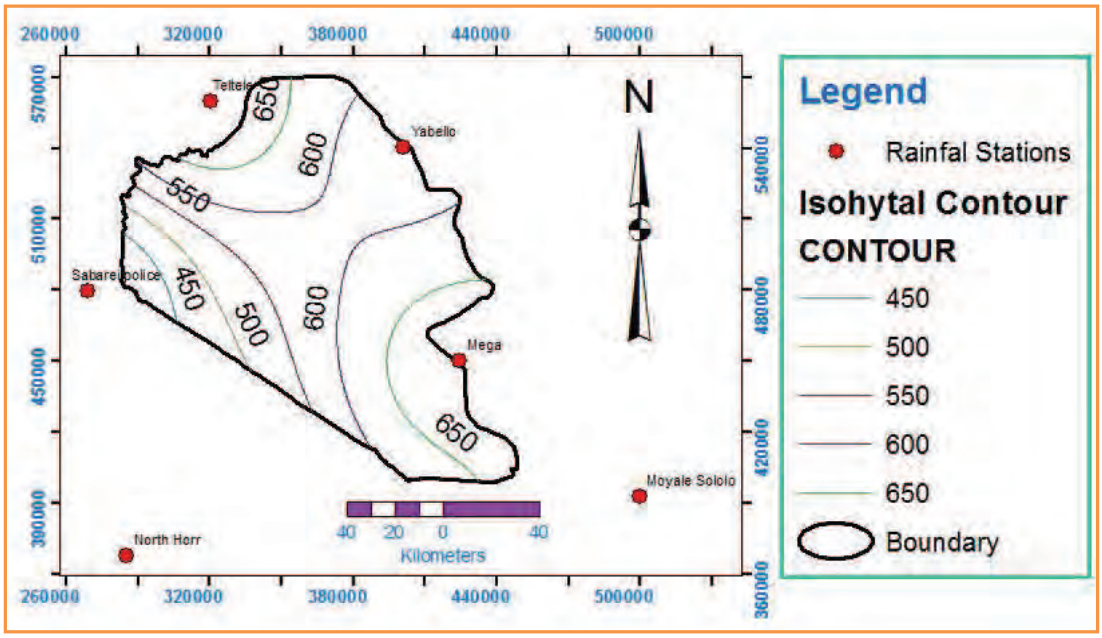

Figure 3-4*: Isohyetal Contour map.*

Table 3-3: *Areal depth of precipitation calculated using the isohyetal method*

Rainfall Range (mm)	Average Value of Isohyets	Area between Isohyets (km^2)	Weighted area (%)	Weighted Rainfall (mm)
<450	450	392.6	2.4	10.7
450-500	475	981.6	6.0	28.3
500-550	525	1683.5	10.2	53.6
550-600	575	5048	30.6	176.0
600-650	625	5484.1	33.2	207.8
>650	650	2905.2	17.6	114.5
Total		16495	100.0	**590.8**

The areal depth of precipitation obtained from the three methods is nearly similar. However, due to orographic effect the Isohyetal result was considered as the areal mean depth of precipitation for this work and is **590.8**mm/yr.

3.4. LAND USE AND LAND COVER

The land cover of the area is mostly shrub grass land, shrubs and grass lands. As most of the area is occupied by pastoralist, there is no cultivated land but small Agricultural work is practiced near Yabello and Mega (Figure 3.5). According to OWWDSE, the western and north-west high lands of the project area and the low lands close to ridge escarpments are relatively well covered with mixed type of vegetation. The vegetations in these areas are dry lowland woods, mixed with hard wood coniferous Shrubs consisting of Podocarpus and Juniperous trees.

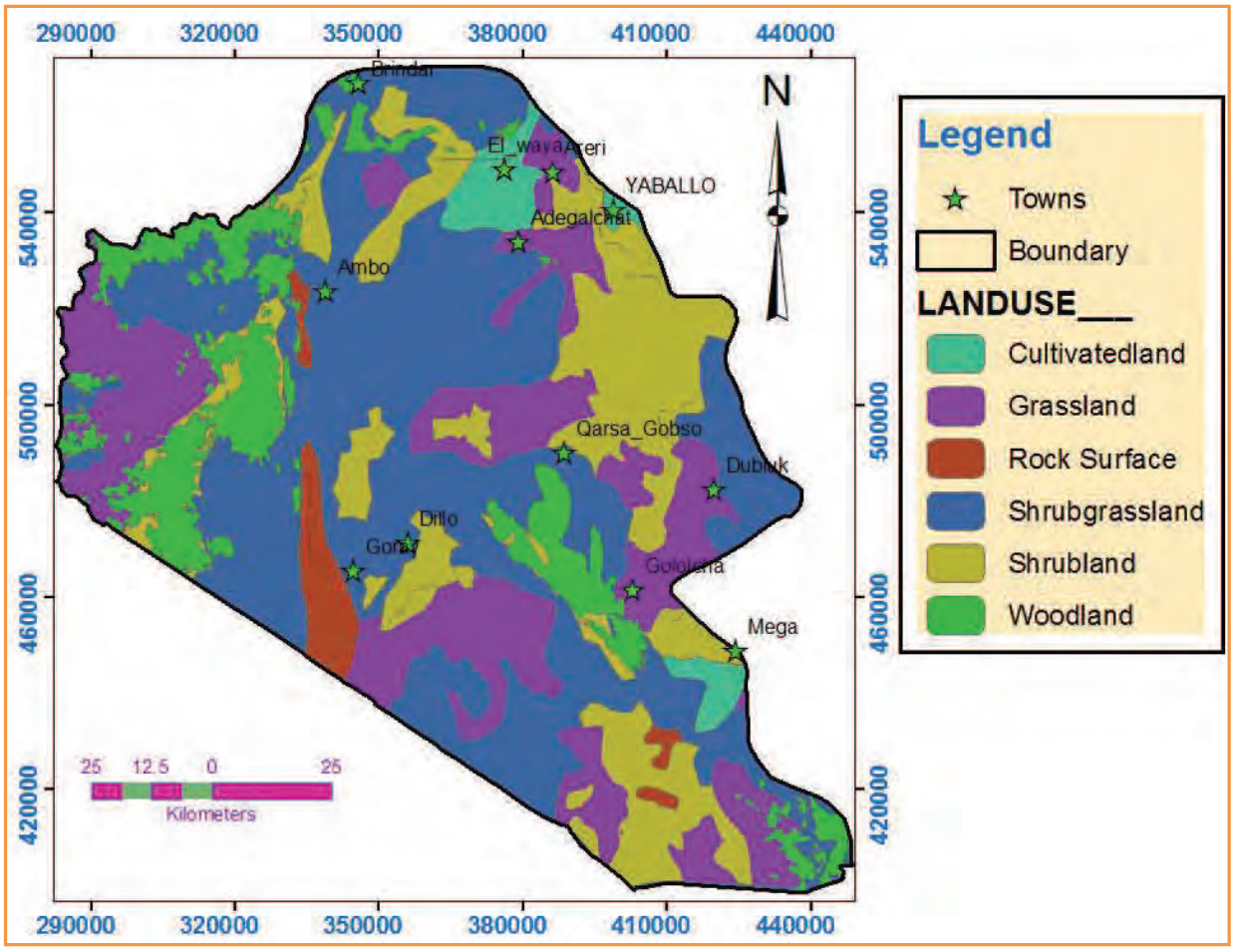

Figure 3-5: *Land use/cover map; adopted from OWWDSE, 2006*

3.5. GEOLOGY

Three major chronostratigraphic units are known to occur in Southern Ethiopia in general, namely Precambrian crystalline basement, Mesozoic sedimentary rocks, and Cenozoic volcanic rocks with sporadic sediments and superficial deposits (Kazmin, 1972; Davidson, 1983; and Teferra *et al*., 1996). In the present study area, however, Mesozoic sedimentary rocks are absent. The geology of the study area was compiled and modified by OWWDSE (2006) from four separate sheets which are Hageremariam, Yabello, Sololo and Ommo River Projects, previously mapped by EGS at 1:250,000 scales.

For the purpose of this thesis work brief descriptions of the geology and hydrogeology were extracted from different previous works, particularly from BGPA report; OWWDSE (2006 and 2011).

3.5.1. Basement Rocks

The Precambrian crystalline rocks of the study area comprise high-grade gneisses, and weakly to moderately metamorphosed rocks. The rocks mainly occupy the eastern part of the project area. Most of the dotted hills in the volcanic plains are also made up of basement rocks, for example, Mt. Kanchero, Bufa-Guda, Gara-Arba, Arbole, etc. Exposures are often extensive and continuous in the mountain ranges, blocky and fragmental in the ridges and hills, whereas patchy and discontinuous in the flat lying areas (MAB Consult, 2009). According to unpublished geological map prepared by OWWDSE (2006), the crystalline basement rocks in the study area comprise different lithologic units with variable degree of weathering and fracturing. These are gneisses, granulites and intrusive rocks (Figure 3.8).

3.5.2. Volcanic rocks

3.5.2.1. Tertiary Basalts

The tertiary basalts are lower basalt, middle (Teltele) basalt, upper basalt, and Bulal basalt from older to younger age. Each is briefly outlined below.

The lower basalt: This mainly occurs as erosion remnant and/or depositional margin of the unit, in the form of patches or discontinuous outcrops of boulder nature. Its thickness is generally in hundreds of meters farther north outside of the project area, but within the project area, the thickness may not be significant, mostly being in tens of meters. It generally dips 5-10^0 towards west (W/Gabriel et al., 1991).

Middle (Teltelle) basalt: It is generally dark gray, fresh aphanitic and partly vesicular. It contains small phenocrysts, as well as zeolite and calcite amygdales. It commonly shows columnar jointing. With basal parts of the Middle (Teltelle) basalt unconformably overlying the Precambrian crystalline basement rocks, these volcanic successions have significant thickness that may range in hundreds of meters in some places.

Upper basalt: The upper basalt is composed of a single flow and is fresher than the Teltelle (middle) basalt. Columnar joints are common and at places outcrops are blocky. It covers small areal coverage in Northwestern extreme of the study area.

Bulal basalt: is the most widespread post rift volcanic rock and horizontally layered sheets of basalt flows mapped in the area. This informal lithostratigraphic unit was introduced first by Davidson (1983). The total thickness of the Bulal basalt section over large part of the area so far explored is in the range of 140 to 250m with an average of 185m. However, within this general domain, there are some localities where the total thickness is not yet known (OWWDSE, 2011).

In hand specimen, rock of the Bulal basalt is dark to greenish gray, fine-grained and usually vesicular where the vesicles are mostly elliptical in shape and rarely reaches up to 3cm in size. It is sometimes amygdaloidal, in which the secondary minerals, for example calcite, forming the amygdales are leached out. The low-lying plain areas south and southwest of Yaballo and Mega towns of the project area are mainly underlain by these rocks. These rocks are exposed in the form of rubble rock fragments of up to boulder sizes at surface, with columnar joint structures and prominent Northwest and Northeast trending fractures. Bulal basalt is mainly characterized by fine-coarse vertical columnar joints, also commonly vesicular and locally scoraceous that have a “young look”

or fresh surface at exposures. The rock is tectonically jointed in the direction of mostly East-West, and Northeast-Southwest in which these joint sets have open structures of up to 70cm apertures. The open joint structures are clearly observed in the internal walls of Dillo volcanic crater (Figure 3.6). The joints are sometimes filled by precipitates of carbonate materials such as travertine.

3.5.2.2. *Quaternary Basalts*

These include Lapilli Tuff, Scoria, and Goray basalt. Each unit is briefly described below:

Lapilli Tuff: The unit consists of thinly bedded fall deposit with poorly sorted and abundant rock fragments of pyroclastic surge. Thickness of the unit is reaching up to 5m near vents. It occurs mainly in the central and southwestern parts of the project area where volcanic activities of the Quaternary Period prevail. The areas include Dillo and Magaddo and few localities west of Mega Town, blanketing relatively gentle gradient slope surfaces and flat topographies in areas of its occurrence.

Scoria: The scoria unit is fine grained, reddish brown, dark grey or greenish grey and highly vesicular. It occurs as volcanic cones and volcanic crater rims sporadically punctuated in many places of volcanic plains of the project area. The unit also occurs in highland terrains of Romso graben structure located just south of Mega Town. These volcanic cones and crater rims made mainly of the scoria are usually aligned, perhaps, marking a structural trend.

Goray Basalt: This youngest volcanic unit, overlying all volcanic units, is dark green, fine grained and very fresh, with cognate xenoliths of olivine aggregates up to 7cm in diameter (Dubois, 1976). The rocks commonly contain xenoliths of frequent mantle nodules of olivine aggregates (dunites).The olivine is crystal green and some is of gem quality. The rock is highly vesicular (5-6%), the vesicles rarely being filled by secondary minerals. Main areas of occurrences of this map unit are Goray (the type locality) found in the southern central part, and Magado and Mega in the southeastern reaches of the area. Thickness of this unit is generally variable, the maximum tongue of the flow at Didibe Ramso reaching 15 to 20m.

3.5.3. Quaternary Superficial Deposits

These deposits include Calcrete and Ferricrite, Elluvium, and Alluvium deposits. The Calcrete and Ferricrite deposit is found in eastern periphery of the project area. It is fine grained yellowish gray to creamy buff colors with slight to high degree of weathering. It is locally reaching up to 5m thick. It consists of calcite cemented angular fragments of mostly basement derived rocks, and commonly occurs as discontinuous patches over the area and in the eastern periphery of the project area in the vicinity of Dubluk village.

The Elluvium deposit occur throughout the project area and comprises of residual and transported soils occupying flat lying and gentle topography represented by sand, silt, clay, and gravels in various proportions. It occurs both in basement and volcanic units, but extensively in the metamorphic area. It has low permeability and a thickness of less than 10m; it could contain shallow groundwater in low lying areas where they are overlain by some alluvium (MoWR, 2005).

Alluvial deposit occupies streambeds, flood plains, stream banks, and rarely defines alluvial fans at the mouth of some rivers. It is dominated in Ririba valley, Mansagerdo stream channels and Utallo areas. It mainly consists of sand, silt, clay in various proportions with some Pebbles and Cobles and the color varies from grayish white through reddish brown to black. The constituent minerals of the sand and silt are chiefly quartz, feldspar, rounded to sub rounded rock fragments, and subordinate magnetite, biotite, and white micas. The crater floors of Megado, Dillo, and Goray are covered by light grayish to whitish alluvial deposits. The deposits in these maars are made up of evaporates derived from carbonate bearing materials that dissolve due to seasonal lakes in the craters/maars. A travertine deposit is observed in Dillo craters (Figure 3.7).

Figure 3-6*: Photograph showing columnar basalt with open fissures exposed in Dillo crater*.

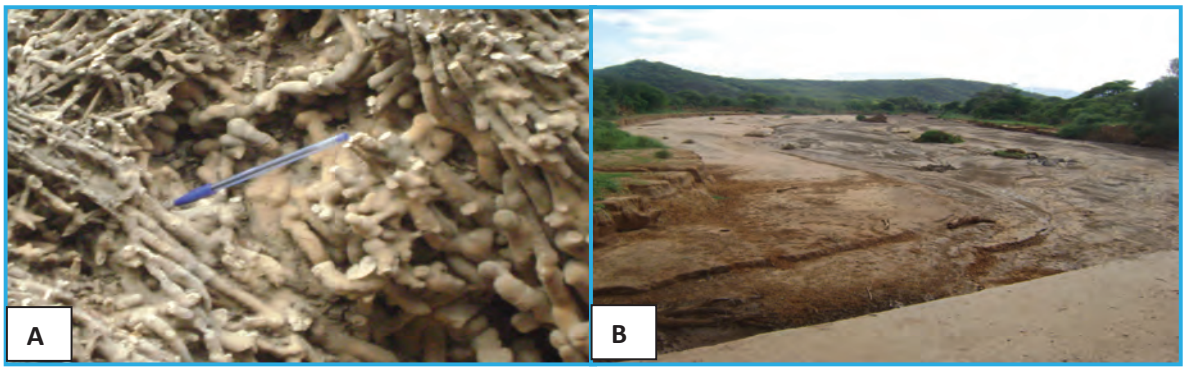

Figure 3-7: A) *Travertine formed in Dillo Craters and* ***B)*** *alluvial deposit along Mansagerdo ephemeral River course*

3.6. GEOLOGICAL STRUCTURES

The Ethio-Arabian swell and the formation on the rift valley in the Late Mesozoic and Early Tertiary times had a great effect on the nature and orientation of the present day river basins (Tesfaye Cherinet, 1993). The development of secondary porosity and permeability through the fracturing and jointing of rocks during tectonic movements throughout the geologic history are also another factor in hydrogeology. The main Ririba and Mega faults crossing the study area are nearly aligned North-South and Northwest-Southeast respectively (Figure 3.8). The Ririba fault is the continuation of the Ethiopian Main Rift. The main faults and fractures crossing the volcanic plains, particularly near Gelchet are good passage and storage for the groundwater reservoir of the Bulal basalt. This could be confirmed by the dominance of high discharge wells drilled in Gelchet area.

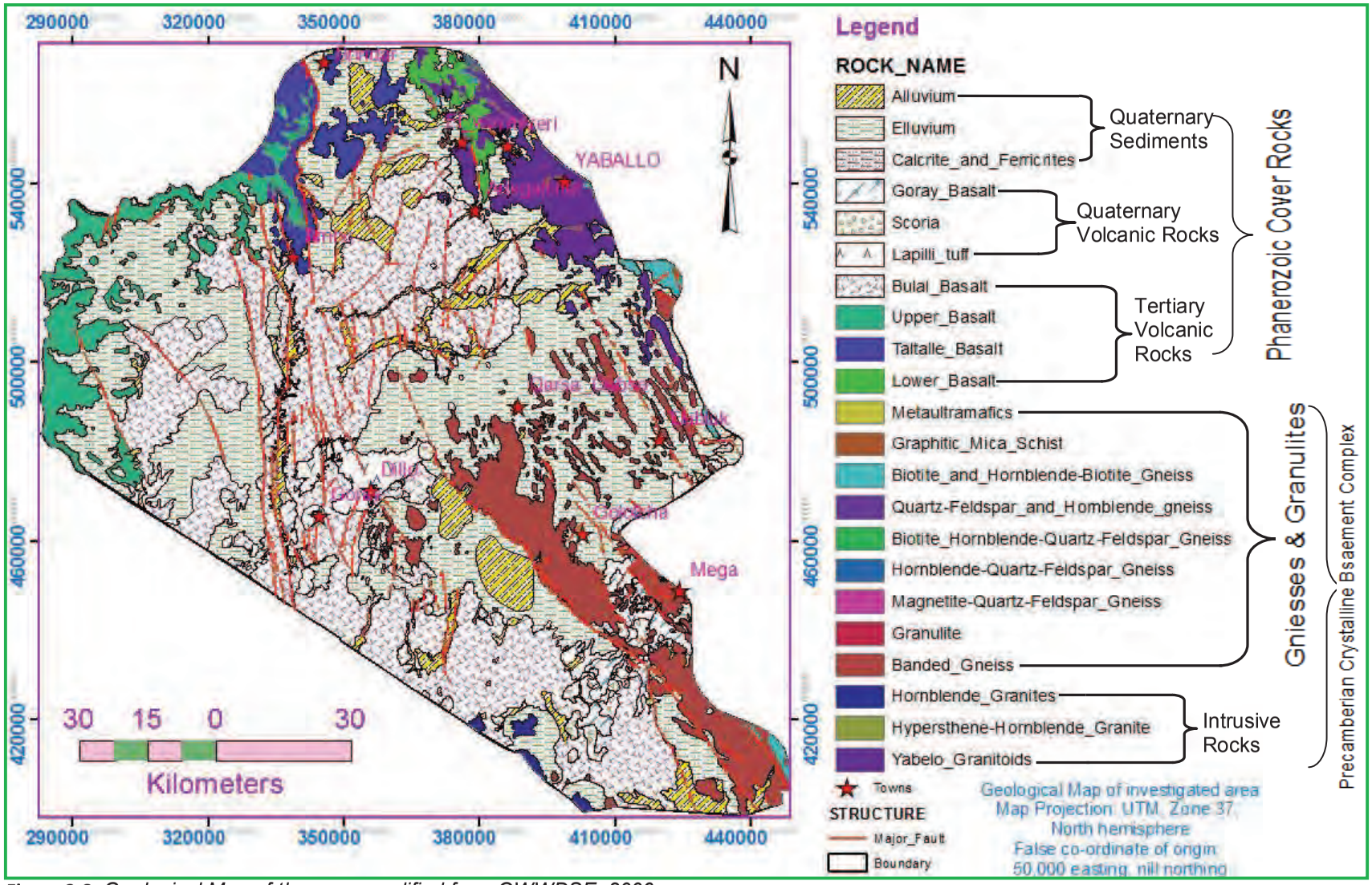

Figure 3-8: *Geological Map of the area, modified from OWWDSE, 2006*

3.7. HYDROGEOLOGY

The hydrogeological configuration of the study area is controlled by the geomorphological, structural and lithological formations. The variations in the aquifer distributions and the groundwater flow system are the result of structural and lithological differences over the project area. The volcanic rocks are the regional aquifers with variable hydraulic capacities. The aquifer classification takes in to account both the aquifer types and the aquifer productivity.

3.7.1. Aquifer Types

According to OWWDSE (2011), the aquifer types in the study area is divided in to 1) Extensive aquifers with intergranular permeability (unconsolidated sediments; alluvium, elluvium, colluviums, lacustrine sediments) 2) Extensive aquifers with fracture permeability (volcanic rocks) and 3) Localized aquifers with fractured and intergranular permeability (basement rock).

Extensive aquifers with intergranular permeability: Alluvial deposits in the area show gradation from clay and silt to coarse sand and gravel at their bottoms and thus possess moderate to good permeability. Their thickness ranges in most cases, from about 2m to 40m, while at the localities of Mermero, Brindar and Harewayu thicknesses varies from 65m to 125m. The thick depositional environments are believed to be zones of old river channels (OWWDSE, 2011).

Extensive aquifers with volcanic fracture permeability: These rocks store water within fissured porosities, flow breccias, porous zones between successive lava beds, lava tubes, cracks and joints. Besides their lithological and porosity variations, relative geomorphologic positions and connections to recharge sources are the fundamental controlling factors for these aquifer systems. From the volcanic aquifers, Bulal basalt is the principal aquifer and covers about 4,684 km2, forming about 29 % surfaces out crop of the study area. The Teltele basalts are classified as aquifers with low to moderate permeability, while the upper and middle basalts covering the area are considered as aquiclude or locally very poor productivity aquifers (OWWDSE, 2011).

Localized aquifers with fractured and intergranular permeability (basement rock): Due to its inherent poor permeability, basement rocks are generally known to be non-aquifers. However, at localities where the rock mass is intensively fractured and weathered, or along open fault zones connected with recharge sources, it can form localized shallow aquifer system for instance, Dubluk area. The basement underlying the Bulal basalt aquifer dams the deep vertical percolation of groundwater and hence helps storage within the overlying Bulal basalt. However, the most upper thin weathered potions of the basement below the Bulal basalt could bear groundwater and can be included to contribute to the main volcanic aquifer (OWWDSE, 2011).

Most of the aquifer in the area is under confined condition because the water table rises from its strikes to a level where it creates its regional hydrostatic balance (see Annex 10).

3.7.2. Aquifer Productivity and Property

The aquifers of the area have variable aquifer properties and classified as high, moderate, low and poor productivity aquifer (figure 3.9 and 3.10). The productivity determined from pumping test data for wells yielding less than 14l/s shows transmissivity ranges from 4.42m^2/day to 398.25m^2/day and hydraulic conductivity from 0.053m/day to 9.83m/day (Table 3.4). However, this cannot represent the general productivity of the aquifer as wells yielding more than 14l/s were not included. Because there is no drawdown, the actual productivity of the aquifers could not be determined. For this reason large diameter well that accommodate high capacity pump size are required.

Table 3-4: *Hydraulic parameters; adopted from OWWDSE, 2011 unpublished technical report*

Parameter	Min	Max	Average
Transmissivity (T,m2/d)	4.42	398.25	65.34
Hydraulic Conductivity (K, m/d)	0.053	9.835	1.38
Specific capacity (Sc, l/s/m)	0.1	1.25	0.3

In general, the potential of main volcanic aquifer depends on its degree of fracturing, the continuity of fracture openings in the horizontal and vertical direction, and the way it is hydraulically connected with an area where recharge takes place (OWWDSE, 2011).

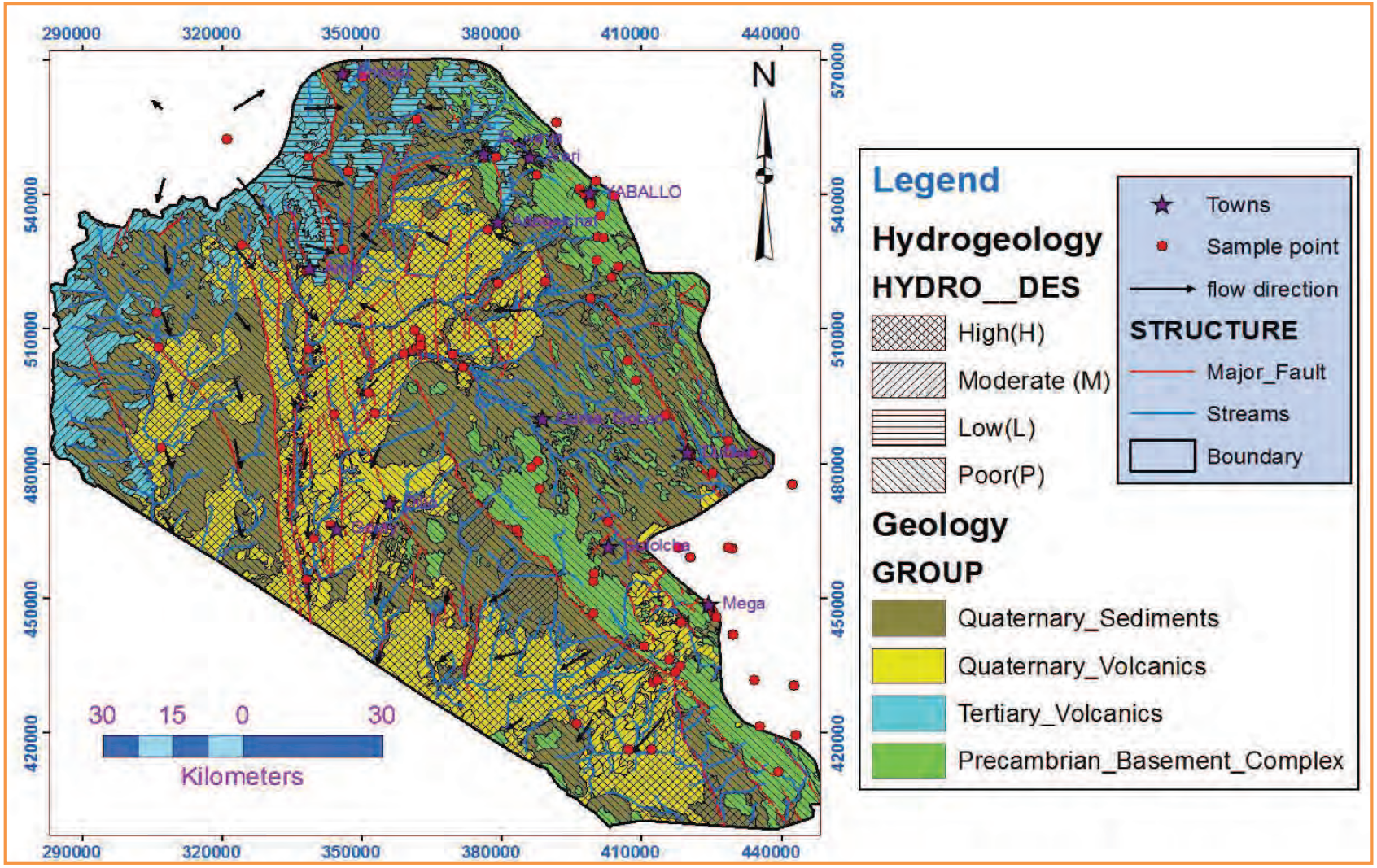

Figure 3-9: *Hydrogeological map; modified from OWWDSE, 2011.*

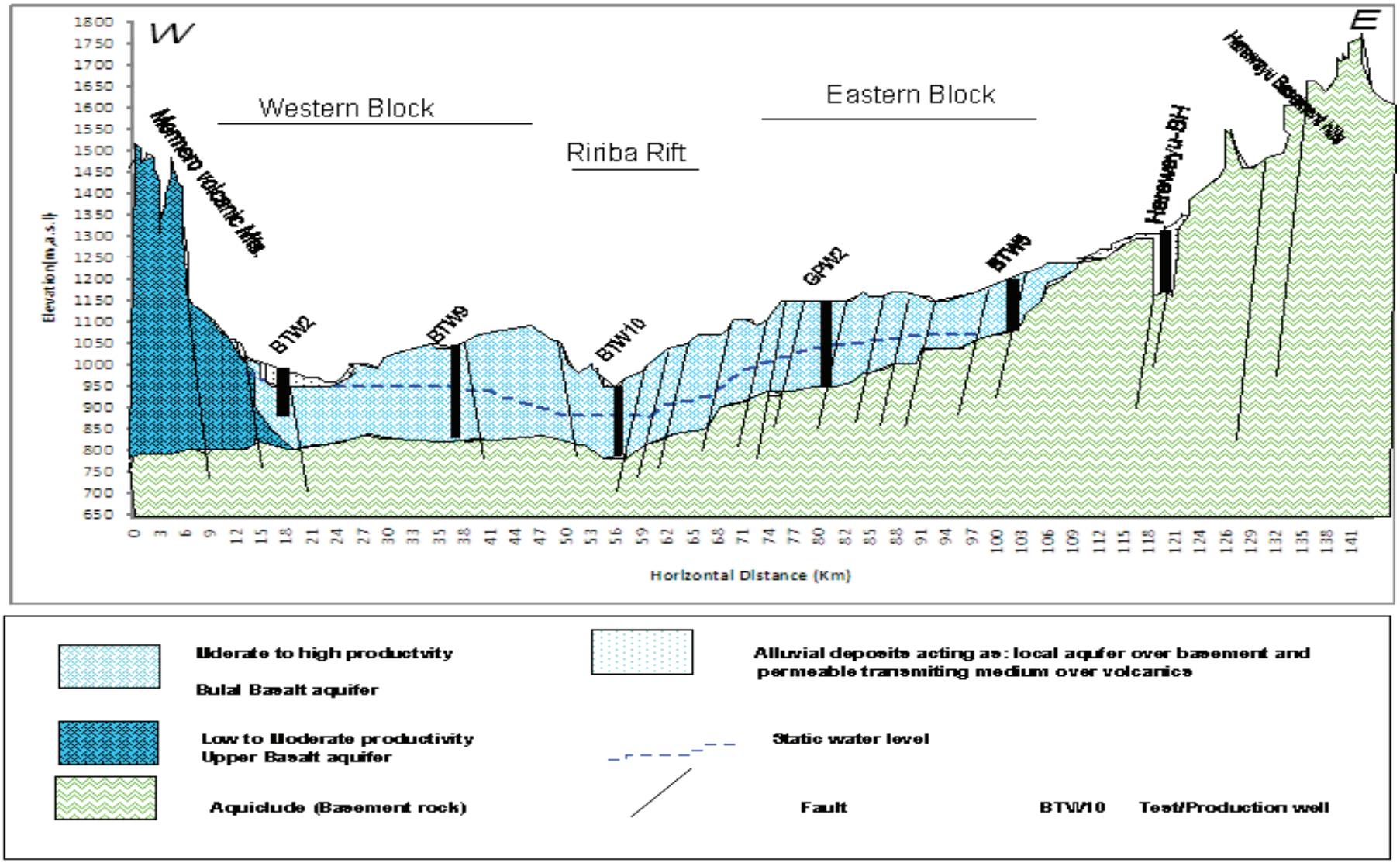

Figure 3-10: *Representative hydrogeological Section; Source OWWDSE 2011.*

4. HYDROGEOCHEMISTRY

4.1. GENERAL

Hydrogeochemistry is an interdisciplinary science that relates the quality of groundwater to various processes and reactions in aquifers and aquitards that is the study of the geological and hydrological controls on the groundwater chemistry (Kovalevsky *et al*., 2004). Water chemistry data can be used to infer groundwater flow directions, to define intended use of water, identify sources and amount of recharge and to define local and regional flow systems (Anderson and Woessner, 1992).

The concentration of inorganic constituents in groundwater are controlled by the availability of the elements in the soil or rock through which the water has passed, by geochemical constraints such as solubility and adsorption, by the rates (kinetics) of geochemical processes, and by the sequences in which the water has come into contact with various minerals occurring in the geological materials along the flow paths (Freeze and Cherry, 1979). The chemical composition of groundwater is the combined result of the composition of water that enters the groundwater reservoir and reactions with minerals present in the rock that may modify the water composition (Appelo and Postma, 1992). As water moves through subsurface geological formations, the composition will start to change gradually from dilute rainwater to concentrated ionic compositions. This is as a result of interaction between slowly moving water and the mineral in contact with water. Hence, hydrogeochemistry has a great importance to investigate groundwater sources, evolutions and quality.

4.2. RELIABILITY CHECK

Hydrochemical data analysis has to be checked to evaluate the quality of data and accuracy before using in interpretations of hydrogeochemical investigations. Water is naturally balanced in its cations and anions so that the principle of the cation-anion balance was used to check electroneutrality of the analyzed data.

$$\text{Electroneutrality} = \frac{\Sigma\text{Cations} - \Sigma\text{anions}}{\Sigma\text{Cations} + \Sigma\text{anions}} * 100$$

Based on the electroneutrality, analysis of water samples with a percent balance error <5% is regarded as acceptable (Fetter, 2001). But in very dilute or saline water, up to 10% error may be considered as acceptable due to the errors introduced in measuring major ions in dilute groundwater or in the multiple dilution require for analysis of concentrated groundwater (Fetter, 2001; cited in Alema, 2009). In this investigation, therefore, the balance error ≤10% is considered as high concentrated water there in the data set. All the chemical analysis obtained from BGWPA data base, OWWDSE, is found to be reliable. 92.6% of the data falls in the acceptable 5% criterion and the rest 7.4% falls in the acceptable 10% criterion (Figure 4.1A). However, most of the original analyzed samples were discarded owing to more than 10% balance error.

Figure 4.1A shows more positive than negative errors that are more cations than anions which suggest a systematic error with some anions being under measured. This is most probably also due to alkalinity being measured in the lab rather in the field as carbonate material precipitate and removes bicarbonate from anions while waiting for analysis (Fetter, 2001).

The ionic balance can also be checked by the sum of cations and anions comparing with the electrical conductivity divided by 100 as summation of cations or anions should be balanced with EC/100 (Figure 4.1B & C). Figure 4.1D shows good correlation among these three parameters.

$$\Sigma\text{cations (meq/l)} = \Sigma\text{anions (meq/l)} = \text{EC } (\mu\text{s/cm})/100$$

This equation is valid for EC measurement value up to 2000 $\mu s(cm)^{-1}$ and for dilute solutions the result should be a straight line. Besides to this, the equation is particularly important when the samples are transported long distances as there might happens chemical reactions in the samples bottles and precipitations of some ions presents (Getachew, 2008). The Descriptive statistics of the total data set (n=94) used in this work were summarized as in Table 4.1.

Table 4-1: *Descriptive statistics of hydrochemical parameters in the study area*[1]

Variables	Min.	Max.	Range	Mean	Harmean	Variance	Std.Dev.	Stnd. Error
pH	6.3	8.6	2.3	7.5	7.5	0	0.5	0.05
TDS*	80.0	8826.0	8746	1194.7	518.5	2182673	1477.4	152.4
Na*	11.5	1900.0	1888.5	195.3	61.6	86501	294.1	30.3
K	1.3	375.0	373.7	24.4	6.9	2504	50.1	5.5
Mg	1.1	734.4	733.3	59.5	13.2	10229	101.1	10.4
Ca	2.7	704.0	701.4	105.9	47.6	9698	98.5	10.2
Cl*	8.67	2330.0	2321.4	212.8	47.5	135657	368.3	37.9
SO_4*	0.57	1692.0	1691.5	245	7.5	113611	337.1	34.8
HCO_3*	29.37	3733.2	3703.9	452.9	228.5	364296	603.6	62.3
NO_3	0.17	44.6	44.5	7.7	0.7	124	11.1	1.15
F	0.07	7.8	7.8	1.3		1	1.2	0.12

Table 4-2: *Reliability check of hydrochemical data sets used in this work*[2]

Reliability Test	Attention Value	Theoretical facts	Remarks
$\frac{K^+}{Na^+ + K^+}$	<20%	Na >>k; because K^+ is more rapidly removed from solution by plants and clays than Na+.	6.4% of the data set is more than 20%; in this case either the dissolution of mica and feldspar or gradual decay of plant material/organic matter will release K+ to solutions.
$\frac{Mg^+}{Ca^{++} + Mg^{++}}$	<40%	Ca > Mg, unless provided by the dissolution of dolomite.	4% of the data set is greater than 40%. As there is no dolomite in the area, the dominance of Mg^{++} ion here is might be from olivine and amphibole minerals from basic rocks. Dominated in deep wells sunk to the volcanic rock of southeast corner of the area *(Figure 4.6B)*.
$\frac{Ca^{++}}{Ca^{++} + So_4^{--}}$	<50%	Most SO_4 concentration can be attributed to the dissolution of gypsum. Therefore the Ca/SO_4 ratio must be 1:1 or lower, if some Ca is also provided by the dissolution of carbonate.	64% of the data set is greater than 50% that indicate addition of more Ca by dissolution of calcerite sediments. Observed in all formations, particularly *in Northeast, East and central plains at Gelchet of the area (Figure 4.6B)*.
$\frac{Na}{Na^+ + Cl^-}$	>50%	Chloride is mainly provided by the dissolution of Halite (NaCl). Therefore the ratio Na/Cl is 1 or higher, if some Sodium is added from silicates or by ion exchange	18% of the data set is less than 50%. This is due to high Cl^- concentration due to evaporation or groundwater evolution. Observed in most shallow and deep wells of thick sediments.

[1] *All units are in mg/l except pH. * are shows high standard deviation and error due to high variation of variables in the area*

[2] *Note that, if the calculated values are not within the attention values (i.e. the result is below or above the given permissible value), then it does not necessarily signify an error; it does mean however there is more source and/or supply of ions in respective to the other (unit is in meq/l). Except the third quality check method the rest result were found to be fair.*

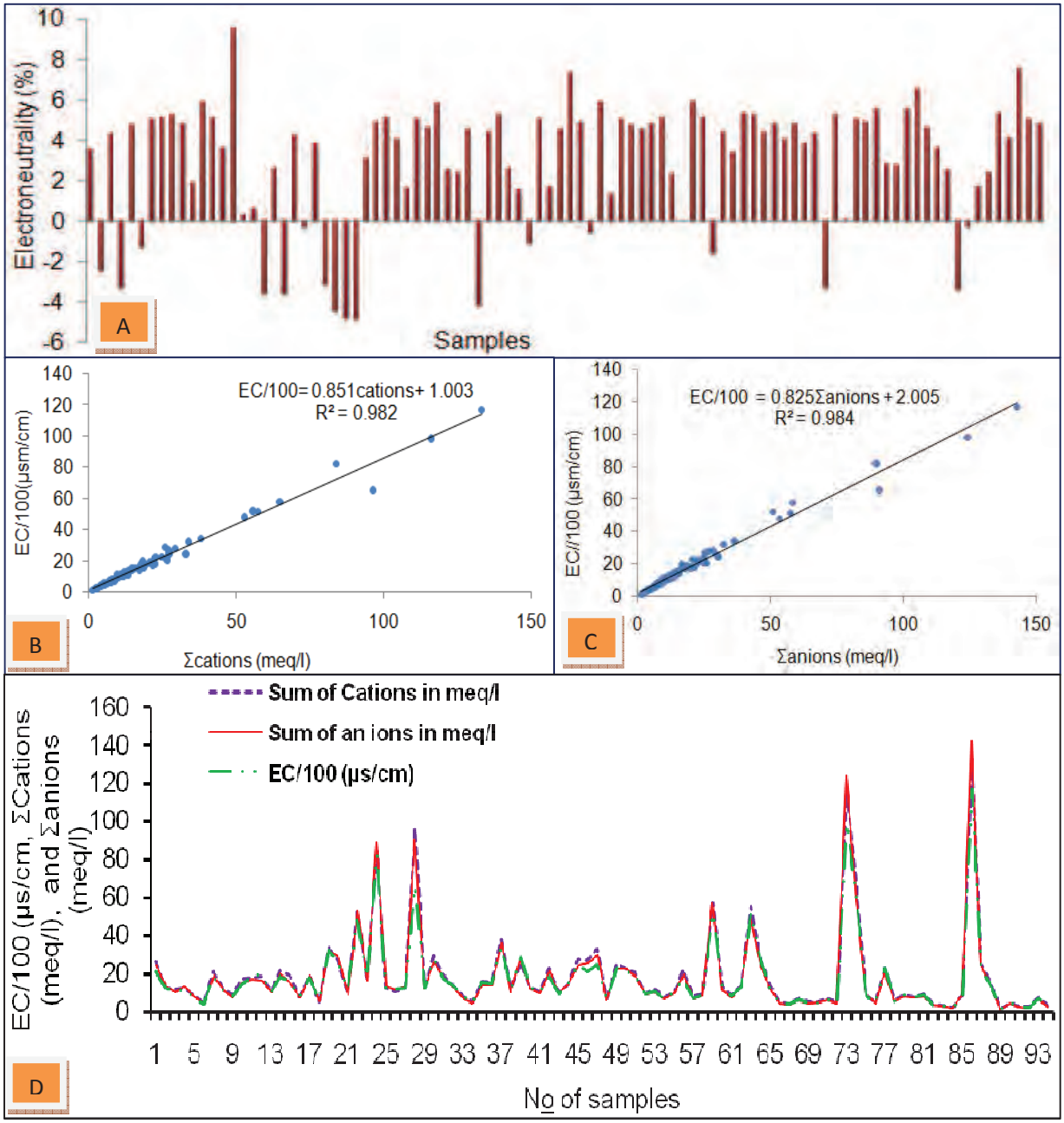

Figure 4-1: ***A)*** *Cation-anion balance error accepted below 10% balance error for the present work,* ***B)*** *Σcations vs. EC/100,* ***C)*** *Σanions vs. EC/100,* ***D)*** *relation among EC/100, Sum of cations and Sum of anions of the total chemical data set; balance error more than 10% was not included.*

4.3. PHYSICAL PARAMETERS

Temperature, pH, Eh, EC, TDS, and Alkalinity (bicarbonate concentration) are physical parameters, which all are should preferably be measured immediately in in-situ since they will changes rapidly after sampling. In this investigation, pH, Eh, Temperature, EC and TDS were measured in-situ for collected primary data (Annex 3).

4.3.1. The Hydrogen Ion Activity (pH)

The hydrogen-ion activity in an aqueous solution is controlled by interrelated chemical reactions that produce or consume hydrogen ions. The pH of natural water is a useful index of the status of equilibrium reactions in which the water participates (Hem, 1985). The primary control over pH in most potable groundwater is the carbonate system including gaseous and dissolved carbon dioxide, bicarbonate, and carbonate ions. The pH value of water between 6.5 and 8.5 is potable according to WHO standards.

The pH values from the study area is ranging from 6.33 to 8.6 in which nearly all samples falls in permissible range. Low pH is observed in most escarpments and middle plain sectors and increasing dominantly to rift parts (Figure 4.2). The low pH at discharging zones is owing to CO_2 gas source from deeper volcanic gases.

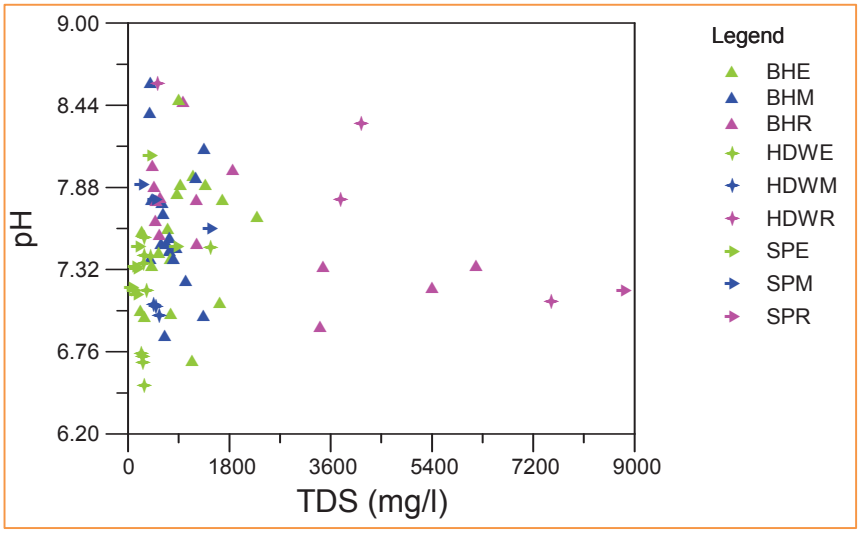

Figure 4-2: *TDS Vs pH in the area*[3]

[3] *BH, HDW, and SP are stands for Borehole, Hand-dug well and Spring respectively where as the letters E, M and R after BH, HDW and SP represents Escarpments, Middle plain and Rift & lowland plain sectors respectively.*

4.3.2. Electrical Conductivity (EC) and Total Dissolved Solids (TDS)

TDS is the total amount of solids, in milligrams per liter that remain when a water sample is evaporated to dryness. It describes all solids (usually mineral salts) that are dissolved in water. The more salts are dissolved in the water; the higher is the value of ion concentrations and thus the higher electric conductivity. Therefore, EC and TDS are related to one another. The EC against TDS from all sources of water measured in laboratory shows a straight correlation line (R^2 = 0.997) and equation of TDS = 0.75EC (Figure 4.4). As it can be seen from spatial distribution map of TDS (Figure 4.3), and EC versus TDS chemical data plot (Figure 4.4), both are increasing from highland plateau to the rift and lowland plain sector. However, water from alluvial and elluvial sediments over different formations show relatively higher EC and TDS in all topographic formations.

A simple classification but widely used scheme for categorizing groundwater based on total dissolved solids (Freeze and Cherry, 1979) is presented in Table 4.3. Fresh water is water that contains less than 1000 mg/l of dissolved solids; generally, more than 500 mg/l of dissolved solids undesirable for drinking and many industrial uses (Hem, 1985).

Water from open hand dug wells and spring from Dillo and Megado craters are classified under brackish water classes. Deep wells from Sarite, Brindar, Mehair/Furole and Dubuluk area also has brackish water class. Most of the sources from highland plains and middle sector of the area has fresh water class (Figure 4.4**).**

Table 4-3*: water class based on TDS*

Water class	TDS(mg/l)
Fresh	0 - 1,000
Brackish	1,000 - 10,000
Saline	10,000 - 100,000
Brine	>100,000

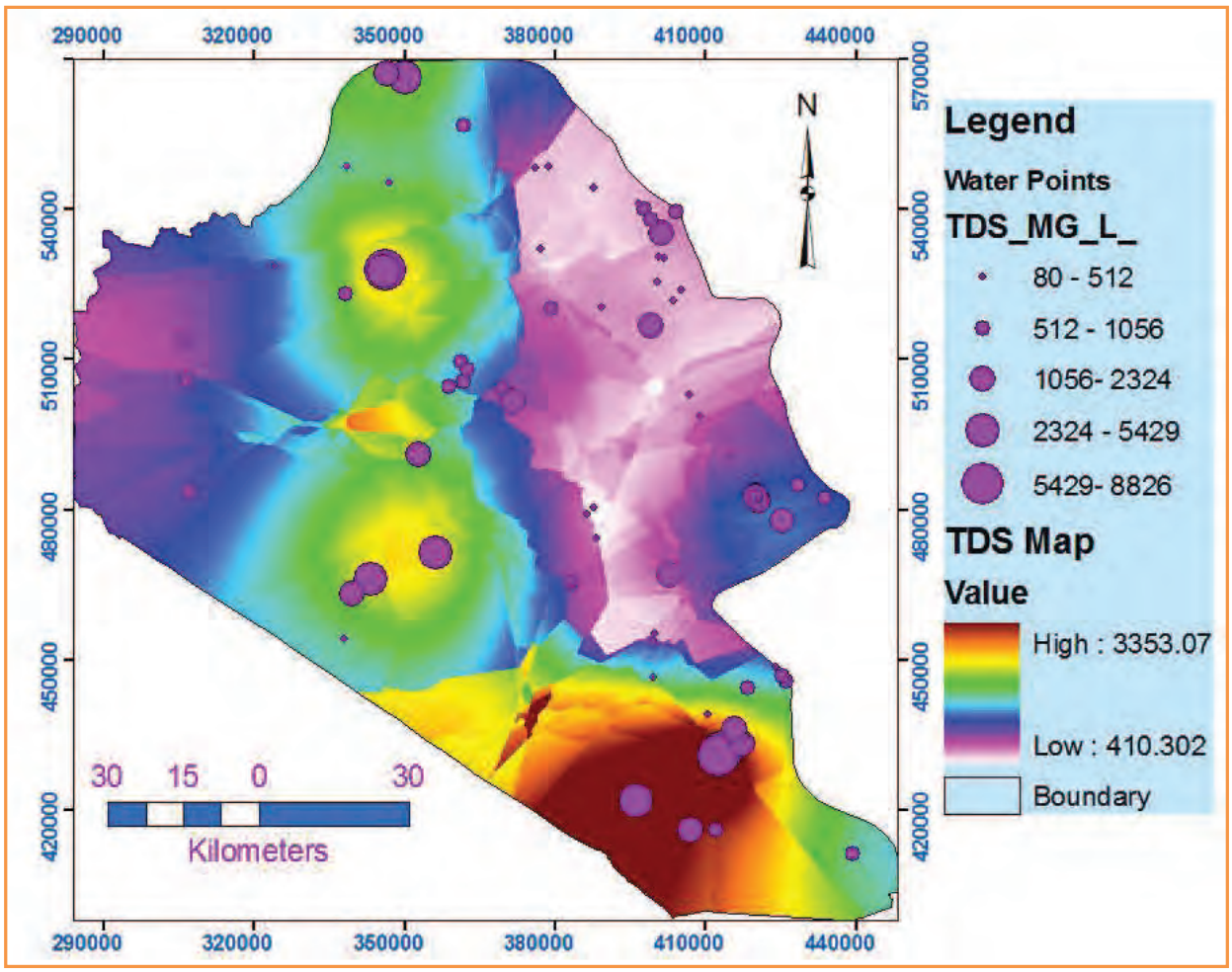

Figure 4-3: *TDS map; very high TDS is mapped along Ririba fault axis and at Megado craters*

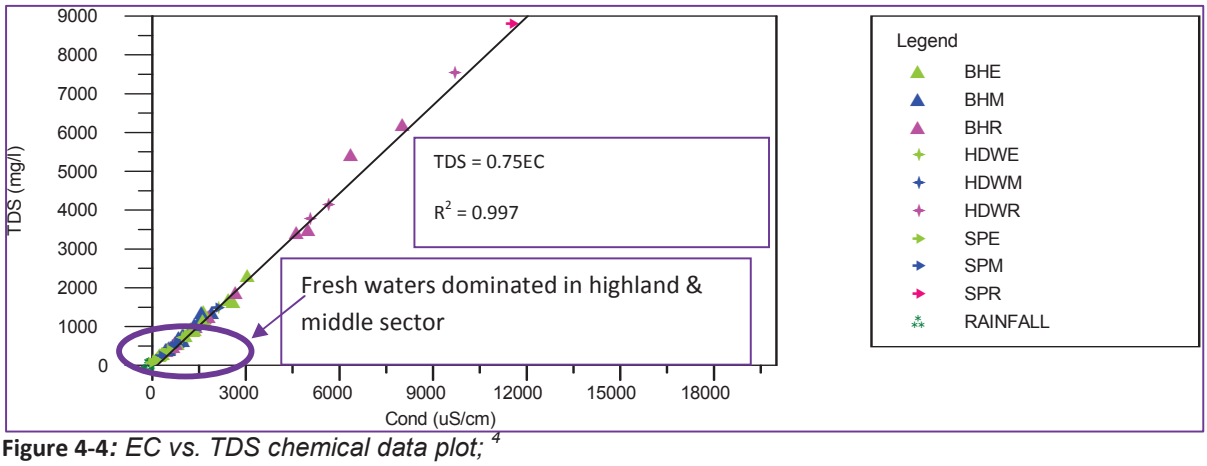

Figure 4-4*: EC vs. TDS chemical data plot;* [4]

[4] *BH, HDW, and SP are stands for Borehole, Hand-dug well and Spring respectively where as the letters E, M and R after BH, HDW and SP represents Escarpments, Middle plain and Rift & lowland plain sectors respectively.*

4.3.3. Water Temperature

Temperature of groundwater is important for numerous applications. For example, temperature measurements are critical in identifying recharge from nearby surface water sources and deep circulating waters. Thus, Temperature can depict clearly groundwater flow in deep and shallow circulations (Figure 4.5B). Groundwater temperature data may also be used to study rates and directions of groundwater movement, identify areas of recharge and discharge zones, because it vary with depth, owing to the geothermal gradient, and aerially because of heat transport by groundwater movement.

Water temperature is an important factor of the utility of water. Domestic water below 10°C (Celsius) is considered to be satisfactory for drinking (Stevens *et.al*. 1978). Chemical and biochemical reactions induced at higher temperatures produce undesirable tastes and odors in water.

Temperature is also affecting the various parameters such as alkalinity, salinity, electrical conductivity. Although shows less EC-Temperature correlation, Figure 4.5A gives highlights how groundwater varies with topographic locations. The overall groundwater temperatures measured from the study area have values ranging from about 18.5 to 41.4^{0}c (Figure 4.5A).

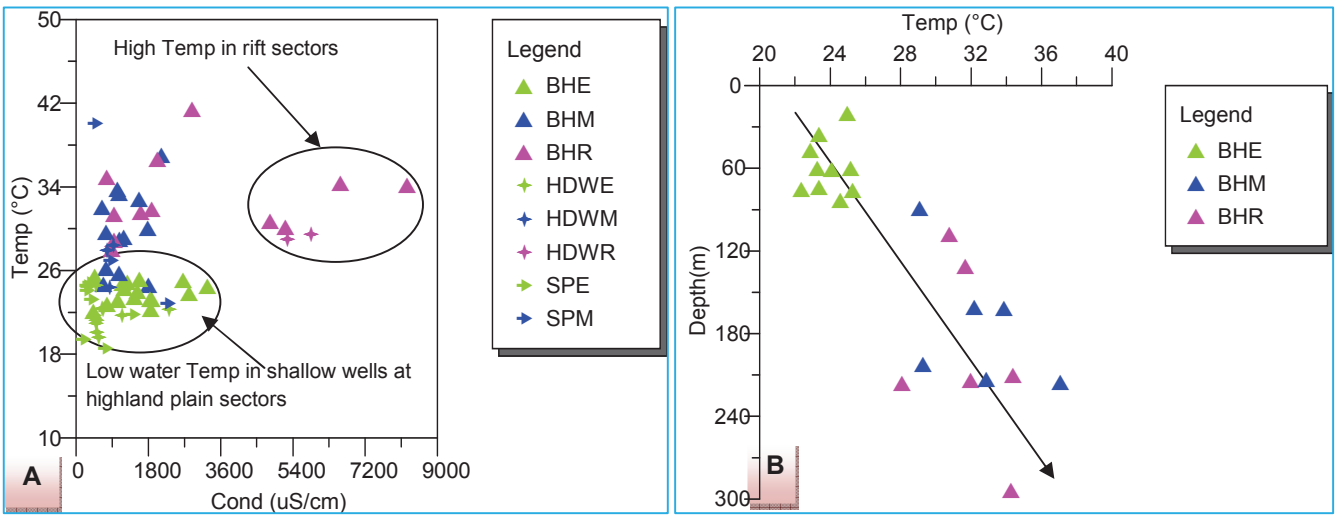

Figure 4-5*: **A)** EC versus Temperature plot of chemical data, **B)** Temperature versus Depth profile plot.*

4.4. MAJOR ION CHEMISTRY

4.4.1. Hydrogeochemical Facies

As the study area is found in dry basin where no perennial River exist, all primary and secondary water samples were collected from groundwater (shallow, deep and hand-dug wells and springs). The chemical composition from these groundwaters varies over a wide range and high standard deviations and error was observed (Table 4.1). This indicates that the groundwater in the study area is not uniform but differs by far, both in salinity and ionic composition. They are broadly distributed rather than forming distinct clusters (Figure 4.6). Thus, most of the groundwater in the area is characterized by different water facies even within few kilometer intervals. For the sake of simplification, however, it can be distinguished and grouped in to three main water types by their position on a Piper diagram (Figure 4. 6A). These are:

I) Ca-Mg-HCO_3,
II) Na-HCO_3 and
III) Ca-Mg-SO_4-Cl/Na-Cl/SO_4

Such various water type in a basin shows that the water has passed from source to sink through sediments, volcanics, and basement formations that have different soluble minerals to induce variable water facies. These rocks and sediments were often deposited over long periods of time and under a variety of geologic conditions. Thus, the chemical composition of the rock or sediment matrix of aquifers is seldom constant. In addition, a high evaporation rate under such semi-arid climate causes an increase in mineralization of groundwater in short distances due to the reaction with host rocks.

Water types in most of the high laying plains and middle slope sector, particularly in the northeastern sectors, are dominated with Ca-Mg-HCO_3 that are rich in calcium and/or magnesium and bicarbonate and is recently recharged groundwater (Figure 4.6). In the general groundwater chemical evolution model these types of waters are often regarded as recharge area waters which are at their early stage of geochemical evolution (Plummer *et al*., 1990; Adams *et al*., 2001; Edmunds and Smedley, 2000) cited in Seifu, 2005. However, some water samples for example, BR-BH21 (Gololcha) and BR-BH11

(Olla-Bersa/Yabello) are grouped in to Ca-Mg-SO_4-Cl/Mg-Ca-Cl-SO_4 water types. Both were sampled from weathered gneiss overlain by sediments of silts and sands where no or shallow circulating groundwater occur. In alluvial aquifers higher dissolved ions can be an indicator of areas of lower permeability, reflecting longer residence times of groundwater and the associated increased weathering reactions of the aquifer materials (Garcia *et al*., 2001; Acworth and Jankowski 1993; cited in Andrew, 2005). Hence, such hydrochemical facies may be acquired owing to slow flows in sediment or intensive evaporation before percolation.

Most of the groundwater from Rift zone and lowland plain sector of the area is grouped under Na-HCO_3 and Na-Cl/SO_4 water types (Figure 4.6A). This shows groundwater evolution along its path from highland to the discharging point. Furthermore, water sample from the western volcanic middle plains are characterized by Na-HCO_3 water types that shows deep groundwater circulation as located at very short distances to the recharging escarpments (Figure 4.6B).

The water types rich in bicarbonate with increasing sodium and potassium concentrations is in the process of moving while waters that is generally rich in Ca, Mg, Na, Cl and SO_4 can be classified as stagnant and is actively being mixed (Adam, 2001). Most of the water clustered in subgroup 2 (section 4.4.4) has shown Na-Ca-HCO_3/Na-HCO_3 and thus is in the process of moving. Waters sampled from open dug wells and springs of Goray, Dillo and Megado craters are classified to Na-Cl/Na-SO_4 water types (Figure 4.6A/C). This could be resulted either from the end stage geochemical evolution, stagnant or slow circulating groundwater that undergone a pronounced water rock interaction or from extensive evaporation from the pool. Groundwater with high sodium, chloride and/or sulphate values is stagnant and relatively old (Adam, 2001). Generally Ca-Mg-HCO_3 type waters occur in areas of recharge (generally topographically higher areas) and Na-Cl/Na-SO_4 type waters in discharging rift (i.e. the lower lying areas). The intermediate water types are a result of hydrogeochemical processes that occur between the two end members of Ca-Mg-HCO_3 and Na-Cl/Na-SO_4 and thus are mixed in type.

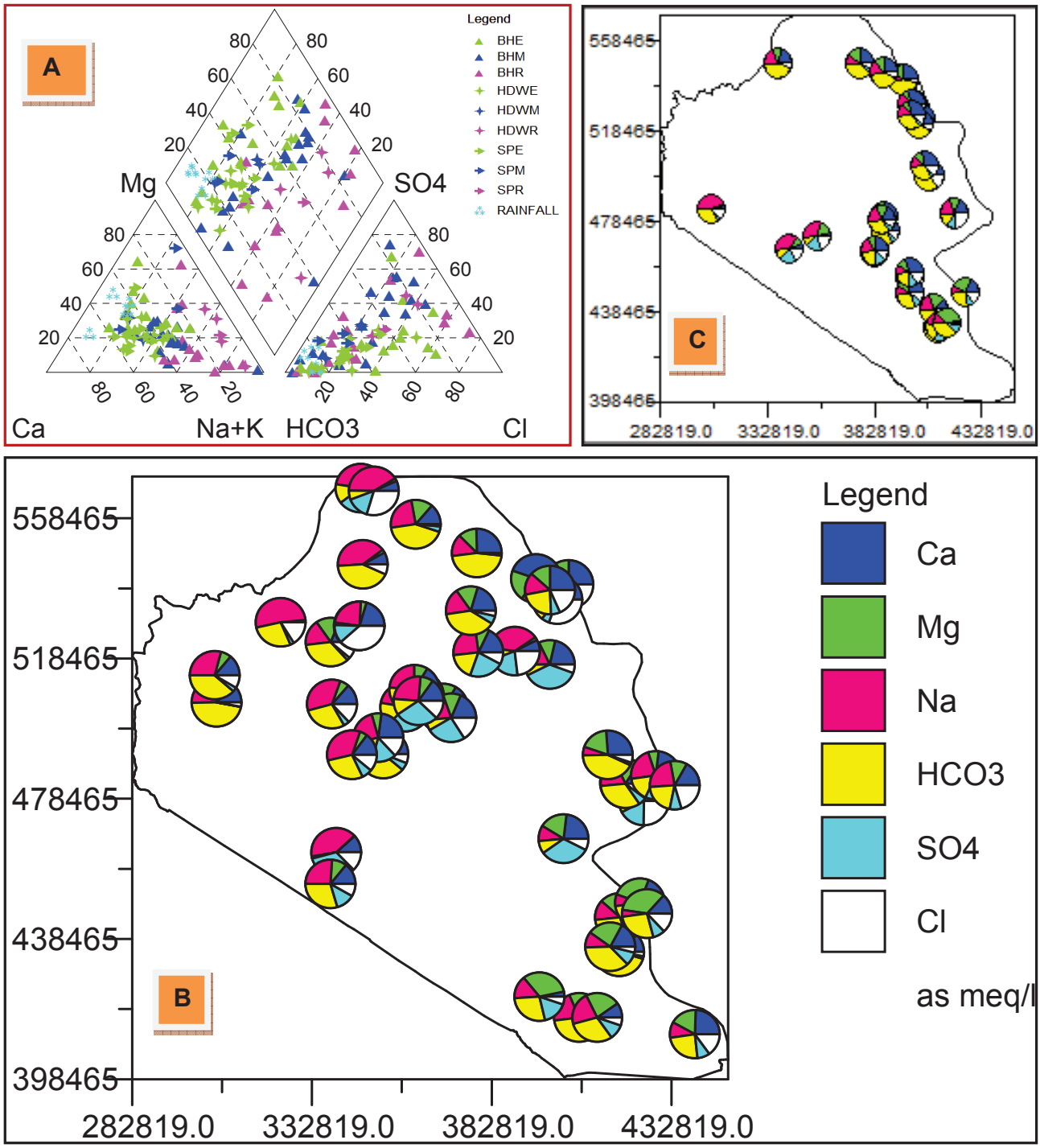

Figure 4-6*: **A)** Piper plot of chemical data of groundwater in the study area, **B**) Boreholes and **C**) Hand-dug wells and springs water type spatial distribution map represented by pie chart.*[5]

[5] *From the three major cations Na^{+} is dominated in NW and along the axial of rift, Ca^{++} is dominated in NE, E and central plains at Gelchet and Mg^{++} is Dominated in the SE extreme of the area.*

4.4.2. Composition Diagrams

Plotting of each major cation and anion versus total dissolved ions (TDI) can give insight understanding on major composition sources in groundwater concentrations. Figure 4.7 show that most of the Ca, HCO_3, and Mg concentration moderately correlates with TDI. In relative to Ca and Mg, the HCO_3 ions are randomly distributed almost nearly at one cluster than linearly increasing with TDI. This might be owing to laboratory measurement error as HCO_3 precipitates during sample transportation from field to laboratory. Water in Sarite (BR-BHR30), Megado (BR-HDW19), and Megado (BR-SPR13) and Maheir (BR-BHR35) shows a cluster for Ca, Mg and HCO_3 at higher TDI.

According to mazor, 2004, when either cations or anions plotted against TDI gives one cluster it may indicate all sources in a cluster are fed by one type of water, or in hydrological terms, by the same aquifer. Hence, the water clusters indicated in green ellipse in Figure 4.7 can be interpreted as water having the same source of water that fed by similar aquifer property or by the same aquifer. This was confirmed by similar trends and clusters of the three Ca, Mg and HCO_3 plots against TDI for Megado HDW and springs and Mahier wells. The more parameters that are checked, the higher is the confidence of the conclusion. Therefore, the clusters illustrate most likely interconnected/similar aquifer. Furthermore, except for the case of Sarite, the high concentration of Ca, Mg and HCO_3 here is by crystalline rock hydrolysis rather than sediment dissolution or leaching.

The plots of Na, SO_4, and Cl ions against TDI revealing a strong positive correlation with R^2 equal to 0.882, 0.834 and 0.724 respectively. Thus, these are vastly contributing for the concentrations of total dissolved ions in the area. These can also reveal the groundwater flow trends as these ions gradually evolve along the flow path with high water-rock interactions.

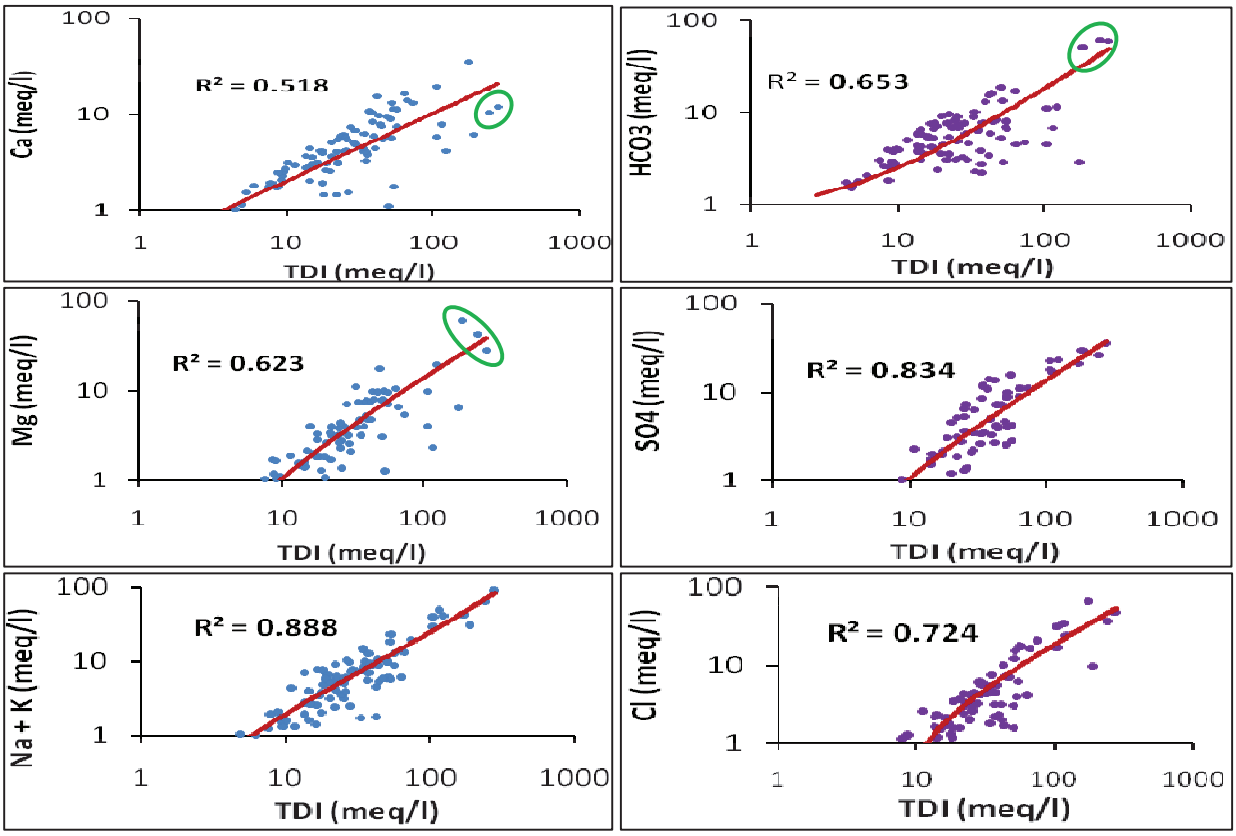

Figure 4-7: *Composition diagram of chemical data; TDI vs.Ca, Mg, Na, HCO3, SO4 &Cl ions respectively*

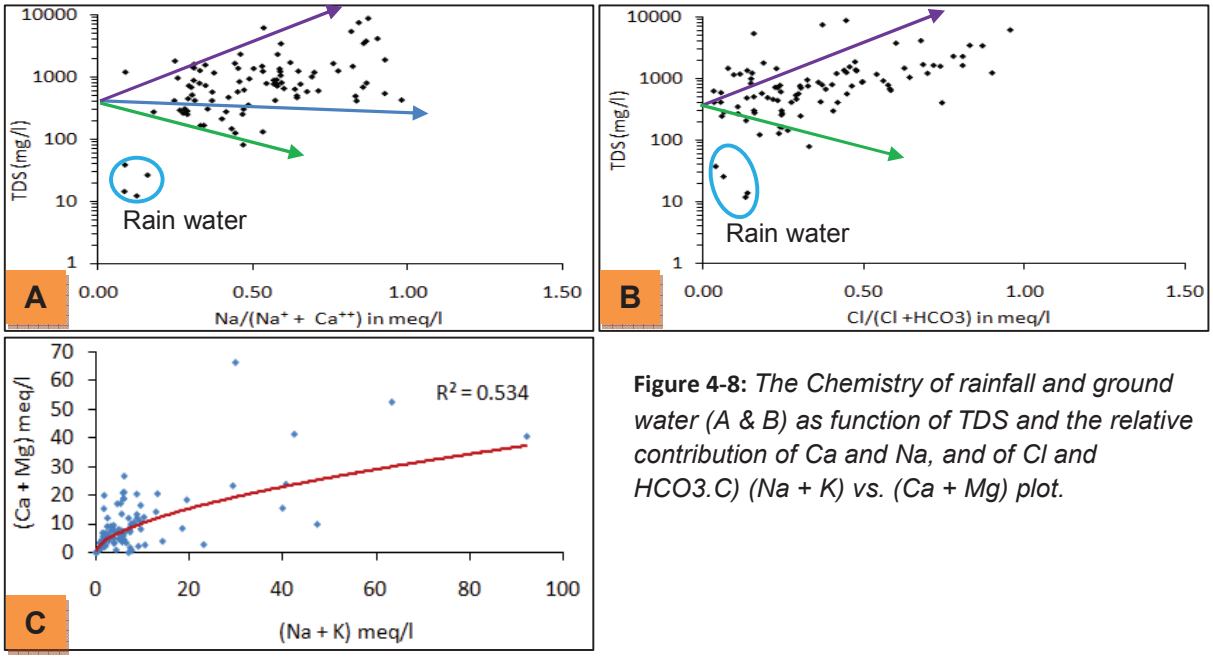

Figure 4-8: *The Chemistry of rainfall and ground water (A & B) as function of TDS and the relative contribution of Ca and Na, and of Cl and HCO3.C) (Na + K) vs. (Ca + Mg) plot.*

Plotting TDS as function of the dominance of Na^+ or Ca^{2+} and of Cl^- or HCO_3^- can help to understand the process in groundwater quality (Appelo and Postma, 2005). Figure 4.8 illustrates the source of mineralization from the relations of Ca, Mg, Na, K cations and HCO_3, SO_4 and Cl anions. From Figure 4.8A and B one can easily distinguish that at low TDS the dominant ions are Na and Cl (green arrows), most probably contributed by rainwater without much geochemical reactions or at very early stage of water-rock interactions. Most of the water samples from shallow wells, springs and hand-dug wells in and near the escarpments have this character.

Contact with rapidly dissolving calcite and Ca-silicates increases the relative content of Ca^{2+} and HCO_3^-. If subsequent evaporation concentrates the solution, Ca^{2+} and HCO_3^- are lost by precipitation of $CaCO_3$ (Appelo and Postma, 2005). As Ca^{2+} and HCO_3^- precipitates with increasing TDS along groundwater flow path, the water composition in turn becomes dominated with Na^+ and Cl^- content and moves upwards as in figure 4.8A & B (the purple arrow). Figure 4.8A also shows an increase of Na/ (Na + Ca) at constant horizontal TDS of about 500mg/l (middle blue arrow) that might point out mixing of fresh and saline water along flow path or constant supply of Ca from the calcerite sediments. This also indicates weathering effect of host rocks with water in contact. Mixing of waters can lead to sub-saturation with respect to calcite, even if the original waters were at saturation before mixing (Appelo and Postma, 2005).

Figure 4.8C indicates nearly a positive correlation among the exchangeable cations of Ca, Mg, Na and K. First the relations highly rose with power regression type and gradually becomes constantly increasing, $R^2 = 0.534$. Hence in the study area the role of cations exchange as a source of mineralization has postulated to be insignificant. This has also been supported by correlation matrices result (section 4.4.5).

4.4.3. Groundwater Equilibrium Conditions

Groundwater chemistry exchanges matter with the various minerals and gases within the aquifer. It can be taken in the form of the dissolution or precipitation of minerals. Equilibrium calculations are most commonly used to assess whether the groundwater is in equilibrium with respect to one or more minerals. The saturation state of minerals in the water can be expressed by saturation index (SI). The SI index of zero indicates that a mineral is in thermodynamic equilibrium with the solution. If the SI is less than zero, the solution is undersaturated with respect to the mineral and that mineral may dissolve. Conversely, SI greater than zero indicates the solution is oversaturated with respect to the mineral and that the mineral may precipitate. These considerations are useful in determining the kinds of reactions that are possible in groundwater systems.

SI of aragonite, anhydrite, calcite, dolomite, fluorite, gypsum and halite were calculated for the groundwater in the study area (Annex 6). About 71.3% of calcite has positive indices which are slightly over saturated where as the rest of the samples are negatively under saturated with calcite, particularly for those samples categorized in subgroup 1 (Figure 4.9A &C). For anhydrite and halite, all indices are negative, which indicates under saturation. TDS vs. SI_{halite} plot shows an increase of saturation of halite from recharge to discharge area but all are undersaturated (Figure 4.9D). The Ionic strength of chemical data strongly correlated with TDS (Figure 4.9B). Fresh water has low Ionic strength and thus, the plot of Ionic strength vs. TDS indicating groundwater flow directions.

The percentages of SI calculated for each of the above mineral are shown in Table 4.4. Most of the water samples show deposition with respect to aragonite, calcite and dolomite suggesting that these mineral phases are extensively present in the corresponding host rock. The rest minerals are under saturated and thus dissolving with groundwater flows.

Table 4-4*: percentage (%) of SI for some minerals in the area under target*

SI	Anhydrite ($CaSO_4$)	Aragonite($CaCO_3$)	Calcite ($CaCO_3$)	Dolomite ($CaMg(CO_3)_2$)	Fluorite (CaF_2)	Gypsum ($CaSO_4$:$2H_2O$)	Halite (NaCl)
SI < 0	100	34	27.7	31.9	97.9	97.9	100
SI > 0	0	66	71.3	68.1	2.1	2.1	0
SI = 0	0	0	1	0	0	0	0

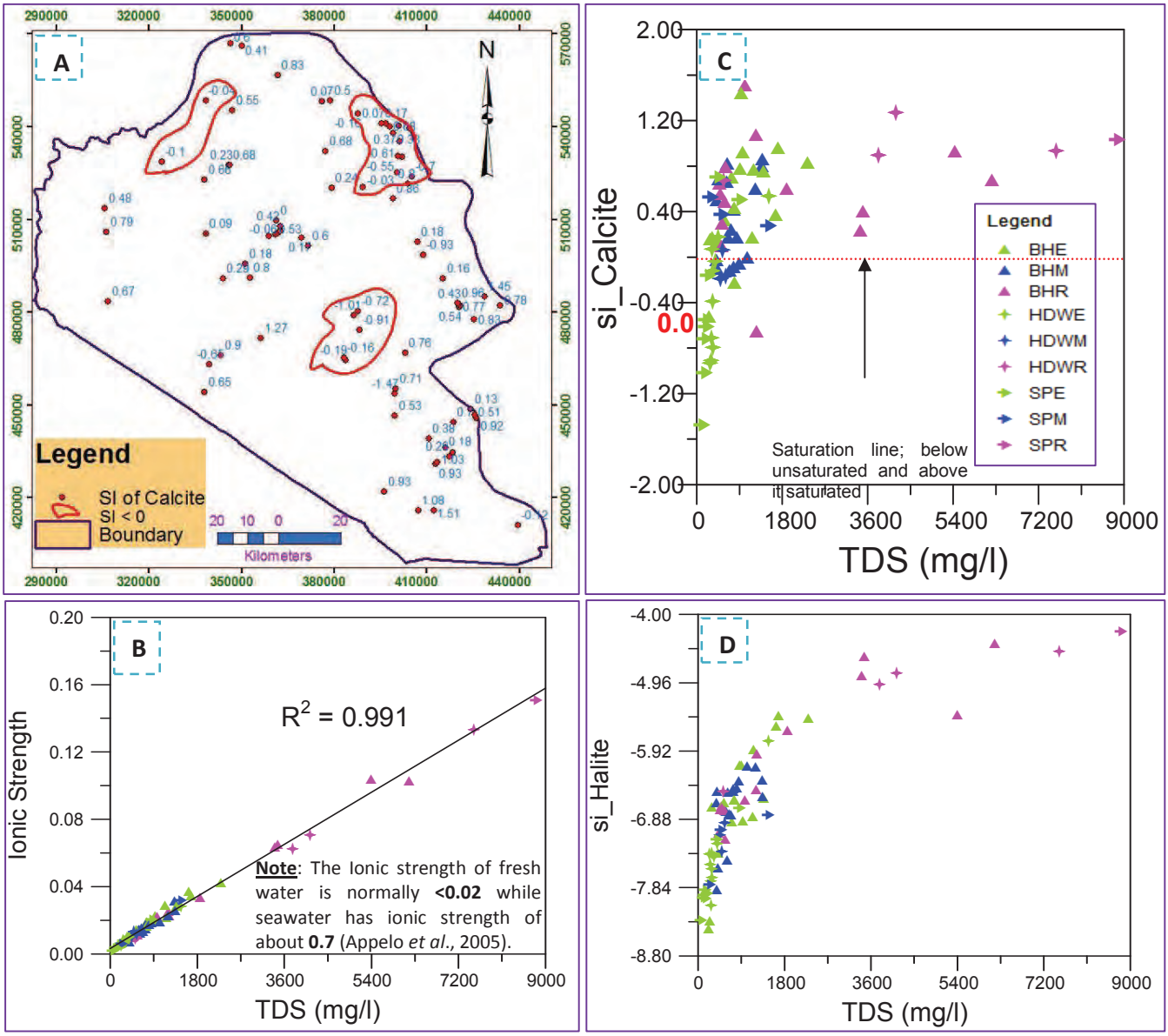

Figure 4-9: A) *Spatial distribution of SI_{Calc},* ***B)*** *TDS vs. Ionic strength,* ***C)*** *TDS vs SI_{Calc} and* ***D)*** *TDS vs. SI_{halite}*

4.4.4. Hierarchical Cluster Analysis (HCA)

The use of graphical techniques proved to have limitations compared with the multivariate methods for large data sets (Cüneyt *et al*., 2002). The most efficient grouping was achieved by statistical clustering techniques. Clustering is the assignment of a set of observations into subsets (called cluster*s*) so that observations in the same cluster are similar in some sense (Andarge, 2009). However, these techniques do not provide information on the chemistry of the statistical groups and thus the combination of graphical and statistical techniques provides a consistent and objective means to classify large numbers of samples while retaining the ease of classic graphical presentations. Before using the raw data for HCA, the data were log-transformed (except for pH) so that they more closely corresponded to normally distributed data. Then, the selected variables were standardized by calculating their standard scores (*z*-scores) as the following equation.

$$Zi = \frac{Xi - \overline{x}}{S}$$

Where zi is standard score of the sample i; xi is value of sample i; $\overline{x}$ is mean; S = standard deviation

Standardization scales the log-transformed data to a range of approximately –3 to +3 standard deviations, centered about a mean of zero. In this way, each variable has equal weight in the statistical analyses. Otherwise, the Euclidean distances will be influenced most strongly by the variable that has the greatest magnitude (Judd 1980; Berry 1995). The raw data were used for the graphical analyses, whereas the transformed (log-transformed and standardized) data were used for the hierarchical cluster analysis (HCA). Comparisons based on multiple parameters from different samples are made and the samples grouped according to their "similarity" to each other. The classification of samples according to their parameters is termed Q-mode classification. The linkage rule used here is Ward's method (Ward 1963). Linkage rules iteratively link nearby points (samples) by using the similarity matrix.

In this investigation, eleven parameters (pH, TDS, Na, K, Ca, Mg, Cl, HCO_3, SO_4, NO_3 and F) were used in HCA. 94 samples having complete analysis of these 11 parameters were used and the result was presented as a dendogram (Figure 4.11). From the dendogram, three major groups were selected based on their TDS value and ten

subgroups were selected based on visual examination. However, as this evaluation is subjective, more or less subgroups could be defined by moving the dashed horizontal red line (phenon line) up or down.

Mean chemical compositions for samples grouped under each subgroups was presented in Table 4.5. Depending on average chemical composition of each subgroups and correlations among the groups; interpretation of geological, hydrogeological, groundwater recharge sources and mechanisms, water-rock interaction and relations with topographic location in the sub basin were presented in Table 4.6.

Table 4-5: *Mean hydrochemical composition of sub-groups, (*(meq/l)) and all others except pH in mg/l).*

Subgroup	pH	TDS	Na	K	Mg	Ca	Cl	SO_4	HCO_3	NO_3	F^-	RA*	$\frac{Ca^*}{Mg}$	$\frac{Ca^*}{SO_4}$
1 (n=16)	7.16	224.75	23.6	7.4	10.8	37.9	23.5	14.5	162.4	2.03	0.8	-0.1	2.1	6.3
2 (n=26)	7.68	501.38	90.2	7.3	21.2	56.9	60.4	50.2	319.2	5.91	1.3	0.6	1.6	2.7
3 (n=20)	7.64	830.45	125.8	16.4	40	89.9	117	186	335.12	15.8	1.2	-2.3	1.3	1.2
4 (n=7)	7.06	1388.57	126.4	26.1	119.1	185.8	93.9	237.7	979.37	5.1	0.6	-3.2	0.9	1.9
5 (n=15)	7.67	1454.93	219.1	23.4	65.1	146.7	291.9	387.3	321.04	7.9	2.1	-7.5	1.4	0.9
6 (n=2)	7.84	2318.5	348	46	73.4	273.4	643.2	534	282.55	21.9	1.3	-15.2	2.2	1.2
7 (n=4)	7.6	3720.5	875	49.3	109.8	186.7	934.9	960.2	517.37	6.1	2.2	-10	1	0.5
8 (n=1)	7.2	5429	640	80	734.4	123.5	341.8	1428.3	3132.96	0.6	0.6	-16	0.1	0.2
9 (n=1)	7.35	6210	930	79	77.8	704	2330	1002.7	175.68	0.5	1.8	*-38.8*	5.4	1.7
10 (n=2)	7.14	8181	1590	337.5	432.5	224	1490.5	1480.8	3678.3	0.9	1.1	13.1	0.3	0.4

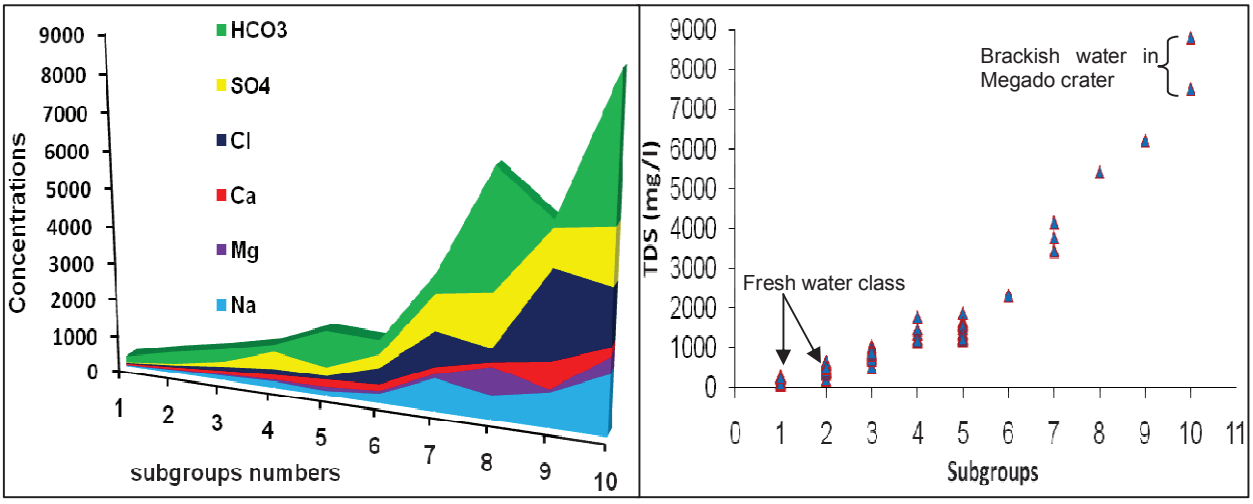

Figure 4-10: *Subgroups vs. Na, Mg, Ca, Cl, SO_4, & HCO_3 concentrations in mg/l* ***(Left)*** *and Subgroups vs. TDS plot* ***(Right)*** *of all chemical data in the research area.*

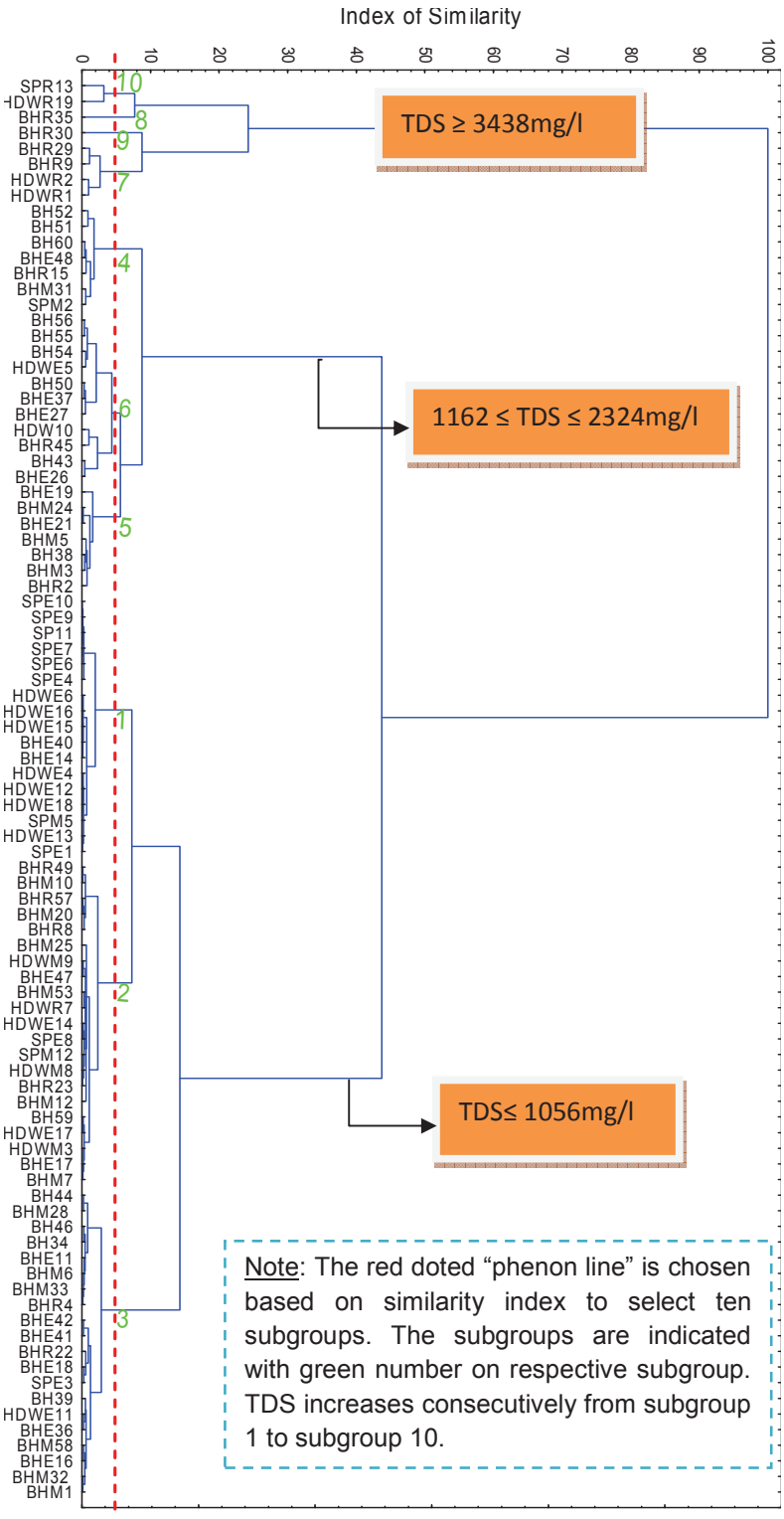

Figure 4-11: *Dendrogram of the hydrochemical data*

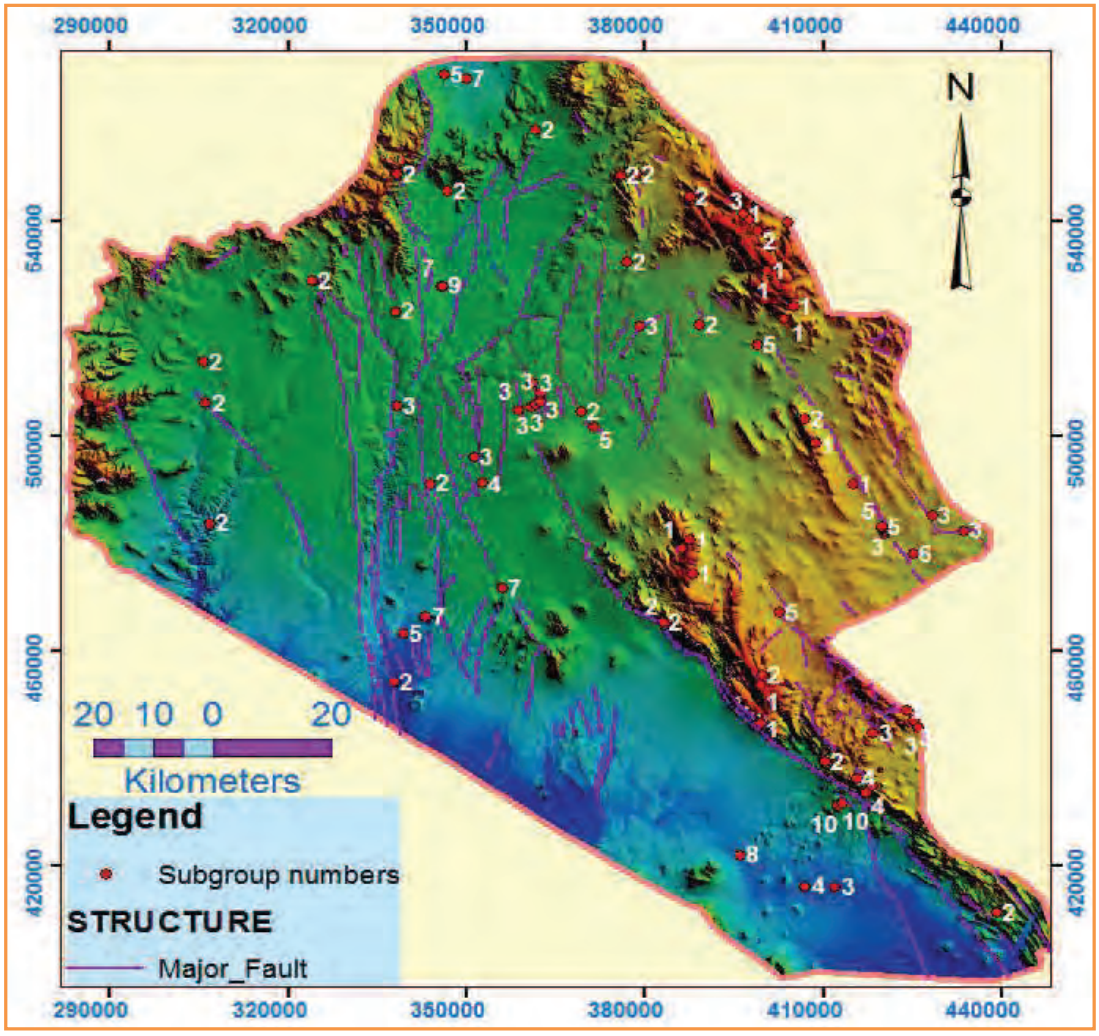

Figure 4-12: *Spatial distribution Map of subgroups*

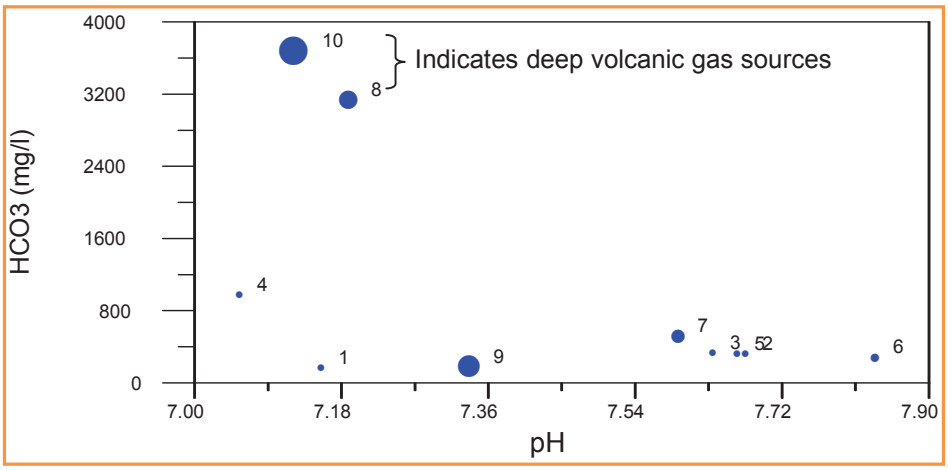

Figure 4-13: *PH vs.HCO_3 Plot of mean subgroups; size varies with TDS. Numbers stands for subgroups.*

Table 4-6*: Descriptions of each subgroup clustered by HCA.*

SG	Descriptions
1	This subgroup entirely falls in higher topographic plains in northeastern part of the area near Yabello, Dubuluk and Gololcha area. They are known for their diluted water chemistry with 224.8mg/l mean concentration of TDS. Most of the samples were from hand dug wells and springs discharging from weathered granite and gniesses. Almost all chemical data from these groups have Ca-Mg-HCO_3 and Ca-Na-HCO_3 water types. Their typical association with the shallow systems and the water facies signifies their direct contact with the recent recharge and/or early stage of chemical evolution. They are, therefore, indicators of the recharge area for the groundwater system in the flow path.
2	They include chemical data that fall dominantly in middle and higher plain sector over all the area in contouring manner. These falls also in the rift sector of south extreme. This might be due to fast flow of groundwater in nearly North-South aligned fault. Mostly falls in volcanic rocks. These have moderately diluted water with mean TDS of 501.38mg/l. Relative to subgroup 1, each parameter increased in concentration. This signifies that water-rock interaction is on verge for chemical hydrolysis that adds chemical concentration to water. This group, therefore, represents early stage of chemical evolution next to subgroup 1. The dominant water type is Ca-Na-HCO_3 and Na-HCO_3 and so the water is moving and represents intermediate rock-water interactions and groundwater residence time. As this cluster falls dominantly in recharge area, such facies could indicate groundwater evolution along vertical deep circulation. It could also be associated with less permeability of the aquifer, as most of the basalt in which this subgroup falls is tertiary middle (Teltele) and upper basalt.
3	These groups are dominantly clustered in Gelchet newly drilled well field. They are similar to group 2, but relatively higher in TDS (830.45mg/l), Ca, Cl and SO_4 that indicates rather there is more water-rock interaction and chemical hydrolysis. Relative to subgroup 1, the samples were collected from deep wells in basalt rock having average depth of greater than 150m. However, those falls near Yabello and Dubuluk obtained from shallow wells sunk in to sediment and weathered basement rocks. Fast selective recharge/regional recharge mechanisms is speculated near Gelchet from isotope Oxygen-18 analysis and hence, the higher Ca in this subgroup is mostly from local flushing of recharge rather than from calcium bearing rocks and calcite sediments.
4	These group falls dominantly in middle sector in SE of the area. The groups have the lowest brackish water class that is 1388.57mg/l and have similar chemical properties with subgroup 3, but have low pH and high HCO_3. The lower pH value and very high HCO_3 indicate there is volcanic gas source from deeper (Figure 4.13). Na-Ca-Mg-HCO_3 and Na-Ca-Mg-SO_4-Cl water type is dominated. They were clustered near Megado in fractured quaternary volcanic. The high concentration of parameters is from prior evaporation and groundwater flow evolution.
5	Similar to subgroup 4 but relatively lower in Mg, Ca and HCO_3. The groups fall near Goray, Gololcha, Dubuluk, Yabello and Brindar. Except Goray (basalt) all are obtained from sediment and weathered parts of basement rocks. Na-Ca-SO_4-Cl water type is dominating. In contrast to the other subgroups this is spatially randomly distributed.
6	These groups consists of two samples from east of the area near Dubuluk. Mean TDS is 2318.50mg/l more brackish than the former groups. Similar to group 5 obtained from thick residual deposit and weathered basement. Ca-Na-Cl-SO_4/Na-Ca-Cl-SO_4 water type is characterizing the group. The wells are shallow but brackish water class is due to intensive evaporation prior to infiltration as the residual sediment is less permeable.
7	These groups fall along the Rift sector in Brindar, Sarite, Goray and Dillo localities. The mean TDS concentration is 3720.5mg/l. The Brackish water from BR-BH29 (Sarite) and BR-BH9 (Brindar) wells is due to salt dissolution from sediment, while that of Dillo and Goray

	open hand dug wells might shows either intensive evaporation or end stage of chemical evolution. This was testified by Cl vs. $\delta^{18}O$ plot. Brindar well has depleted $\delta^{18}O$ where as the dug wells have enriched $\delta^{18}O$.
8	Consist single well and located in Rift sector at Maheir/Furole (BR-BH35). It is extremely saline water with TDS of 5429mg/l. Situated on Fluviall deposit overlaying volcanic rocks. It has low pH value and High HCO_3 indicating volcanic gas source from deep volcanic (Figure 4.13). Furthermore its Ca/Mg and Ca/SO_4 ratio is lowest compared to other subgroups and has Low negative RA due to high Mg concentration. These characteristics of the water suggest that the water has its origin from end stage hydrolysis reaction in volcanic terrain containing Olivine and pyroxene minerals. Inverse modeling result (section 4.4.7, path-V) confirmed this idea. This water could represent groundwater that has undergone significant rock water interaction in a regional groundwater flow path. The water is Mg-Na-HCO_3-SO_4 type.
9	Similar to subgroup 8 single borehole from Sarite (BR-BH30) was categorized in this subgroup. Located in Rift sector and extremely saline water with TDS of 6210mg/l. Situated on very thick fluvial deposit overlaying volcanic rocks. In contrary to subgroup 8, it has low Mg, HCO_3, and RA value and Very high Na, Ca, Cl and SO_4. Its water type is Na-Ca-Cl-SO_4. This is due to salt dissolution from the fluvial, mainly lacustrine deposits, rather than in consequence of evaporation. The isotopic composition taken from neighbor of the localities ascertains the prominent salt dissolution than evaporation.
10	Two samples from Megado Crater/Maars, one spring and one hand-dug well, were clustered in this subgroup. The highest brackish water (mean TDS of 8181mg/l) is observed in this subgroup. Similar to group 5 and 8 characterized by low pH and higher HCO_3 but low Calcium, (Figure 4.13). The water type is Na-Mg-HCO_3-Cl-SO_4. It shows a significant groundwater evolution as indicated by highest HCO_3 that originated from deeper source.

4.4.5. Correlation Matrices

Samples showing $r > 0.7$ are considered to be strongly correlated whereas $0.5 < r < 0.7$ shows moderate correlation at a significance level (p) of < 0.05. Strong correlations have seen between TDS and the major elements of Na, K, Mg, Cl, SO_4 and HCO_3; $r > 0.7$, (Table 4.7). These relationships clearly identify the main elements contributing to the groundwater salinity and their tendency to follow a similar trend (e.g. due to concentration by evaporation, dissolution/precipitation).

A strong correlation between SO_4 and Cl indicates that these ions tend to increase in concentration as the salinity of the water increases. Moderate correlation between Ca and SO_4 indicates that these ions tend to originate from the same sources. The increase in SO_4 is due to dissolution of salts from thick sediments which are common all over the flat lands, particularly at Utalo, Harewayu, Gelchet, and Goray. In semiarid and arid regions the soils are generally not fully leached, and surplus solutes may accumulate near the surface. The amount of drainage water that leaves such an area is a small fraction of the total received in precipitation. Because of these factors, the supply of solutes is large in proportion to the water volume in which it can be carried away. As a result, surface and underground waters in semiarid regions tend to be comparatively high in dissolved solids. Sulfate is a predominant anion in many places (Hem, 1980). Hence, the high concentration SO_4 observed in Borena lowlands where carbonate/ gypsifrous rocks absent is vindicated by this fact and may be attributed to little rain, high temperature and strong evaporation. The source of the SO_4 in the aquifers with low SO_4 (≤ 5.5 mg/L) could be the rainfall. One month rainfall mean chemistry data shows the SO_4 content in the area is in the order of 0.2 - 5.5mg/l.

The low correlation between Ca and HCO_3 signifies the source of Ca from Crystalline rocks is less significant in the study area. Therefore, the source of Ca in the study area is mostly from calcerite dissolution rather than the minerals of crystalline volcanic rocks. Figure 4.6B clearly shows this fact that in volcanic rocks very high HCO_3 but relatively low Ca concentration is visible.

Strong correlation between Ca & Cl may signify addition of Ca concentration from Ca bearing sediments along groundwater flow paths. As higher content of Cl indicates intensive evaporation in areas where halite or other source of chloride like weathering

of geological material is lacking, the positive correlation of Ca and Cl could also show dominantly sourced from thick sediment due to intensive evaporation.

In general, in these overall large and variable data sets the dominance of strong positive correlations was observed so that little cation exchange dependencies could be expected in the study area. It can therefore, be assumed that the simultaneous increase/decrease in the cations is the result mainly of dissolution/precipitation reactions and concentration effects, while the effects of cation exchange processes are masked in the overall data set. From Figure 4.14A it can be noticed that, positive correlation is seen between Na and Ca ions although does not show strong positive correlation and, therefore, this testifies the above assumptions as ion exchanges has little or no paramount effect in groundwater mineralization. However, the more increases of Ca in escarpments and middle plain sector and the more increase of Na in rift sector than in respective to one the other might show groundwater evolution rather than cation exchanges. To a lesser extent negative correlation was seen between Ca and pH (Figure 4.14B). This indicates concentrations of Ca decreases to a lesser extent with increase of pH along groundwater evolution. In general, from the correlation matrix it can be recognized that HCO_3 has weak correlation with Ca where as strong positive correlations obtained between Ca cation and Cl, SO_4, and TDS. Hence, the source of Ca is dominantly from sediment leaching containing calcite and gypsum rather than crystalline hydrolysis. SI of calcite in most volcanic rocks shows slightly saturated in calcite and hence deposited instead of adding minerals to water (section 4.4.3). This supports the above idea.

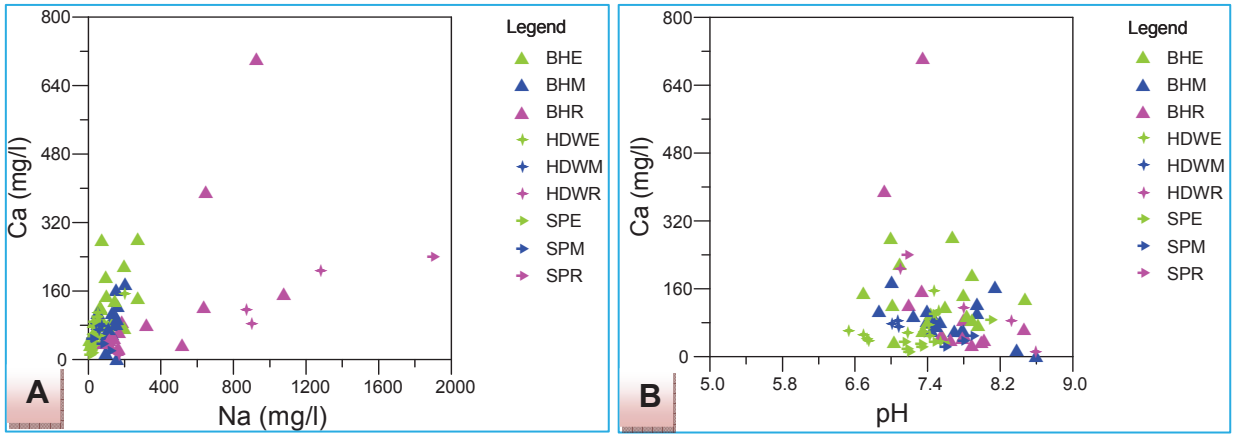

Figure 4-14: ***A)*** *Na vs. Ca scatter plot and* ***B)*** *PH vs. Ca scatter plot of chemical data set.*

Table 4-7: *Correlation matrices of elements in Borena groundwater; all values are in mg/l unless otherwise indicated. All bolded correlations are significant level at p < .05; N=94.*

	pH	TDS	Na+	K+	Mg++	Ca++	Cl-	SO4-	HCO3	No3-	F-
pH	1.00										
TDS	-0.05	1.00									
Na+	0.04	**0.94**	1.00								
K+	-0.07	**0.86**	**0.83**	1.00							
Mg++	-0.11	**0.75**	**0.59**	**0.67**	1.00						
Ca++	**-0.23**	**0.61**	**0.45**	**0.34**	**0.28**	1.00					
Cl-	-0.04	**0.88**	**0.86**	**0.67**	**0.43**	**0.74**	1.00				
SO4-	0.03	**0.92**	**0.88**	**0.72**	**0.70**	**0.54**	**0.75**	1.00			
HCO3	-0.17	**0.77**	**0.67**	**0.84**	**0.89**	**0.23**	**0.43**	**0.64**	1.00		
No3-	0.14	-0.06	-0.06	-0.04	-0.08	0.02	-0.03	-0.06	-0.11	1.00	
F-	0.12	0.11	0.20	-0.01	-0.08	0.02	0.11	**0.25**	-0.10	0.02	1.00

4.4.6. Geomorphologic Setup and Groundwater Chemical Compositions

In most cases the rate and direction of surface water and groundwater flow varies with topography as well as with the differences in geology and hydrogeology (i.e. differences in hydraulic conductivities). All other factors being constant the steeper the topography assists the fastest runoff where as the gentle and flat topography facilitates more infiltration. The local topography, rate of evaporation and vertical permeability typically determine the location and rate at which salts accumulate. Most of the low-lying areas are flat and overlain by young sediments in which the extent of flushing with groundwater is low and hence more salt accumulated in flat areas. Cl and TDS increase with decreasing topography from higher escarpment to the lower rift and flat areas (Figure 4.15A). This shows that in lower and flat topography the possibility of ponding water is high and thus evaporated water percolates to groundwater than hills and sloping topography where high runoff is more prominent. TDS versus altitude further demonstrates the highest brackish water class is observed at lowest altitude at Megado, Dillo and Sarite localities where as the freshest water class from Gololcha/Choresa spring is at the highest altitude (Figure 4.15B). Some sampling points located on lower lying areas also show properties representing higher lying areas and vice versa, indicating that topography alone does not determine the

salinity of the groundwater. Factors other than evaporation, thus, also affect groundwater salinity and chemical composition. Rapid recharge through preferential pathways in lower lying areas where fractures are exposed to the surface could be a possibility (Adam, 2001). The salinization of groundwater would also be expected to result from the ionic concentrations increasing due to both evaporation of recharged water and to the effects of interactions between the groundwater and the geological formations.

Except Ca and Cl the rest dominant ions increase from escarpments to lower topography where gentle and flat land predominated (Table 4.8). This is generally attributed to salinizations of groundwater. The high Cl concentration in upper topography ascribes intensive evaporation from sand deposits at bottom foot of mountain escarpments, for instance, Yabelo alluvial fan.

Table 4-8*: Mean value of dominant variables in escarpments, middle and rift sectors*

Topographic division	TDS	Na	Mg	Ca	Cl	SO_4	HCO3
Escarpment	654	75.44	40.38	91.93	125.39	95.18	293.18
Middle Sector	722.95	111.57	42.68	82.19	83.01	146.46	352.98
Rift sector	2886.22	578.28	137.21	149.5	578.11	621.22	937.5

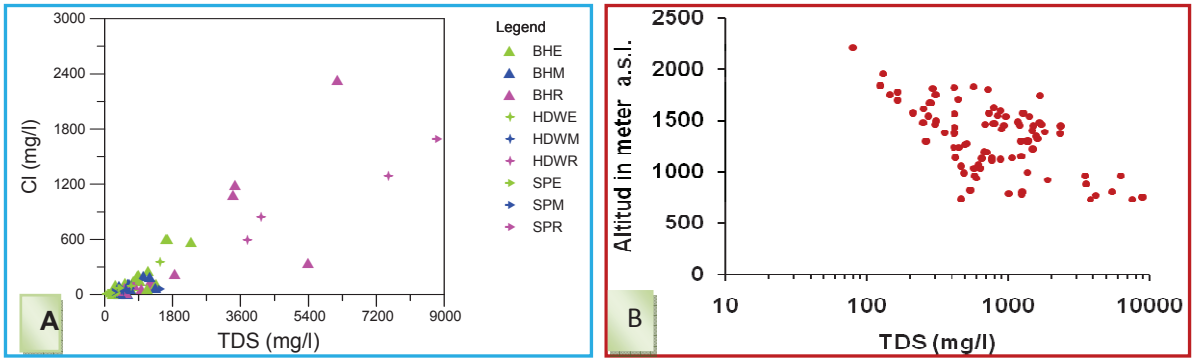

Figure 4-15: ***A****) TDS vs. Cl and* ***B****) TDS vs. Altitude scatter plot of the chemical data set*

4.4.7. Inverse Geochemical Modeling (IGM)

Inverse modeling is often used for interpreting geochemical processes that account for the hydrochemical evolution of groundwater (Plummer *et al*., 1983, 1992, 1994). This mass balance approach uses two water analyses represent initial and final water compositions along a flow path to calculate the moles of minerals and gases that must enter or leave solution to account for the differences in composition (Parkhurst *et al*.,

1980). Hence, using inverse geochemical modeling amount of mole transfers either through dissolution or precipitation of phases that account for changes in water chemistry between initial and final water composition along the groundwater flow path has determined in this work. The initial and final water points were selected based on general information of geological and topographical setting up, groundwater flow direction deduced from previous works, geochemical evolution trends, HCA cluster groups and environmental isotope results. For this modeling the PHREEQC Interactive version 2.8 computer codes was used. The inverse modeling in PHREEQC takes into account uncertainty limits that are constrained to satisfy the mole balance for each element and valance state, as well as the charge balance for each solution within the simulation.

For the modeling, mineral phase selection was done based on the mineral composition of the rocks in the sub basins obtained from geological information and thin section analysis made in BGPA report (OWWDSE, 2006) and saturation indices. As Bulal basalt is the most dominating aquifer from the volcanic formations in the area, rock samples analyzed from this unit at the localities of Goray, Hobok, Utalo, Mahier and Toroba were taken as representative minerals. The thin section studies result in these localities shows that the unit is composed of 44-49% plagioclase, 30-38% pyroxene, 10-13% opaque, up to 10% olivine, 3% calcite and 5% volcanic glass, with minor sanidine, spinel and secondary calcite.

In general silicate minerals dominate the mineralogy of the crystalline basement and volcanic terrains like in this research area. Hence, plagioclase, k-feldspar, olivine, pyroxene, amphiboles are primary silicate and minerals like kaolinite, montimorilonite, illite (k-mica) are among the secondary silicate minerals which are results of incongruent dissolution. Calcite is also dominantly occurring in thick alluvial and elluvial deposits overlying the most crystalline basement and volcanic terrains in the area. Furthermore, gypsum and halite occur in clay, sand or paleosoles due to the pre-burial evaporative process (Tilahun, 2008). In this work water from the subgroups resulted from HCA was used as initial and final water point. Starting point of pristine water was selected from subgroup 1 and 2 because the water in these subgroups is diluted in TDS. Water from subgroups 3, 4, 5, 6 and 7 were used as final water points. At both initial and final water points, chemical compositions of single representative

water source were used. The chemical data used is shown in Table 4. 9. Accordingly five main flow paths are selected for the modeling (Figure 4.16). The results in all flow paths were obtained at uncertainty limit of 0.05 (5%). Table in each respective flow path shows the amount in moles of minerals or gases transfer in dissolving, precipitating, and weathering or in cation exchanging processes. Results and brief discussions of the model output are outlined below.

Table 4-9: *Chemical data of water used in Inverse geochemical modeling*

Paths		group	Locality Name	Sample Code	X	Y	Z	PH	TDS	Na+	K+	Mg++	Ca++	Cl-	SO4-	HCO3	F-	Water type
Path-I	Start	1	Harewayu	BR-HDWE16	403655	521689	1495	6.53	306	27.5	13	8.64	61.6	26.46	5.61	241.3	0.36	Ca-Na-HCO3
	Final	3	Gelchet	BR-BHM1	360826	505258	1118	7.95	860	150	12.5	7.82	104.9	103.6	346.8	180.6	1.72	Na-Ca-SO4
Path-II	Start	3	Gelchet	BR-BHM1	360826	505258	1118	7.95	860	150	12.5	7.82	104.9	103.6	346.8	180.6	1.72	Na-Ca-SO4
	Final	5	Goray	BR-BHR2	339581	463165	811	7.5	1250	325	5.7	1.08	81.44	155.5	550	29.3	7.8	Na-Ca-SO4-Cl
Path-III	Start	1	Gobso/Bule Dhela	BR-SPE6	387650	480489	1750	7.34	146	20	1.7	6.48	22.93	20.16	10.81	96.6	1.16	Ca-Na-HCO3
	Final	5	Gobso	BR-BHM3	371540	501553	1150	7.95	1230	164	14.4	47.5	125.2	190.09	410	140.3	1.58	Na-Ca-Mg-SO4-Cl
Path-IV	Start	2	Elwaya	BR-BHM12	378708	548522	1379	7.4	415	56	5.3	24.3	83.79	9.6	0.534	468.48	0.07	Ca--Mg-HCO3
	Final	7	Sarite	BR-BHR29	345844	527739	966	6.93	3438	650	41	48.6	392	1088	860.6	276.7	2	Na-Ca-Cl-SO4
Path-V	Start	2	Saakee/Megado	BR-SPM12	410499	439266	1269	7.8	496	78	15.5	40.5	37.8	47.3	93.45	322.7	1.31	Ca-Na-Mg-HCO3
	Final	8	Maheir/Furole	BR-BHR35	396126	421963	805	7.2	5429	640	80	734.4	123.5	341.8	1428.3	3132.96	0.55	Mg-Na-HCO3-SO4

Path-I: Inverse geochemical modeling was conducted between Harawayu (BR-HDW16) and Gelchet (BR-BH1); from subgroup 1 to subgroup 3. TDS in initial and final water is 306 and 860mg/l respectively.

Phases	Mole transfers	Composition
Calcite	-5.825e-003	CaCO3
Ca-Montmorillon	-5.340e-003	Ca0.165Al2.33Si3.67O10(OH)2
CO2(g)	2.456e-003	CO2
Halite	2.052e-003	NaCl
Fluorite	3.583e-005	CaF2
Gypsum	3.374e-003	CaSO4:2H2O
Albite	3.578e-003	NaAlSi3O8
Anorthite	4.432e-003	CaAl2Si2O8

The main hydrochemical processes occurring along the flow path here are dissolution of anorthite, albite, gypsum, halite, fluorite minerals and CO_2 gases. In the groundwater flow precipitation of Calcite mineral and clay forming or weathering of Ca-montmorilonnite are occurring. Hence, mainly dissolution and precipitations/weathering are the main hydrochemical processes contributing to the salinity of water in this path.

Path-II: In this flow path inverse modeling was conducted between Gelchet (BR-BH1) and Goray (BR-BH2); from subgroup 3 to subgroup 5. Initial and final water has TDS of 860 and 1250mg/l respectively.

Phases	Mole transfers	Composition
Albite	4.756e-003	NaAlSi3O8
Anhydrite	2.586e-003	CaSO4
Calcite	-3.911e-003	CaCO3
CO2(g)	9.174e-004	CO2
K-feldspar	1.443e-003	KAlSi3O8
Pyroxene	7.927e-004	Mg0.5Ca0.5SiO3
Fluorite	1.602e-004	CaF2
Illite	-2.695e-003	K0.6Mg0.25Al2.3Si3.5O10(OH)2
Halite	1.832e-003	NaCl
Chalcedony	-9.957e-003	SiO2

This inverse geochemical modeling demonstrates that the dissolution of albite, plagioclase, K-feldspars, pyroxenes, fluorite, halite, anhydrite and CO_2 are required to derive the observed natural groundwater chemistry in the area. This dissolution is balanced by the precipitation of Calcite and weathering of illite and chalcedony.

Path-III: In this flow path the modeling was conducted between Bule Dhera (BR-SP6) and Gobso (BR-BH3); from subgroup 1 to subgroup 5. The TDS in initial and final water is 146 and 1230mg/l respectively.

Phases	Mole transfers	Composition
Anhydrite	4.416e-003	CaSO4
Calcite	-4.075e-003	CaCO3
Fluorite	1.109e-005	CaF2
Halite	4.799e-003	NaCl
Plagioclase	1.777e-003	Na0.62Ca0.38Al1.38Si2.62O8
Pyroxene	3.379e-003	Mg0.5Ca0.5SiO3
CO2(g)	4.905e-003	CO2
K-feldspar	3.252e-004	KAlSi3O8
Ca-Montmorillon	-1.192e-003	Ca0.165Al2.33Si3.67O10(OH)2
Chalcedony	-4.635e-003	SiO2

This inverse geochemical modeling demonstrates that the dissolution of pyroxenes, plagioclase, K-feldspars, anhydrite, halite and CO_2 are required to derive the observed natural groundwater chemistry in the area. This dissolution is balanced by the precipitation of Ca-montmorilonite, chalcedony and calcite.

Path-IV: In this flow path water the modeling was conducted between Elwaya (BR-BH12 and Sarite (BR-BH29), from subgroup 2 to subgroup 7. TDS in initial and final water is 415 and 3438mg/l respectively.

Phases	Mole transfers	Composition
Albite	3.386e+001	NaAlSi3O8
Anorthite	4.194e+001	CaAl2Si2O8
Calcite	-5.054e+001	CaCO3
CaX2	1.693e+001	CaX2
CO2(g)	5.053e+001	CO2
Fluorite	4.929e-005	CaF2
K-feldspar	7.930e-004	KAlSi3O8
Halite	2.891e-002	NaCl
NaX	-3.386e+001	NaX
Ca-Montmorillon	-5.053e+001	Ca0.165Al2.33Si3.67O10(OH)2
Gypsum	8.978e-003	CaSO4:2H2O

This inverse geochemical modeling demonstrates that the dissolution of albite, anorthite, K-feldspars, halite, fluorite, gypsum and CO_2 are required to derive the observed natural groundwater chemistry in the area. This dissolution is balanced by the precipitation of calcite and Ca-montmorilonite. Furthermore, cation exchange also plays a great role in groundwater chemistry of this path. The cation exchange between CaX_2 and NaX indicates that Ca uptake (dissolve) and Na release (precipitate) reactions along groundwater flow paths. Dissolution, precipitations/weathering and cation exchanges are the major chemical reactions in driving the natural groundwater chemistry.

Path-V: In this flow path the modeling was conducted between Sake/Megado (BR-SP12) and Maheir/Furole (BR-BH35), from subgroup 2 to subgroup 8. TDS in initial and final water is 496 and 5429mg/l respectively.

Phases	Mole transfers	Composition
Calcite	-4.870e-002	CaCO3
CO2(g)	1.084e-001	CO2
Fluorite	-1.997e-005	CaF2
Halite	8.367e-003	NaCl
Olivine	1.180e-002	Mg2SiO4
Pyroxene	5.392e-002	Mg0.5Ca0.5SiO3
Plagioclase	2.594e-002	Na0.62Ca0.38Al1.38Si2.62O8
Anhydrite	1.404e-002	CaSO4
Illite	-8.157e-002	K0.6Mg0.25Al2.3Si3.5O10(OH)2
K-mica	5.061e-002	KAl3Si3O10(OH)2

This inverse geochemical modeling demonstrates that the dissolution of olivine, pyroxene, plagioclase, anhydrite, halite, K-mica (clay) and CO_2 are required to derive

the observed natural groundwater chemistry in the area. This dissolution is balanced by the precipitation of calcite, fluorite, and clay formation of illite. Dissolution and precipitations/weathering are the major chemical processes in driving the natural groundwater chemistry.

By and large, one can easily see from this inverse geochemical modeling that hydrogeochemical processes such as dissolution of minerals and CO_2 gases, precipitation and/or weathering of calcite and clay minerals, and cation exchange reactions along the flow path controls the chemical composition of groundwater in Borena lowlands.

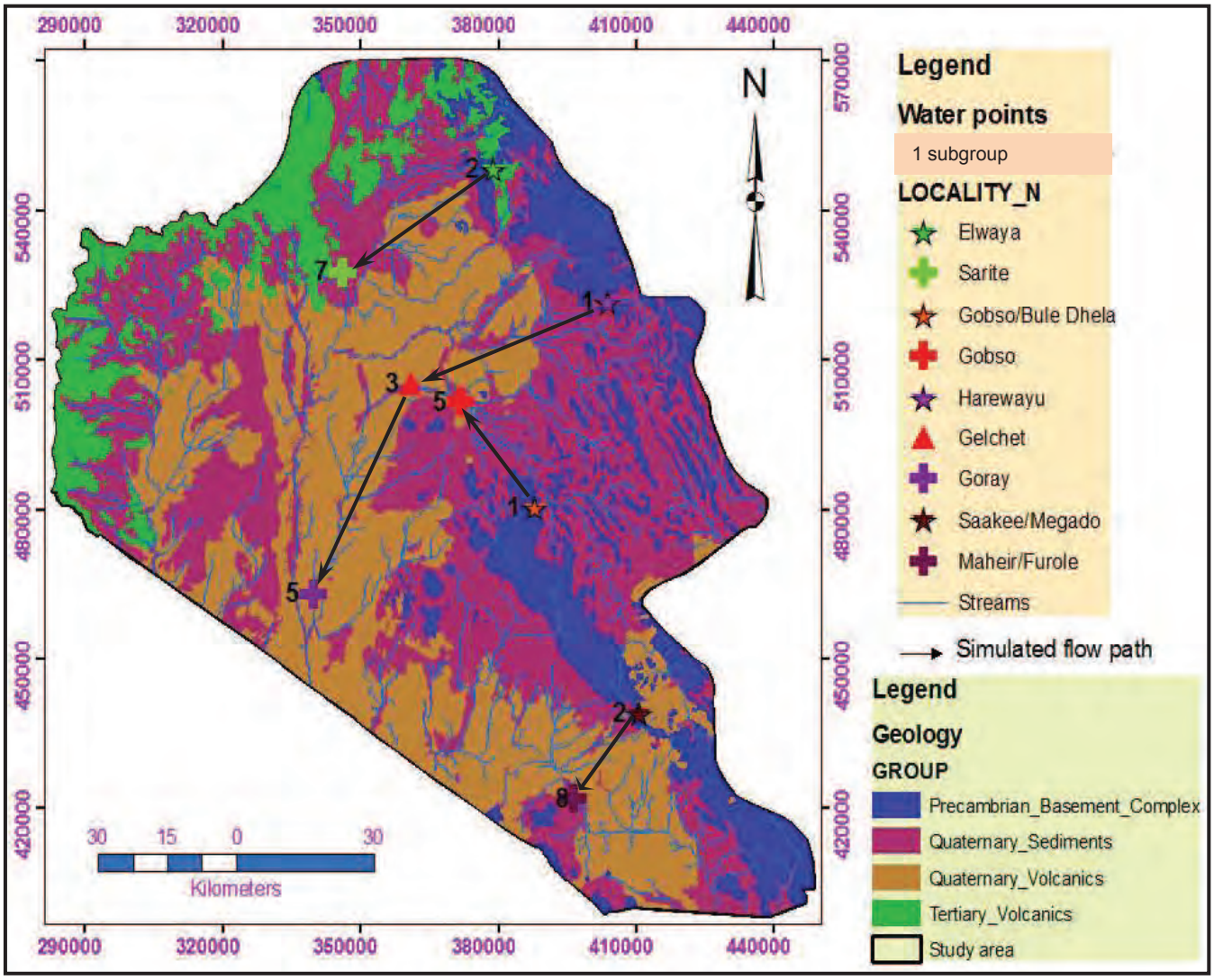

Figure 4-16*: Location map of initial and final water points along simulated flow paths*

4.4.8. Water Quality Assessment

The required water quality is determined by the purpose for which the water is to be used (domestic, urban, agricultural, or industrial). The evaluation of water for use is based on the characteristics of the water compared to a required quality for that use. The quality of groundwater of any region is a result of influences from; geology, hydrologic, human activity. Each factor has its mark on the resulting water. In this work water quality for drinking and agricultural purpose is briefly touched in the following section.

4.4.8.1. Drinking Water Quality

The analyzed samples water quality from the study area is evaluated with respect to the standard guidelines set by World Health Organization (WHO, 2004) as in Ttable 4.10. Generally, those samples out of total samples (see Annex 4) do not fulfill the WHO guidelines were shown in Table 4.10.

Table 4-10*: Drinking water quality standard for selected water quality variables; all are in mg/l unless indicated; N =94.*

Variables	maximum allowable concentration		Analyzed sample from study area			Result > WHO standard	
	WHO (2004)	MoWR (2002)	Minimum	Maximum	Mean	In No	In %age
Turbidity (NTU)	<5	-	nil	100	23.3		
pH	6.5-8.5	6.5-8.5	6.3	8.6	7.5		
Total Dissolved Solids (TDS)	1000	1776	80	8826	1195	33	35%
Sodium (Na)	200	358	11.5	1900.0	195.3	16	17%
Total Iron (Fe)	0.3	0.4				8	8.50%
Manganese (Mn)	0.1	0.5	nil	0.5	0.07	5	5.30%
Sulphate (SO_4)	250	483	0.57	1692	245	19	20.20%
Nitrate (NO_3)	45	50	0.17	44.6	7.7	1	1%
Chloride (Cl)	250	533				17	18%
Fluoride (F)	1.5	3	0.07	7.8	1.3	18	30%

4.4.8.2. Agricultural Water Quality

The relative concentration of Na with respect to Ca and Mg is very important for the suitability of water for agricultural purposes. If water used for irrigation is high in sodium and low in Ca and Mg the cation exchange complex may become saturated with sodium. This can destroy the soil structure owing to dispersion of

the clay particles and this in turn decreases permeability, and aeration of the soil which harm plant growth by limiting the uptake of water and air. The Sodium Adsorption Ratio (SAR) is used for evaluating the danger of high sodium water (Fetter, 1994).

$$SAR\ (meq/l) = \frac{Na}{\frac{\sqrt{Ca + Mg}}{2}}$$

Figure 4.17 and 4.18 shows that about 91.5% of the chemical data in and near the target area have excellent water class for irrigation purpose while the rest 8.5% have a little hazard from sodium (SAR >10meq/l). Of the 8.5% only 2.13%; (Horbate /Dawa and Brindar wells) have SAR more than 18meq/l and hence they are much harmful for plant growth where as all the rest result are within a recommendable range from view of agricultural production. In respect to salinity, most of the samples fall in medium water class for agriculture.

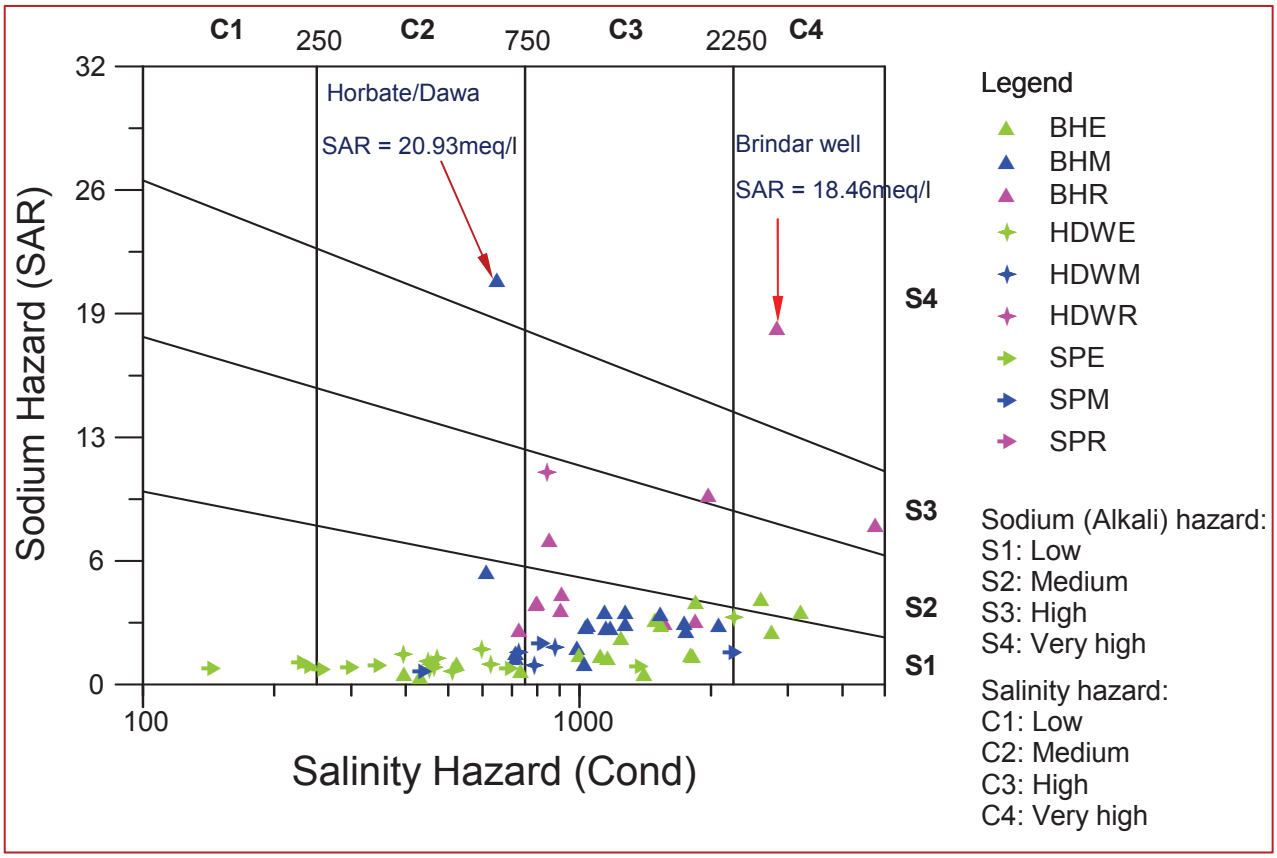

Figure 4-17*: Wilcox diagram for hydrochemical data in study area*

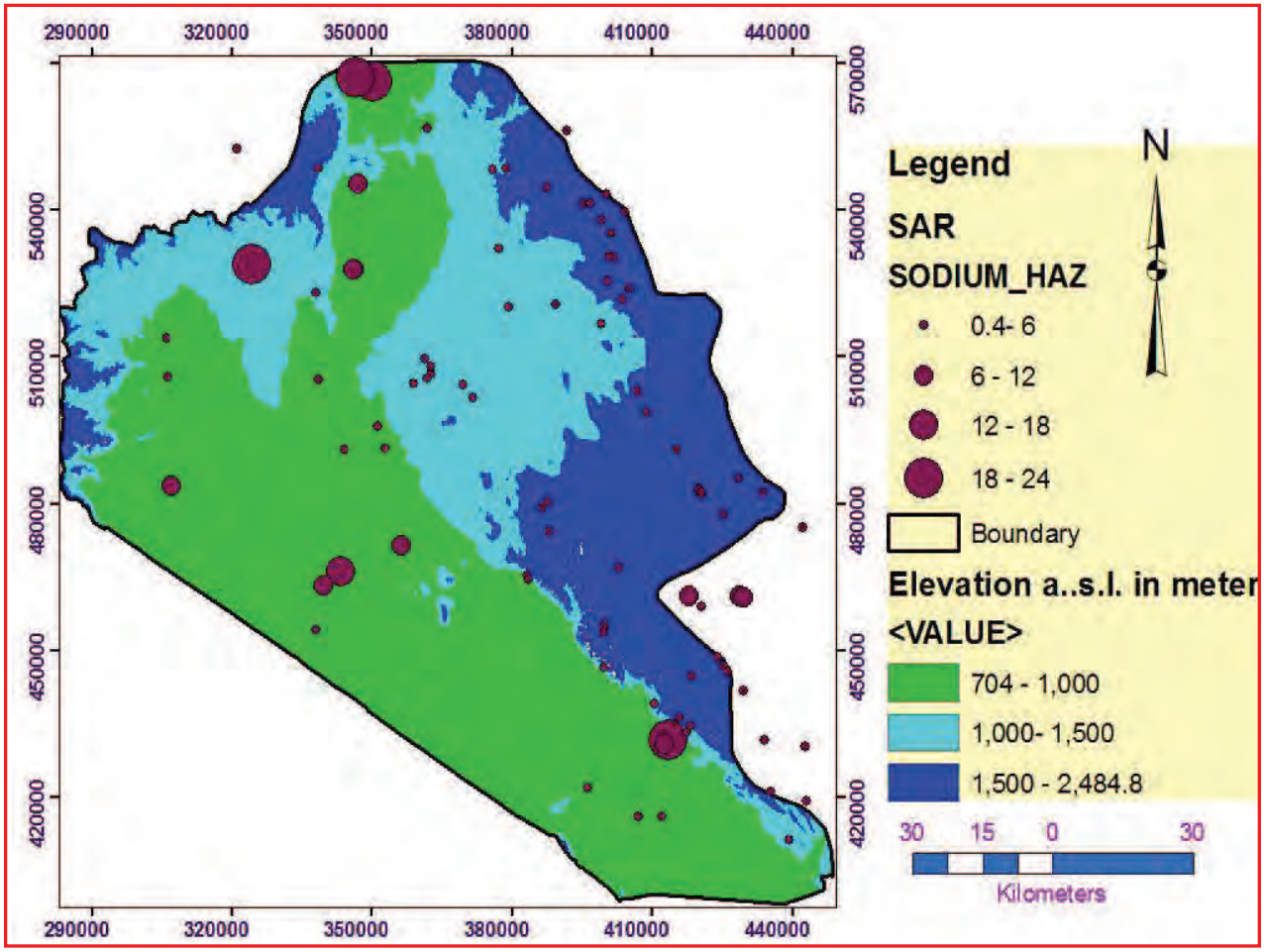

Figure 4-18*: Spatial distribution map of SAR (meq/l)*

Table 4-11: *Suitability of natural waters for irrigation based on their EC and SAR (US Development of Agriculture)*

Water Class	EC (µs/cm)	SAR (meq/l)
Excellent	< 250	Up 10
Good	250-750	18-Oct
Medium	750-2250	18-26
Bad	>2250	>26

5. ISOTOPE HYDROLOGY

5.1. GENERAL

The isotopes commonly employed in groundwater investigations are the heavy stable isotopes of the water molecule, deuterium and oxygen-18 and the radioactive isotopes, tritium and carbon-14 (IAEA, 1981a; Fritz and Fontes, 1980), cited in Fritz *et al*., 1997. In this research, however, only environmental isotopes of δ^2H and $\delta^{18}O$ were used to determine the recharge source, recharge mechanisms and sources of water quality as they are constitute of water by nature and conservative in aquifer. They are part of the water molecule and constitute natural tracers which behave chemically like the water itself.

For this work thirty two water samples were collected systematically from recharge to discharge area. Four samples were from rainfall while the remaining samples were from groundwater sampled from shallow wells, deep wells, hand-dug wells and springs. In addition four analyzed secondary stable isotopes and tritium were included in this thesis from BGWPA report. Total data used for isotope interpretation in this research were 36 (see Annex 3). Figure 5.2 shows points of sampled location.

5.2. DEUTERIUM AND OXYGEN-18 ISOTOPIC COMPOSITION OF WATER

For a regional or local study it is important to compare surface water and groundwater data with a local meteoric water line (LMWL). However, it is not always possible to rigorously monitor precipitations over a representative period of time (at least 1 year), and meteoric water lines must be borrowed from the closest available monitoring station (Fritz *et al*., 1997). Using a large precipitation data set will also improve the confidence limits of the meteoric water line, allowing a better interpretation of groundwater data as the local meteoric water line provides a baseline for groundwater (Fritz *et al*., 1997). As there was no representative station nearby the research area, the average local meteoric water line was derived from mean isotopic composition of rainfall data monitored by IAEA from 1961 to 2007 at Addis Ababa station (Figure 5.1). The station is located at $38^0.73$' longitude and 9^0 latitude and 2360m a.s.l. To derive the LMWL equation 271 data containing both $\delta^{18}O$ and δ^2H downloaded from IAEA/WMO/GNIP data base (**http://isohis.iaea.org**). Hence, the local meteoric water line (LMWL) for the area is represented by $\mathbf{\delta^2H = 7.12\delta^{18}O + 11.9}$, where, δ^2H is

isotopic composition of hydrogen and $\delta^{18}O$ is isotopic composition of Oxygen-18 per mill.

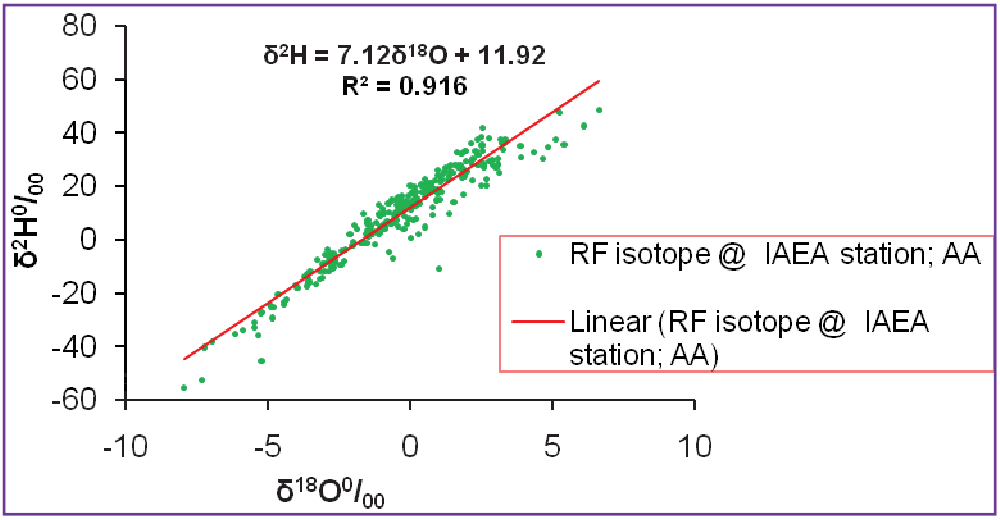

Figure 5-1: *Oxygen-18 vs Deutrium of rainfall data @ IAEA station, Addis Ababa*

The $\delta^{18}O$ and $\delta^{2}H$ compositions of Borena are relatively depleted compared to those of Eastern (for instance in Shinille and Dire Dawa) and central part of Ethiopia which gets rainfall from the same moisture sources. Some part of Ethiopia, like the present study area, gets its rainfall from North Indian Ocean (Seifu Kebede, 2004). The Eastern Ethiopia rains relatively represent the initial stage of condensation for the moist easterly flows from the Indian Ocean (Joseph *et al.*, 1992; cited in Seifu Kebede, 2004) and thus enriched in isotopic composition relative to the current study area that found at the furthest distance from moisture sources (oceans). This indicates the isotopic composition is being depleted along its trajectory line.

Most of the analyzed water samples plot in the right position of the LMWL (Figure 5.3). Precipitation and other waters that have not undergone evaporation (such as most groundwater) generally fall along a LMWL having a slope of about 8, usually lying close to the GMWL of Caraig (1961). Meteoric waters that have undergone evaporation display systematic enrichment in both $\delta^{18}O$ and $\delta^{2}H$, resulting in divergence from the GMWL along evaporation lines having slopes of less than 8 (often in the range 4 to 6). If the analyzed water drops in the right of LMWL, evaporation prior to recharge enriches the recharging water. In contrary, those lies on and to the left of the LMWL most probably indicates fast recharging of groundwater

through vertical fractures or highly permeable media before affected with kinetic evaporation effect. The characteristics of each isotopic composition of water in rainfall, wells (hand-dug, shallow and deep wells), and springs were illustrated below.

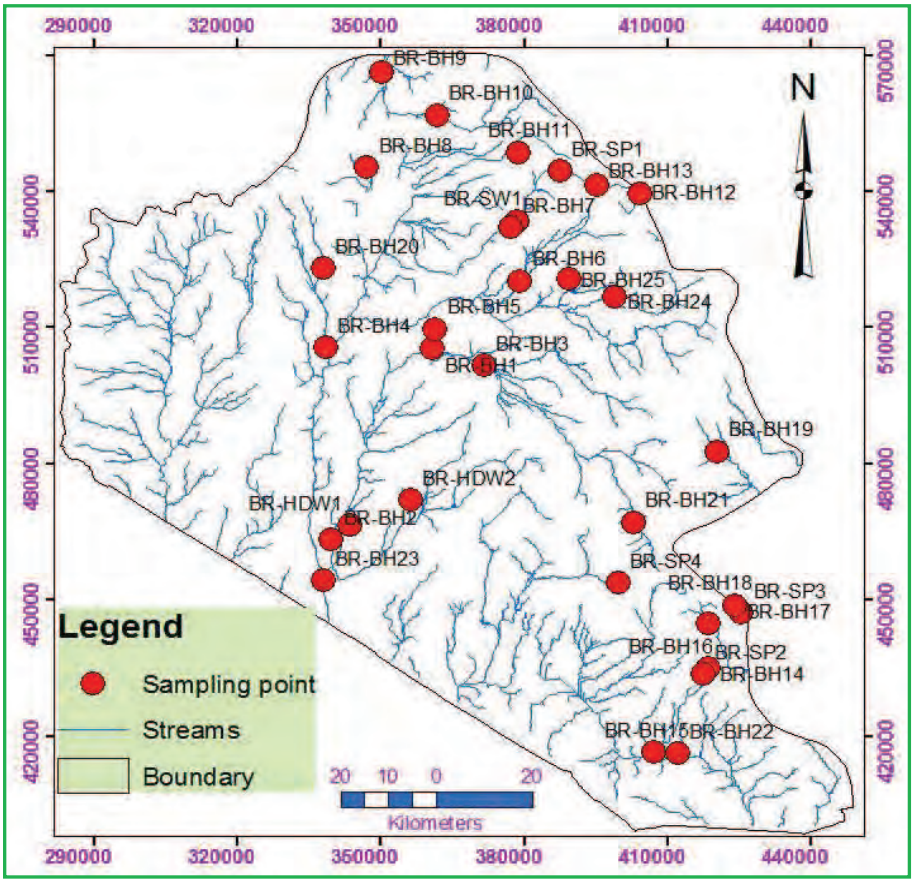

Figure 5-2: *Map of Environmental Isotope Sample points*

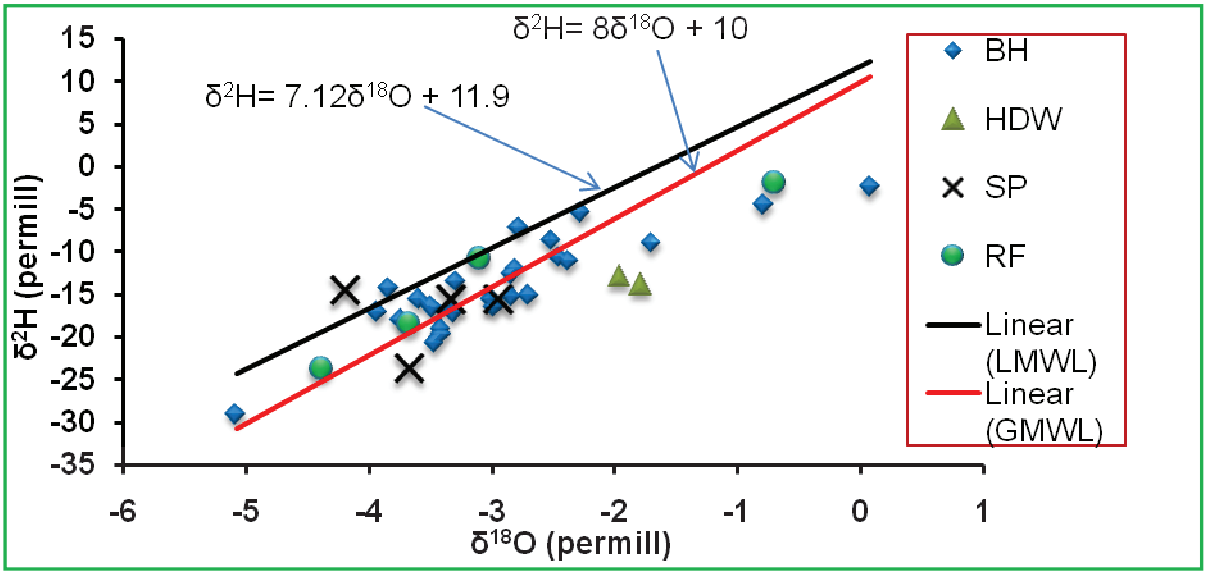

Figure 5-3*: Oxygen-18 vs. Deutrium plot of groundwater and rainfalls in the study area*

5.3. RAINFALL ISOTOPIC COMPOSITION

The isotopic value of precipitation is controlled by isotope value of source, rate of evaporation of source, isotopic evolution of air mass, relative humidity during precipitation (Gat, 1996).

Most of the secondary rainfall data were taken in 1995 during the main rainy seasons which fall between April and July (EGS, 2000) where as the original rainfall data were taken only from a lesser rainy season falls between mid-September and mid-October. Most of the secondary data cluster on LMWL while some plots to right of this regression line indicating that the precipitation has undergone different evaporative effects (Figure 5.4). Similarly, most of the primary isotopic composition plots on the right of LMWL that also indicate kinetic evaporation while raining and subsequent evaporative enrichment. Moreover, it was noticed that the rainfall at Yabello (both from 1^{o} and 2^{0} sample) and Moyale (2^{0} sample) were enriched in isotopic composition not only due to evaporation but also associated with events of low rainfall amount. In contrary, rainfall from Mega stations was depleted in both $\delta^{2}H$ and $\delta^{18}O$ for both data sets and hence, the rains in this station is less evaporated while raining owing to high rainfall amount and saturated atmosphere as the altitude at Mega is higher than Moyelle and Yabello (Figure 5.4).

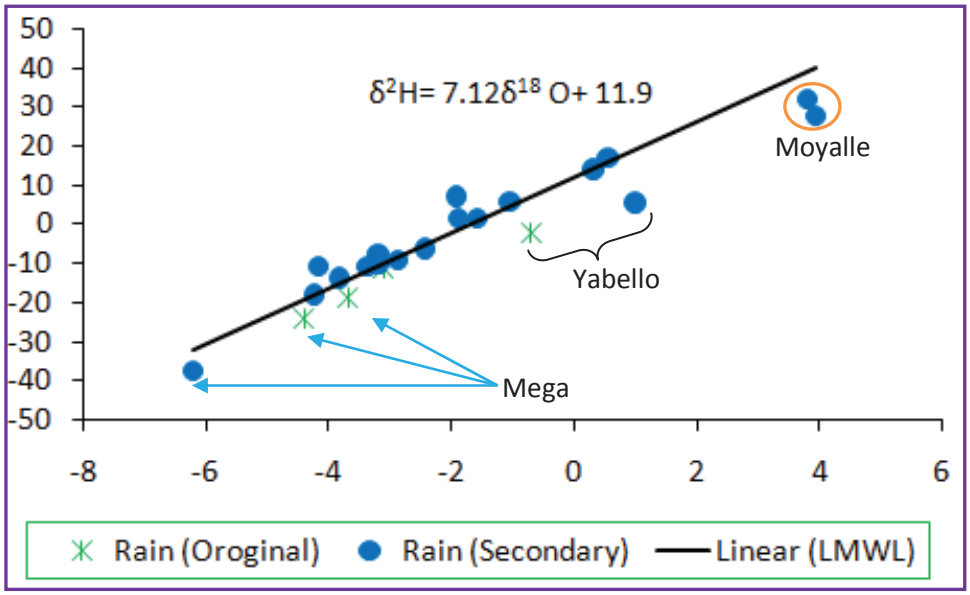

Figure 5-4: *Oxygen-18 vs. Deuterium plot of rainfall isotopic composition*

5.4. GROUNDWATER ISOTOPIC COMPOSITION IN WELLS

The isotopic composition of oxygen-18 and Deuterium in shallow and deep wells varies from -5.08$^0/_{00}$ to 0.08$^0/_{00}$ and from -29$^0/_{00}$ to -2.4$^0/_{00}$ respectively. The mean composition is -2.93$^0/_{00}$ for Oxygen-18 and -13.9$^0/_{00}$ for deuterium. The two hand-dug wells in Goray and Dillo craters shows -1.97$^0/_{00}$ and -1.79$^0/_{00}$ for oxygen-18 and -12.92$^0/_{00}$ and -13.88$^0/_{00}$ for deuterium respectively. These were nearly plot to evaporation slope line indicating intensive evaporation from recharging water while infiltrating (Figure 5.5). Furthermore, as these hand-dug wells were open, the relative enrichment might also be resulted from evaporation after being discharged to the hand dug wells.

Groundwater from Harewayu (BR-BH24) and Alabor (BH-BH15) wells plot on a LMWL indicating a predominantly meteoric source (Figure 5.5). The isotopic compositions in remaining wells were deviated from the LMWL in a direction indicative of fractionation due to possible strong evaporation. Among the enriched isotopic composition of $\delta^{18}O$ and $\delta^{2}H$ Liso (BR-BH4), Ambo (BR-BH20) and Goray (BR-BH2) wells plot along the evaporation line with nearly a slope of 4.2. The groundwater from these wells was enriched with Oxygen-18 and therefore, highly affected by evaporation effects compared to the rest wells. The groundwater sample from Liso (BR-BH4) is plot nearest to the point representing sea water that signifies intensive evaporation.

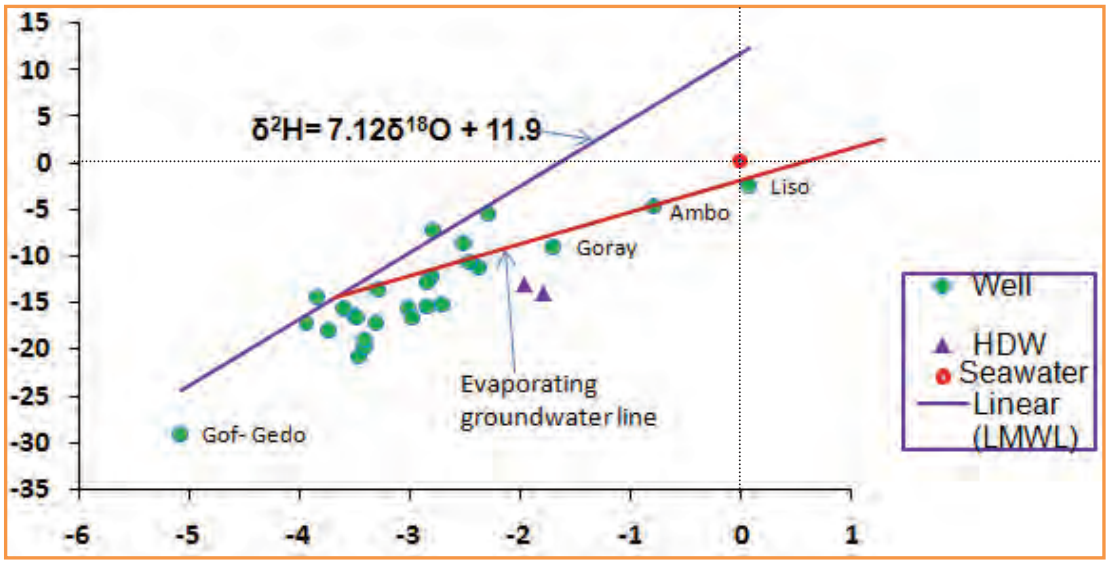

Figure 5-5: *Oxygen-18 vs. Deuterium plot of HDW and BH water isotopic composition*

In general, groundwater show shifting samples towards heavier values of $\delta^{18}O$, which is typical phenomenon prior to recharge in semi-arid areas (Gat, 1981). The strong evaporation of recharge in semi-arid is the result of runoff over the hot landscape like in this research area. As in semi-arid regions, water can be lost by evaporation from the unsaturated zone or from the water table. In the case of this research, however, as the water table is found deep most water samples show the evaporative losses only from the unsaturated zone and the pool collected in flat land during heavy rainfall.

5.5. GROUNDWATER ISOTOPIC COMPOSITION IN SPRINGS

Figure 5.6 shows Choressa spring groundwater from Gololcha area were more depleted in $\delta^{18}O$ compared to the isotopic composition of the rest three springs suggesting it is recharged at higher altitudes and/or lower temperatures. The spring oozes out of fractured gneiss along Mega Northwest-Southeast trending escarpment at an altitude of 2214m above sea level. Additionally, the surrounding aquifer was covered by dense vegetation that can create humidity and thus declines evaporation so that depleted isotopic composition observed in this spring. Even though the entire rest springs plot below the LMWL that indicates effect of evaporation before infiltration to the fractured aquifer they are relatively depleted. From these, a relatively enriched value were observed for the Tesi spring near Megado and for Churessa spring near Mega, hence compared to the other evaporative effects on these springs was indicted.

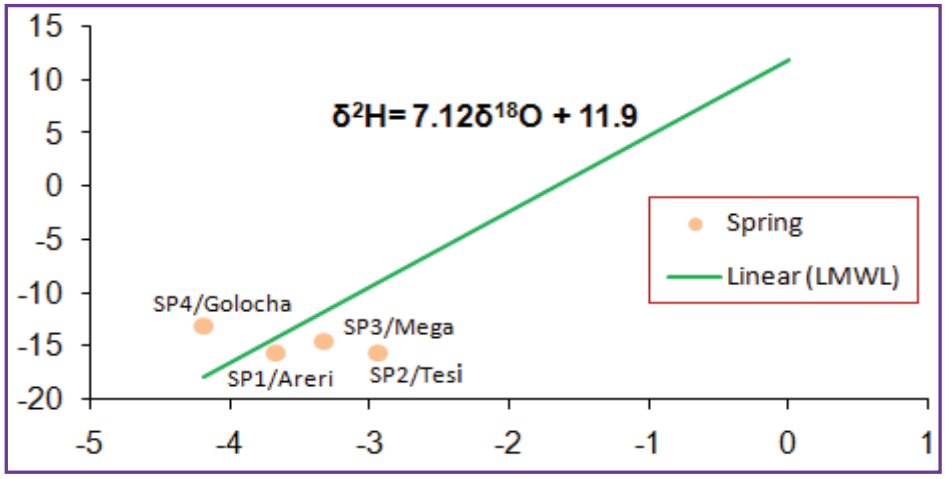

Figure 5-6: *Oxygen-18 vs. Deuterium plot of spring water isotopic composition*

6. GROUNDWATER RECHARGE AND FLOW PROCESSES

6.1. GENERAL

The sources of recharge to groundwater system include both natural and human-induced phenomena. Precipitation is the only recharge in the study area either through direct recharge from percolation of precipitation or indirect recharge from runoff ponding in topographic depressions and wadis channel.

In arid and semi arid regions like the research area localized and indirect recharge are often the most important sources of natural recharges (Figure 6.1). Because direct or diffuse recharge is water added to the groundwater reservoir in excess of soil-moisture deficits and evapotranspiration by direct vertical percolation of precipitation through the unsaturated zone. It is typical of humid climates because frequent, regular precipitation maintains a high water content in the soil, so that there is little additional storage capacity in the vadose zone. Thus, infiltration can be routed quickly through the vadose zone to the saturated zone. In contrary, in semi-arid areas where the climate is hot, soil moisture deficit cannot easily reached as soil moistures quickly removed by high rate of evapotranspiration(Sophocleous, 2004).

The objective of this chapter is to show qualitatively the recharge sources, recharge mechanisms and groundwater flow directions and quantitatively the recharge rates using the techniques and principles of hydrogeochemistry and isotope hydrology as evidence.

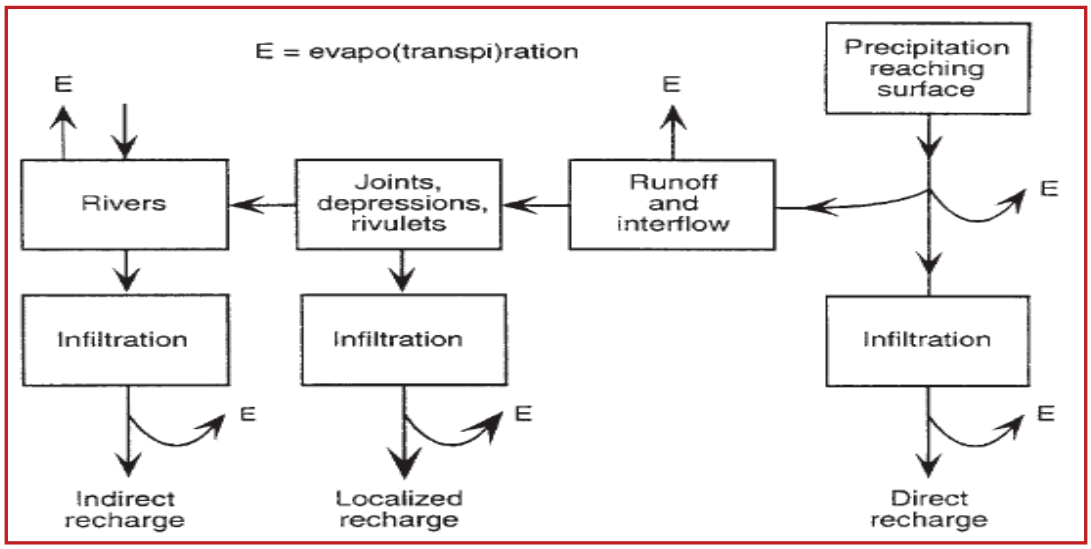

Figure 6-1: *The various mechanisms of recharge in a (semi-)arid area (After Lerner 1997)*

6.2. HYDROGEOCHEMICAL FACIES CONCEPT

According to Chebotarev (1955) and Back (1960, 1966), variation of water composition evolves along groundwater flow direction due to chemical reactions and water-rock contact time even in a homogeneous aquifers. In recharge areas the soil zone undergoes a net loss of mineral matter to the flowing water (Freeze and Cherry, 1979). As groundwater moves along flow lines from recharge to discharge zones, its chemistry is altered by the effects of various geochemical processes. Groundwater chemical evolution can be attributed mainly by two factors namely flow path and the travel time. The general trend of chemical evolution is towards the composition of sea water. Chebotarev (1955) suggested the sequence of major ion evolution as:

Travel along the flow ⟶

$HCO_3^- \longrightarrow HCO_3^- + SO_4^{2-} \longrightarrow SO_4^{2-} + HCO_3^- \longrightarrow SO_4^{2-} + Cl^- \longrightarrow Cl^- + SO_4^{2} \longrightarrow Cl^-$

Increasing ⟶

The geology of recharge area is dominated with weathered gneiss and plutonic granite in the northern extreme while the lower basalt, middle (Teltele) basalt and upper basalt occupies the recharge area of the western extreme (section 3.5). Furthermore, sporadically scattered grabens and bottom foot of basement hills, for instance at Yabello town, filled with thick sand and silt deposits exist in recharge area. For example, the alluvial fan at Yabello town consists of unconfined aquifer. The middle sector covered by elluvial sediments over which calcerite deposit is predominating. The discharge area is covered by variable thickness of sediments overlying the fractured Bulal basalt; the principal aquifer in the area. The main north-south and northwest-southeast trending Ririba and Mega faults respectively also play a great role in complicating geology and water chemistry of the locality.

Hence, it is ideal thinking that water flow from the recharge to discharge area has pass through such complicated geological structures and compositions with variable flow rates and lines. The hydrochemical facies from the Borena lowland, therefore, resulted from different soluble minerals so that variable water types resulted. In northeastern (recharge area), most of the water sampled from shallow wells, hand-dug wells and springs in crystalline basement rocks were dominated by Ca-Mg-HCO_3 water type (Figure 4.6). Rain water collected from the project area also falls in this

category and thus testifies early stage groundwater evolution in recharge area. However, in the same area, particularly in grabens and bottom foot of escarpments where unconfined alluvial fan exist like that of Yabello town, mixed water types like Na-Ca-HCO_3-Cl-SO_4 is dominating. On the other hand, the water type from the volcanic of the western extreme recharge area is dominating with Na-Ca-HCO_3, which shows a little evolution. In this sector, the Ca concentration is being deposited from the flowing water as indicated in SI and thus Na becomes the dominant cations. The northeastern and western recharge area water types were categorized in to subgroup 1 and 2 respectively. The subgroups have diluted water in TDS, which are 224mg/l and 501mg/l respectively. Therefore, Ca-Mg-HCO_3 and Na-Ca-HCO_3 water types are extensively seen in northeastern and western recharge area respectively.

The middle sector of the study area is also characterized by the dominance of Na-Ca-HCO_3 water type coupled with different mixture of water types. This sector is dominated with plain lands where water gets chance to stay rather than fast runoff until infiltrated or evaporated. Thus, it comprises of a mixed groundwater from vertical fast percolation through overlying sediments and underground water flows from the upper extreme of the recharge area. That is why Na-Ca-HCO_3 coupled with variable mixture of water types detected in this sector as well as in lower rift sector. This was confirmed by the isotopic compositions showing similar signature, particularly in Gelchet area, with that of recharge area. From the Q-mode HCA, subgroup 3, 4, 5, and 6 which consists different mixture of water along flow lines were categorized in the middle and rift sector.

Rainwater is the source of most groundwater and a logical starting point for the study of groundwater geochemistry (Appelo and Postma, 2005). Figure 6.2 shows a higher increase of each variable with TDS at the commencement of groundwater evolution from precipitation until their appearance as spring or wells. All parameters greatly increase from subgroup 1 to 3, but the pH is nearly constant from subgroup 2 to 3. Na, Cl, and SO_4, nearly shows systematic increase with TDS while Mg and Ca become slightly decreases or increases starting from subgroup 4 as these solutes precipitate along the groundwater flow paths. The flow path evolution among the anions HCO_3, SO_4 and Cl can be clearly seen, but in subgroup 8 and 10 HCO_3 superimposes the other due to deeper source of CO_2. The pH increases with TDS, however becomes

decline for instance at subgroup 4, 8 and 10 as HCO_3 rises as a result of deep source of CO_2. The increase of Ca concentration in subgroup 9 was resulted from dissolution of thick calcerite sediment. This was affirmed by isotopic composition taken from similar neighboring well showing prominent salt dissolution than evaporation for the salinity of the groundwater.

By and large, even if distinct identification could not attained from the Q-mode clustering and Piper plot as the evolution trend suggested by Chebotarev (1955), the hydrochemical facies illustrates the groundwater flow evolution along its flow path; from Ca-Mg-HCO_3/Na-Ca-HCO_3 to Na-Cl/SO_4. The groundwater flow trend was shown by Durov plot for each HDW, BH, and SP separately (Figure 6.3).

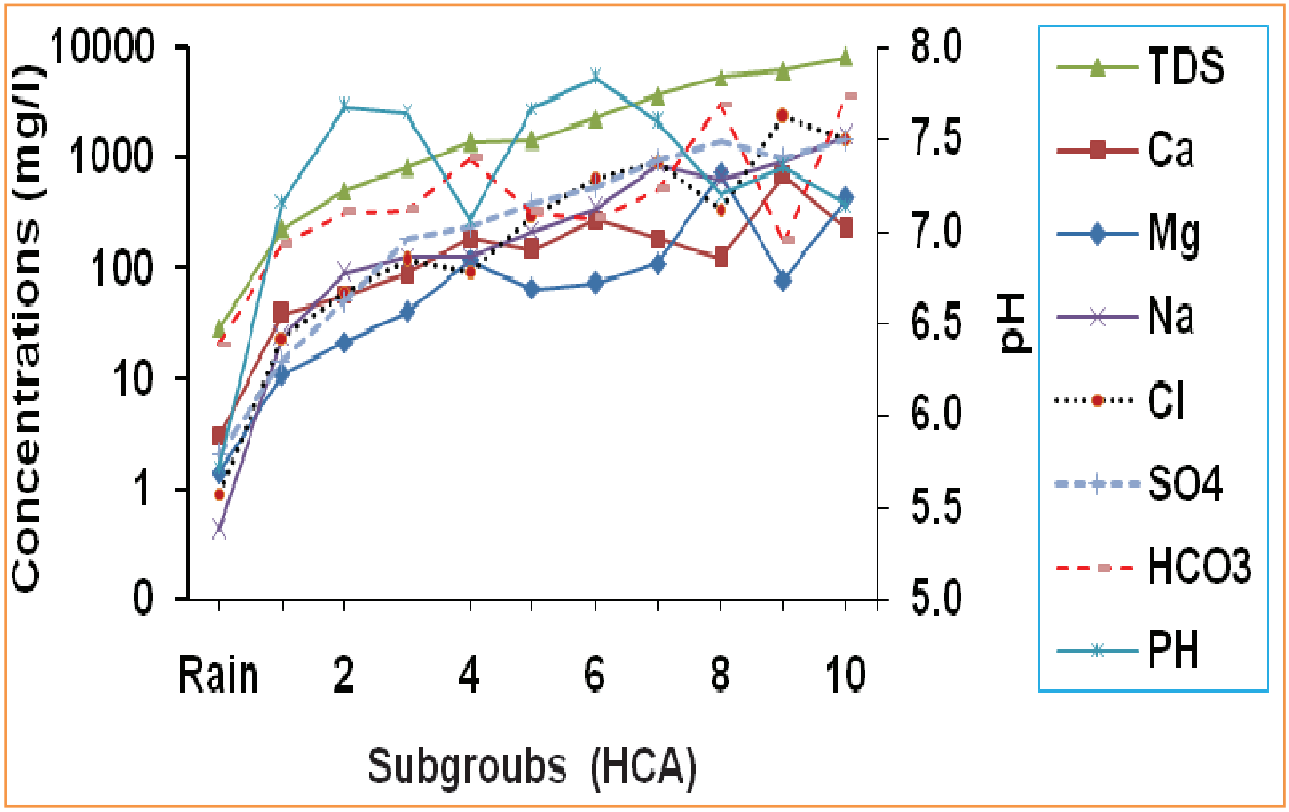

Figure 6-2*: Hydrochemical evolutions from precipitation (Rainfall) to subgroup 10 in the study area. Note that pH values are displayed in right-hand y-axis.*

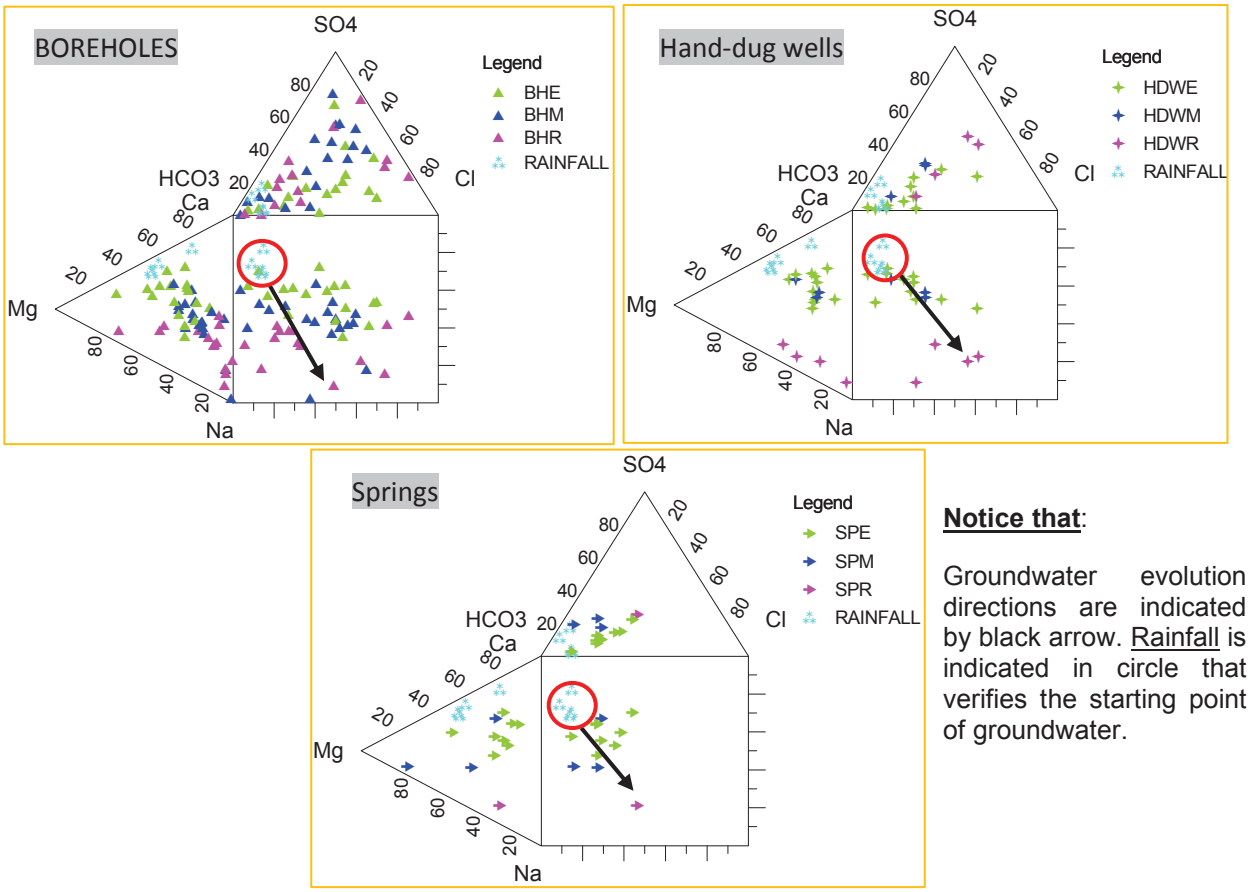

Notice that:

Groundwater evolution directions are indicated by black arrow. Rainfall is indicated in circle that verifies the starting point of groundwater.

Figure 6-3*: Durov plot indicating groundwater flow directions from escarpments via middle to rift sector.*

Figure 6.4 shows the groundwater flow lines along with decreasing of Ca and Mg ion concentrations and increasing of Na, Cl and SO_4 ion concentrations. The assumption here is that for reactive elements such as Ca, Mg, K, Na and F, SO_4, concentration increases until these elements reach their saturation with respect to soluble salts. Removal of soluble salts leads to decrease of these elements. For elements such as Na, F and K in natural groundwater systems the salts cannot reach saturation with respect to stiochiometric minerals (Seifu kebede. 2007; unpublished report). The flow lines indicated in Box and Whisker plot in Figure 6.4 was thus justified by this fact. Blue arrows in this figure show flow lines from escarpment via middle sector to rift zone.

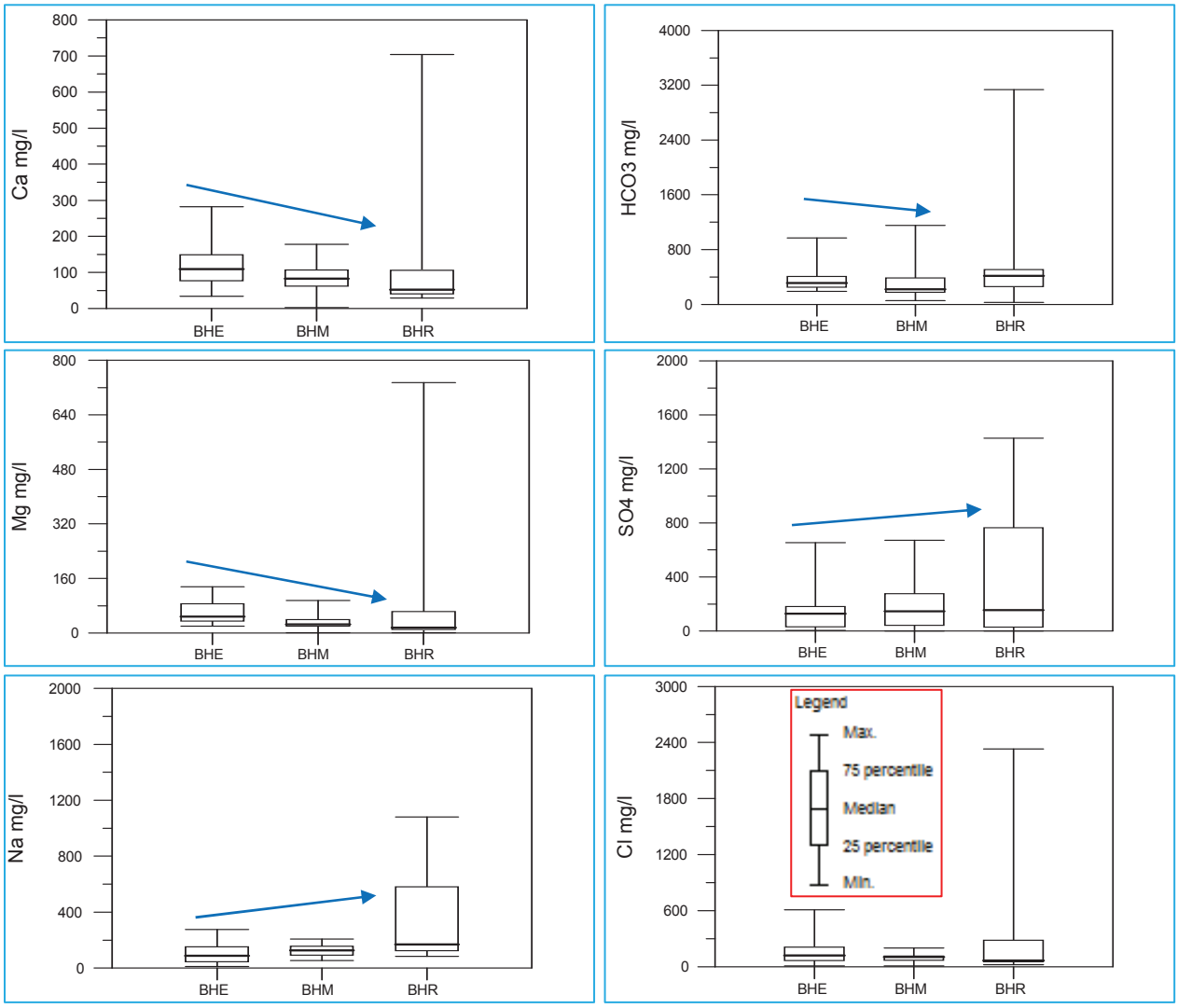

Figure 6-4: *Box and Whisker plot for Ca, Mg, Na, HCO_3, SO_4, and Cl ions against boreholes in Escarpment, Middle and Rift sectors.*

6.3. RESIDUAL ALKALINITY

In many crystalline formations, Residual Alkalinity [RA = (HCO_3) - (Ca + Mg)] in meq/l increases with increasing TDS along groundwater flow directions as Ca ion precipitate rapidly with respect to the other. However, in this investigation, particularly, in Ririba rift to which groundwater flow was hypothesized, the reverse holds true (Figure 6.5, left & 6.6, top). But, a slight increase of RA with TDS was noticed in Mahier/furole (BR-BH35) and moderately raised in spring and open hand dug well of Megado craters; BR- SP13 and BR-HDW19 respectively and in Goray/Melkasedeka well (BR-BH23).The decrease of RA with increasing TDS signifies that high addition/dissolution

of Ca or Mg concentration with respect to HCO_3. The reason is most probably due to either fast groundwater flow in fractures of basic rocks/basalt and local dilute meteoric water flashing from vertical fractures so that low residence time for precipitation of Ca and Mg or from fracture filled calcerite dissolution. Presence of Ca and Mg bearing minerals like Olivines, pyroxenes and plagioclase in the area could also be the reason.

The Sulphate map relatively increases along the speculated flow trends that confirm the groundwater evolutions suggested by Chebotarev (1955) (Figure 6.5, right & 6.6, bottom). High SO_4 concentration was observed at downstream of Ririba streams and at Sarite, Brindar, Dillo, Goray and Megado localities, which are situated in ideal discharging zones.

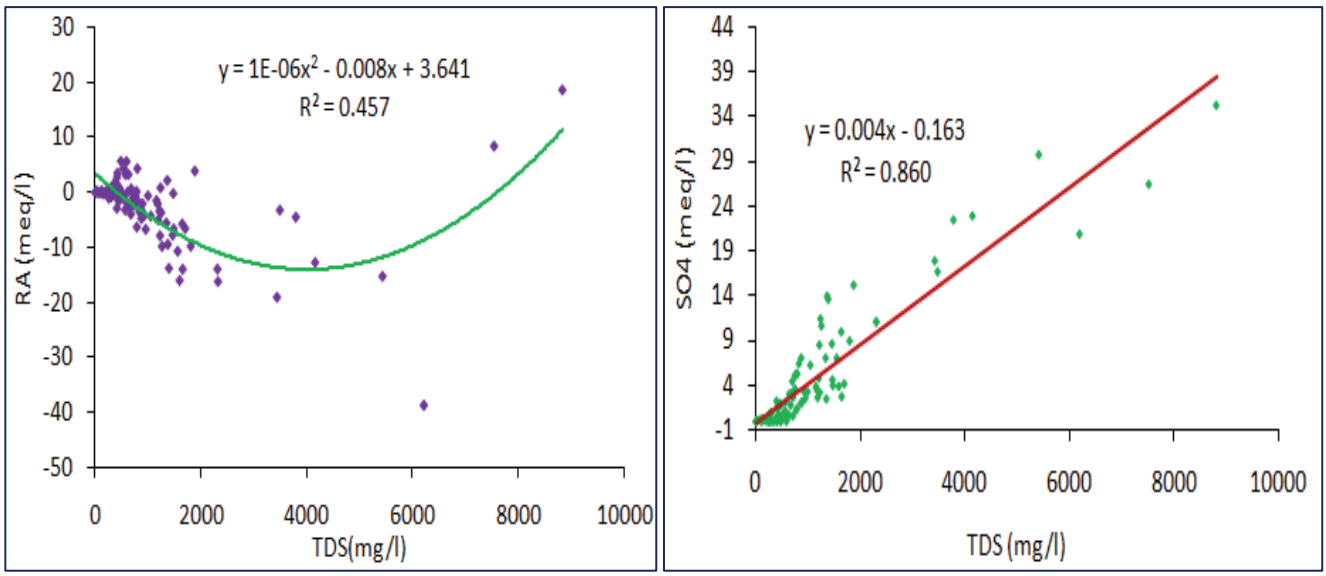

Figure 6-5: *TDS vs. Residual Alkalinity* ***(Left)*** *and TDS vs.* SO_4 ***(Right)*** *plot*

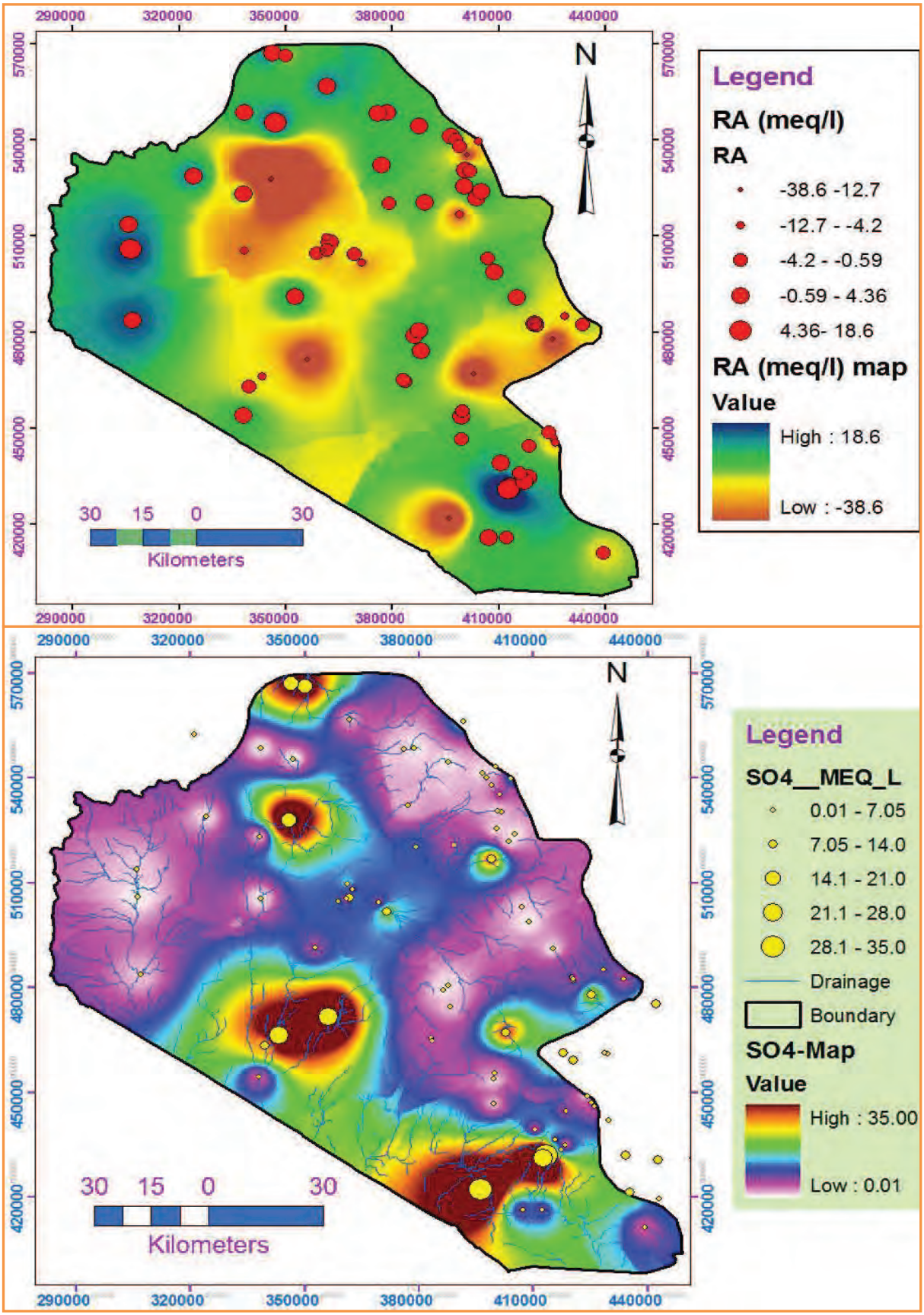

Figure 6-6*: Spatial distribution map of Residual Alkalnity (RA)* ***(top)*** *and Sulphate Map* ***(bottom)***

6.4. ELEMENTAL RATIOS (CA/MG AND CA/NA) AS GEOCHEMICAL TRACERS

The ratio of Ca/Mg ion concentration is one of the geochemical tracers to indicate regional groundwater flow lines in a given catchment or basins. Due to the fact that Ca ion concentration is rapidly removed from the groundwater solution either by precipitation or ion exchange, the ratio of Ca/Mg decreases from recharge area to discharge area. Figure 6.7 clearly indicates a gradual decrease of Ca to Mg ion ratio from Elwaya, Yabello and Utalo locality via Gelchet to Goray locality. In contrary, higher ratio is observed in BR-BH2 (Goray), BR-BH4 (Liso), BR-BH8, BR-BH29 & BR-BH30 (Sarite), and BR-BH9 (Brindar) wells situated in rift and ideally in discharge zone. This could either be due to local flashing of dilute meteoric water through vertical fractures that contribute high concentration of Ca from calcium bearing rocks and calcite filling fractures or from calcerite dissolution from thick sediments particularly in case of Sarite and Brindar. This case had also been observed in RA. The SI of calcite in BR-BH2 (Goray) for example indicates undersaturation where as the other in similar lower topographic position is saturated (Figure 4.9C). This confirms the local flashing of Ca in this area.

The concentration contour and interpolated Ca/Na ratio map clearly illustrates a gradual decrease of Ca with respect to Na along flow path and groundwater evolutions (Figure 6.8). From this the groundwater flow direction is schematized perpendicular to the iso-concentration contour of Ca/Na ratio (Figure 6.10).

Once the rain joins the soil or rocks its chemical compositions starts to change along the flow paths as a function of the lithologies encountered. One can easily understand that the Ca concentration begins declining with respect to Mg and SO_4 concentrations as it moves from rain to each successive subgroup; from subgroup 1 to 10 (Figure 6.9). But higher concentration of Ca with respect to Mg was observed in subgroup 6 and 9 which suggests either local recharge along the flow lines or higher calcerite deposit that can furnish Ca during rainy season.

By and large, based on general hydrogeochemical evidences, the groundwater flow directions are illustrated as follows:

The first major flow directions are from the Northwestern elevated basement rocks (Adegelchet, Utalo, Elwaya and Gololcha) via the middle plains sectors of Gelchet to

the main North-South trending Ririba fault. The second flow direction is from the elevated middle east of the study area (Arbaale/Sayole area) to Megado/Biliko lower plains. Thirdly, from the Southeastern extreme (Shanacha locality) to west direction and then returns to south following the replica of surface flows. Based on the current available data, the flow line from northwest elevated volcanic rocks (Mermero area) seems more vertical deep flow in vertically fractured basalt aquifer instead of directly flowing to Ririba valley. But this needs further investigation for verification.

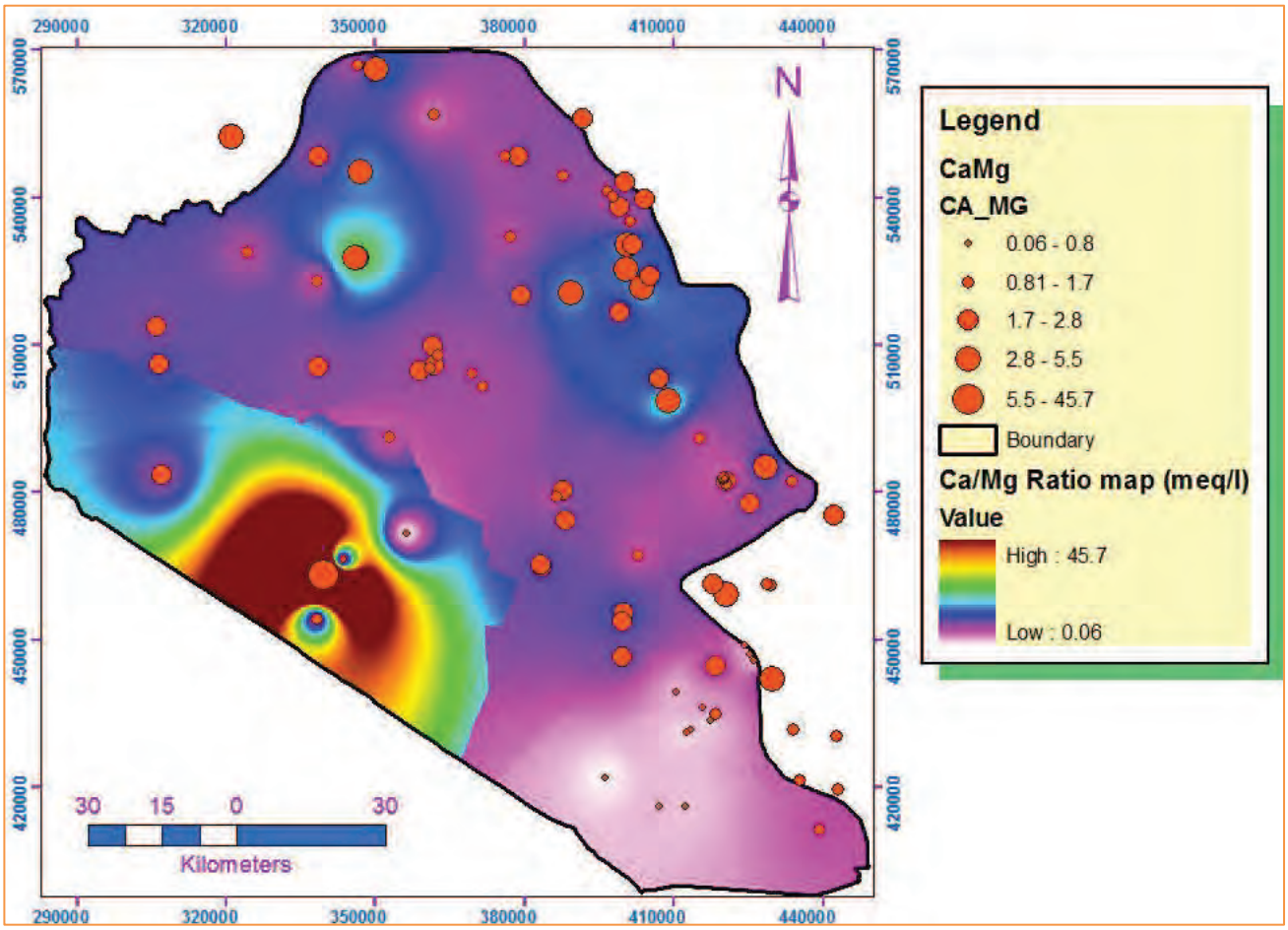

Figure 6-7*: Spatial distribution map of Ca/Mg*

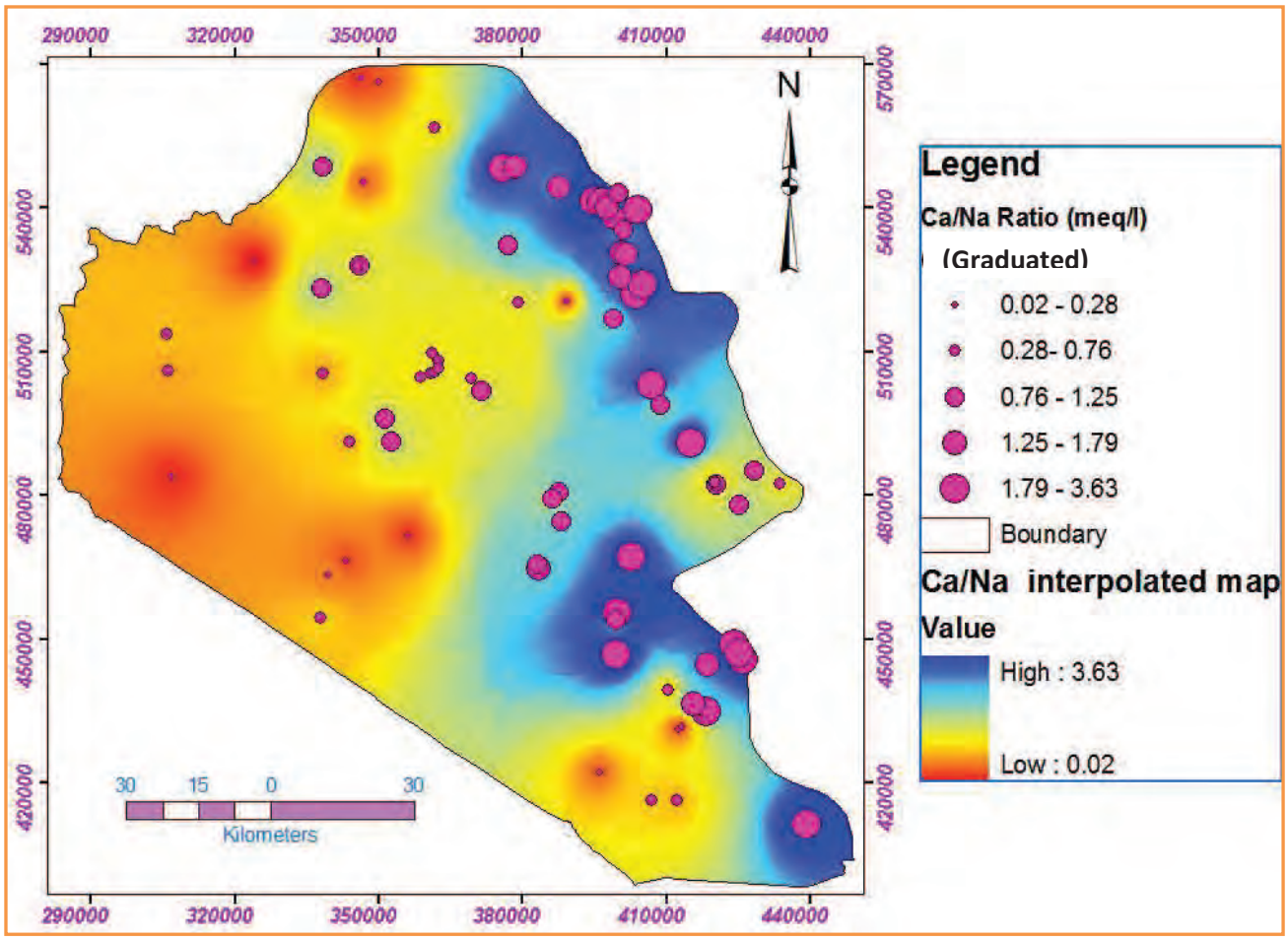

Figure 6-8: *Spatial distribution map of Ca/Na in (meq/l)*

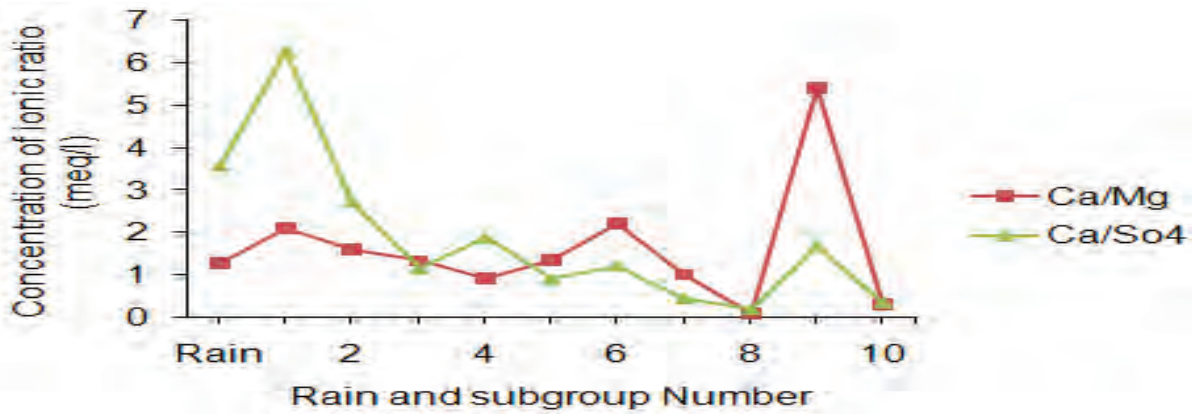

Figure 6-9*: Rain and subgroups Vs. Ca/Mg and Ca/SO4 ratio plot.*

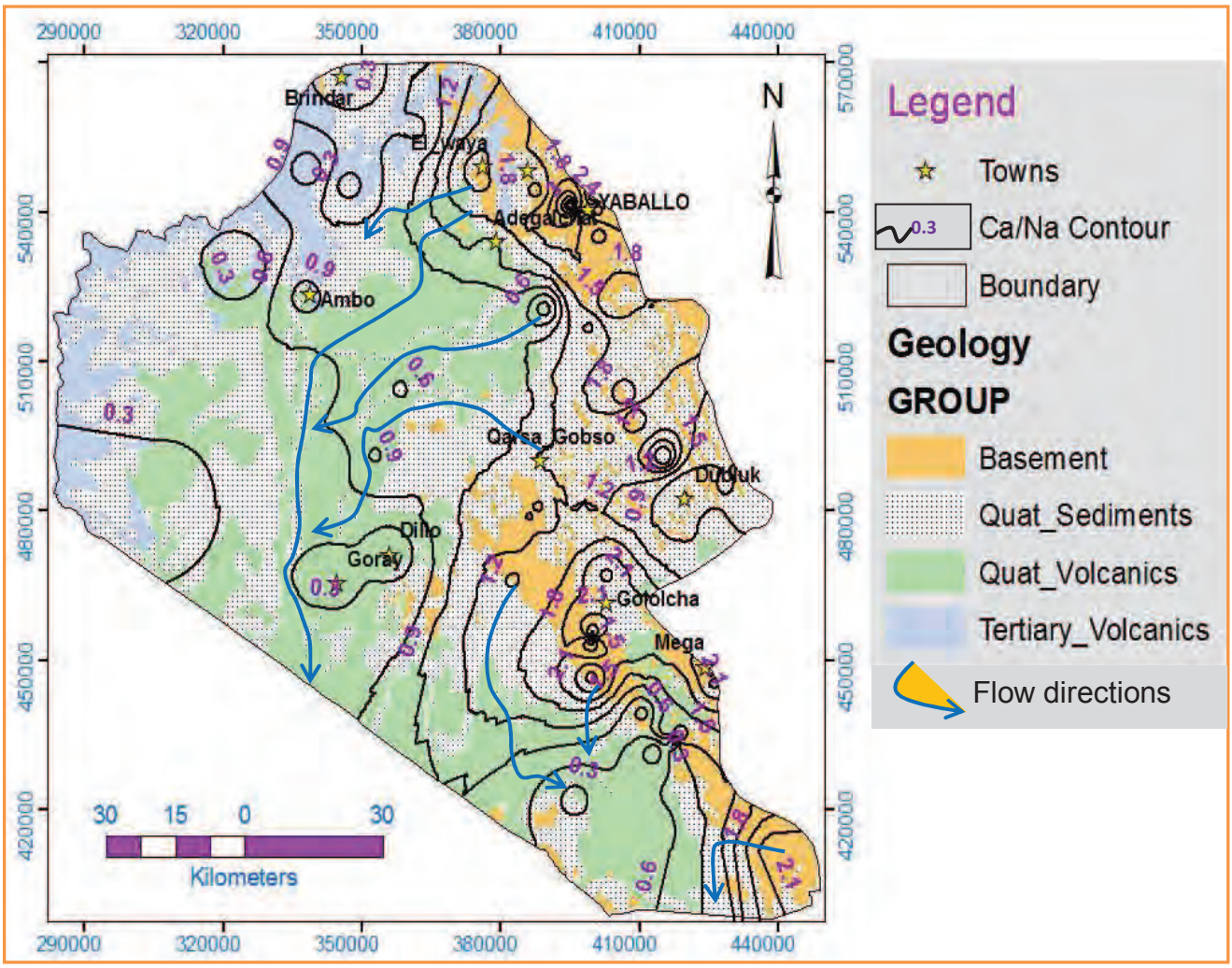

Figure 6-10*: Ca/Na (meq/l) ratio contour map and groundwater flow directions.*

6.5. SPATIAL DISTRIBUTION OF OXYGEN-18 AND $\delta^{18}O$ VERSUS $\delta^{2}H$ RELATION

In this investigation, analysis of $\delta^{18}O$ and $\delta^{2}H$ for different water sample data has been done with the aim of identifying ground water recharge source, recharge mechanisms, and salinity source. Based on the analysis result for the collected sample, interpretation is made so as to identify recharge sources and mechanisms and briefly described below.

The isotopic composition of groundwater from BR-BH24 (Harewayu), BR-BH21 (Gololcha) and BR-BH15 (Alabor) lies on a LMWL suggesting direct infiltration of local precipitation (Figure 6.11). Most of the water from the escarpments lies between LMWL and GMWL (Figure 5.3). These water samples were relatively depleted in both $\delta^{18}O$ and $\delta^{2}H$ isotopic composition. Water collected from middle sector of the area like BR-BH3 (Gobso), BR-BH1 (Gelchet) and BR-BH5 (Gelchet) wells also show a relative depletion that affirms higher altitude recharge sources that is from Harewayu, Gololcha, Adegelchet, and Elwaya localities (Figure 6.12). Moreover, fast selective recharge from intensive rains could also be the recharge mechanism (Figure 6.11 and 6.12). The plain is covered with thin impermeable clay deposits and the under lying rock is permeable fractured vesicular and scoriaceous basalt. The isotopic composition of BR-BH4 (Liso), BR-BH20 (Ambo), BR-BH8 (Sarite) and BR-BH2 (Goray) is somewhat enriched in both $\delta^{18}O$ and $\delta^{2}H$. They lie along evaporation line with nearly a slope of 4.2 (Figure 6.11). This reflects the ground water recharge from flash floods or wadis streams after intensively evaporated (Figure 6.11 and 6.12). In most cases water samples in recharge area and middle plain sector show relatively depleted signature in Oxygen-18 that did not go farther fractionations while the axial of Ririba rift and lower plain sector near Megado depicts a relatively enriched Oxygen-18 that shows fractionation due to evaporation. In general, three recharge mechanisms can be identified from the environmental isotope analysis (Figure 6.11 and 6.12). These are:

1) Recharge from direct precipitation 2) Recharge from regional groundwater and/or fast selective recharge from intensive rainfall and 3) Recharge from flash floods mechanisms.

The first mechanism is observed in the higher altitude of the recharge area. Due to orographic effect the upland mountains receive relatively high rainfall to reach in excess of soil-moisture deficits and evapotranspiration and thus enhance infiltration to groundwater through fractured rock mass. The second mechanism is observed in middle plain sector, particularly at Gelchet well field. Here, recharge to groundwater is attributed primarily to rains on high land plains and runoff at slope breaks (depleted stable isotopes from mountain catchments). The regional faults in the area help to convey depleted recharged groundwater to lower discharge area. There are also many step faults in middle plains that facilitate fast selective recharges on the plains. The last mechanisms observed along the axial Ririba fault, at Ambo and Sarite plains. In this case, the floods sourced from elevated area enter through faulted system to reach groundwater after being evaporated on way of flooding.

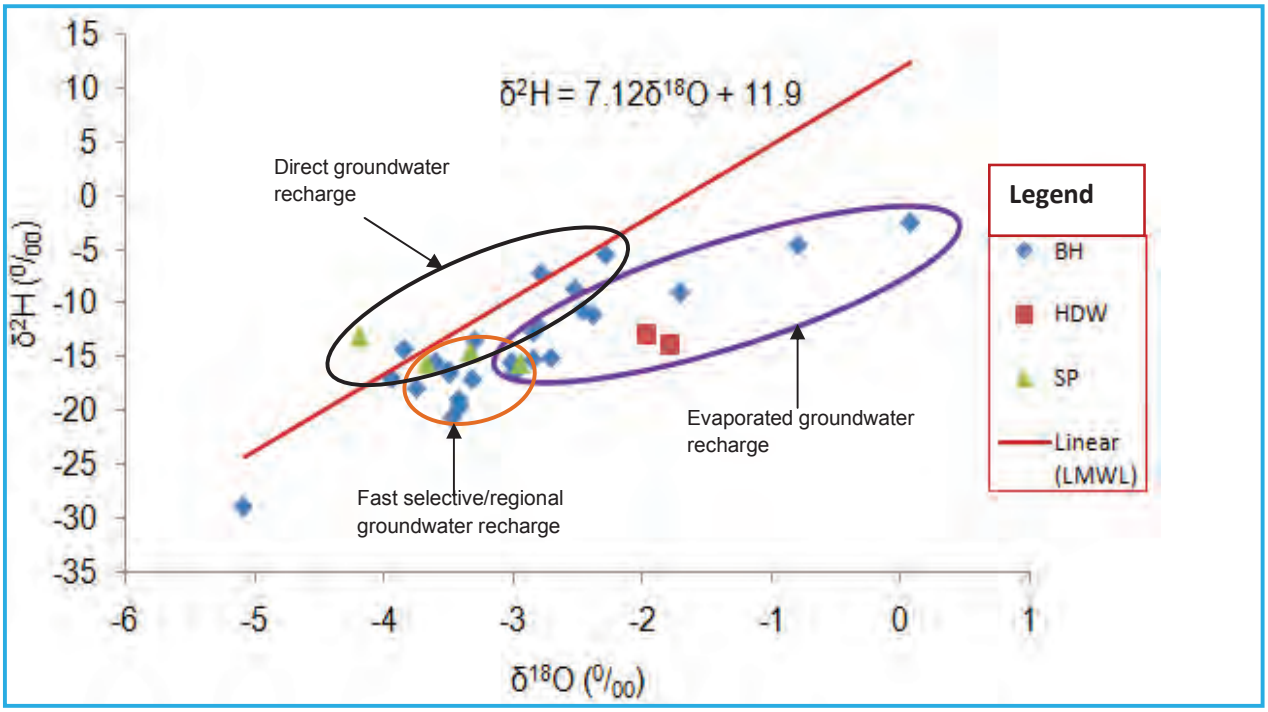

Figure 6-11*: Oxygen-18 vs. Deuterium plot*

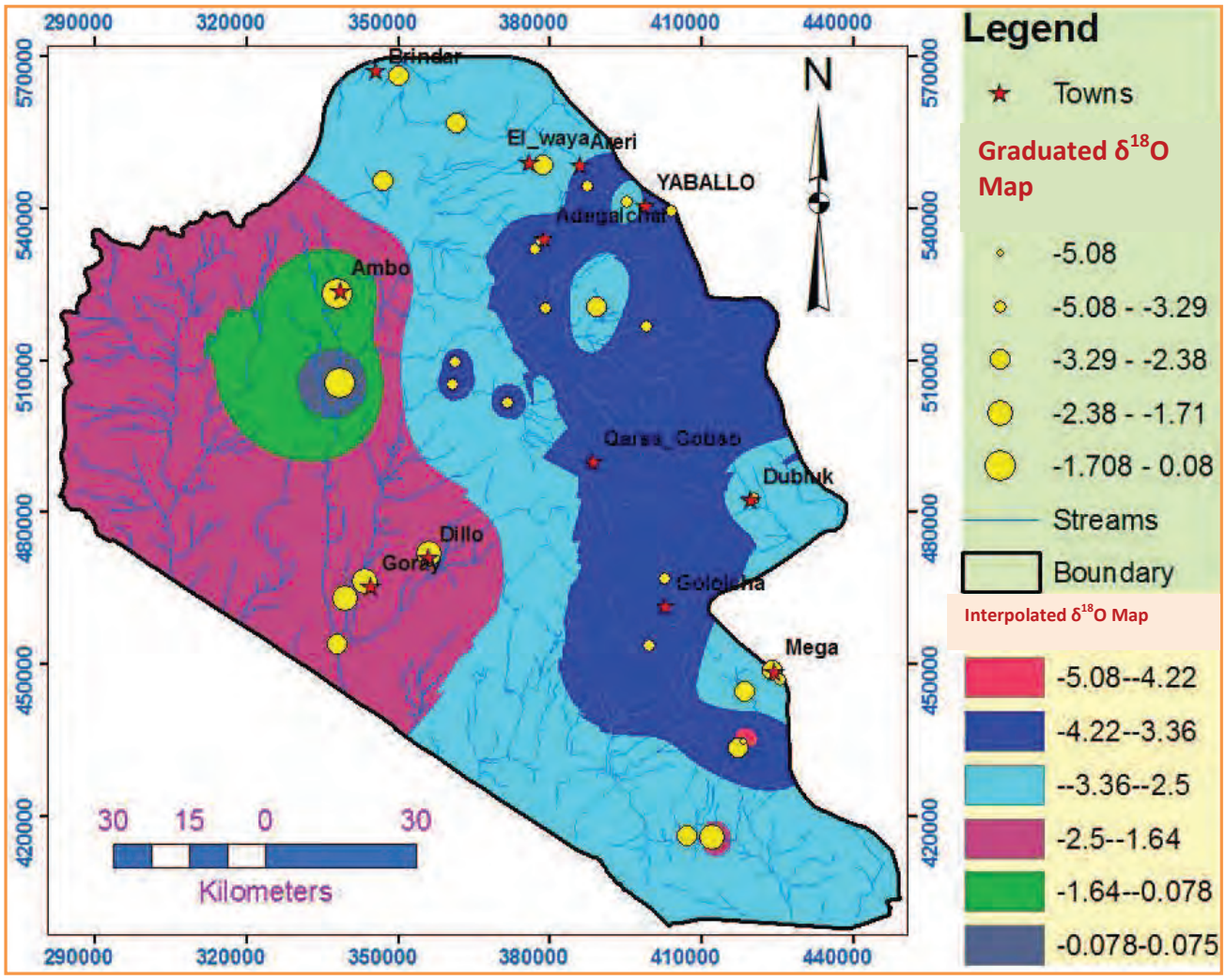

Figure 6-12*: Spatial distribution map of Oxygen-18*

6.6. RECHARGE ALTITUDE

Usually the isotopic composition of precipitation changes with the altitude of the terrain and becomes more and more depleted in $\delta^{18}O$ and $\delta^{2}H$ at higher elevations. This has enabled one of the most useful applications in isotope hydrology, namely the identification of the elevation at which groundwater recharge takes place. This altitude effect is temperature-related, because the condensation is caused by the temperature drop due to the increasing altitude.

The relation between altitude and $\delta^{18}O$ was used to estimate the recharge altitude for Gelchet well field which is postulated to get its recharge from higher elevations. The relation is represented with equation of **$\delta^{18}O = -0.001h - 1.454$; $R^2 = 0.186$**., where **h** is the altitude above sea level in meter (Figure 6.13). Hence, the altitude effect on isotopic composition in the research area shows that $\delta^{18}O$ depletes with $-0.1^0/_{00}$ per 100m elevation rise. From the equation one can notice that there is little relation between the isotopic composition and altitude, hence altitude effect in the study area is not as such significant. However, to estimate the recharge altitude for those water samples like Gelchet well field showing similar isotopic signature with higher altitude, the Biliko isotopic composition ($-2.28^0/_{00}$) and altitude (789m) is taken to represent the lower plains. Based on this the recharge altitude for Gelchet and Alabor wells is estimated (Table 6.1). Because these wells represent the rest wells receiving their recharge source percolating at higher altitudes.

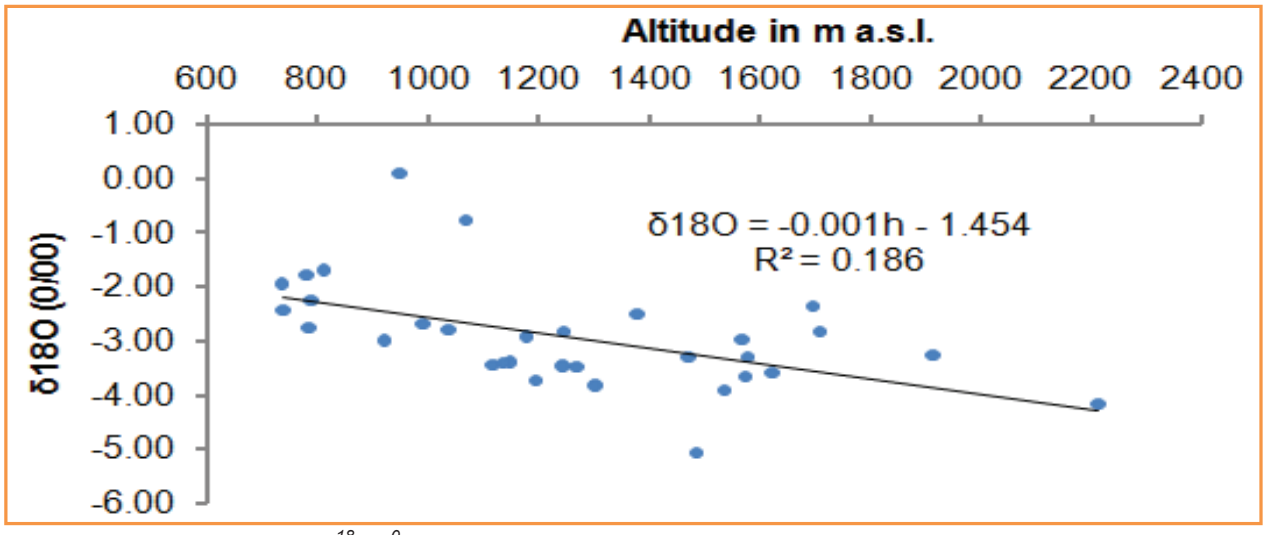

Figure 6-13: *Altitude (m) vs. $\delta^{18}O$ ($^0/_{00}$) plot for water samples collected for isotope analysis*

Table 6-1*: Estimated recharge altitude for Gelchet and Alabor wells.*

Well	Altitude (m) a.s.l.	Well depth(m)	$\delta^{18}O(^0/_{00})$	Recharge altitude (m) a.s.l.	Remark
Gelchet (BH1)	1118	185	-3.47	2308	Recharge area could be near Yabello/Gololcha
Alabor (BH15)	785	214	-2.78	1326	Could be from elevated Mega high lands

6.7. CHLORIDE VERSUS OXYGEN-18($^0/_{00}$)

Stable isotope is a very useful tool in identifying source of groundwater salinity. Salt dissolution from sediment or halite increases the total dissolved solids but does not change the content of stable isotope. However, if the cause of salinity in groundwater is resulted from evaporation simultaneous increase in both stable isotope content and salinity will occur. Figure 6.14 clearly shows that the high TDS for instance, from Brindar, Gelchet and Dubuluk localities is resulted from salt dissolution where as the TDS for instance, from Dillo and Goray craters is from intensive evaporation so as these water sample were from open hand dug wells. The wells at Liso area (center of Ririba rift) and Ambo have relatively moderate TDS but enriched in isotopic composition of $\delta^{18}O$ that signifies locally recharged water from evaporated pools or runoff rather than recharged at high elevated recharge area of the sub-basin. The Gof-Gedo well shows much diluted in salinity and much depleted in $\delta^{18}O$. This signifies the water is originated from precipitations falls on higher altitude that did not undergoes much water rock interactions.

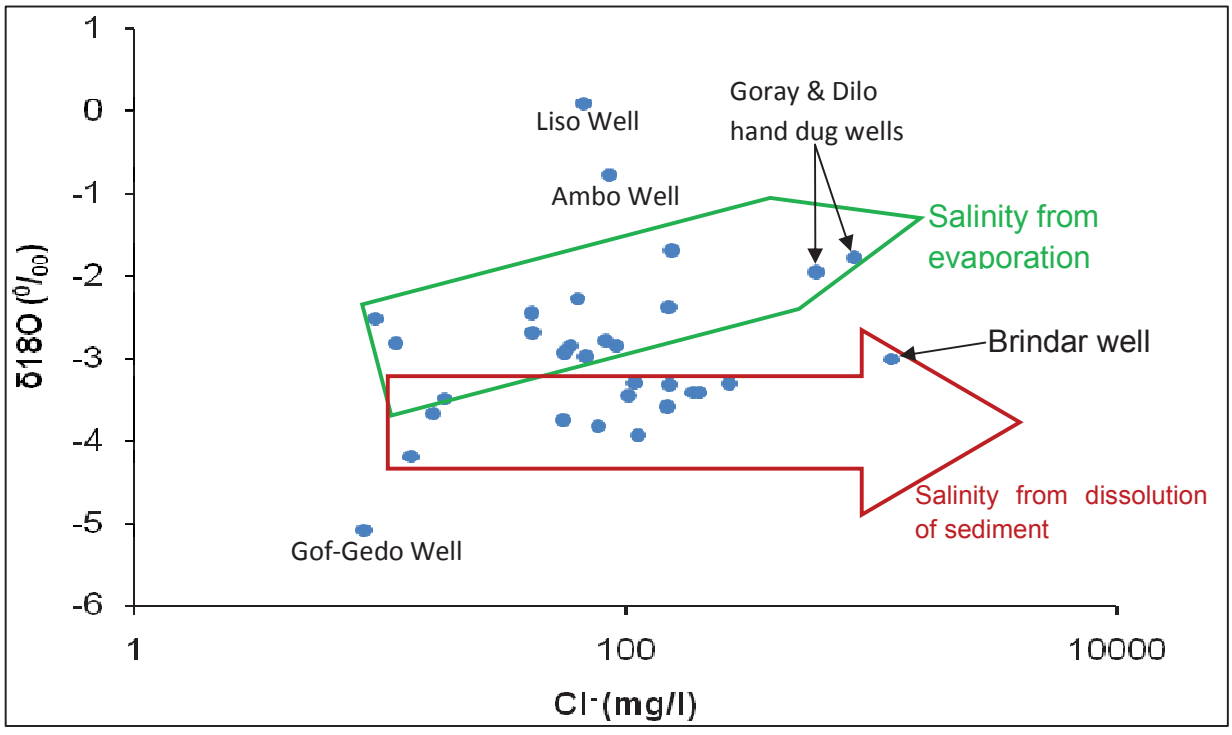

Figure 6-14: *Chloride (mg/l) vs. Oxygen-18 ($^0/_{00}$) plot*

6.8. GROUNDWATER AGE AND SUSTAINABILITY

Determining the mean subsurface residence time or "age" of groundwater is important for several reasons. Groundwater age translates roughly to renewability, which is a critical factor for water resource planning. Unless otherwise groundwater recharge in semiarid and arid area linked to modern day recharge, exploiting it may lead to groundwater mining. Tritium and carbon 14 are the most widely used dating tools for groundwater. Tritium (^3H) is an unstable isotope of hydrogen with a half life of 12.3 years. Prior to atmospheric nuclear bomb testing in the 1950's, tritium's natural average concentrations ranged from approximately 2 to 8TU. The largest tritium concentrations reached peak in 1963. It is assumed that ^3H less than 0.8TU indicates sub modern water (prior to 1950s), 0.8 to 4TU indicates a mix of sub modern and modern water and 5 to 15TU indicates modern water (<5 to 10 years).

Three ^3H results were obtained from OWWDSE, 2011. The samples were collected from Megado/Biliko, Goray and Harawayu and their ^3H content are -0.25, 0.10 and 0.40TU respectively. Harawayu is located at recharge area while the rest are at discharge area. Hence, the result slightly shows that groundwater age increases from recharge to discharge. The tritium content of groundwater in Borena, particularly from crystalline terrain bordering the study area shows over modern age, mainly post 1950's (Figure 15). Few carbon 14 data also reveals that the majority of the waters are modern (see Annex 8). Thus the groundwaters are primarily modern and shows recharge is sustainable (OWWDSE, 2011).

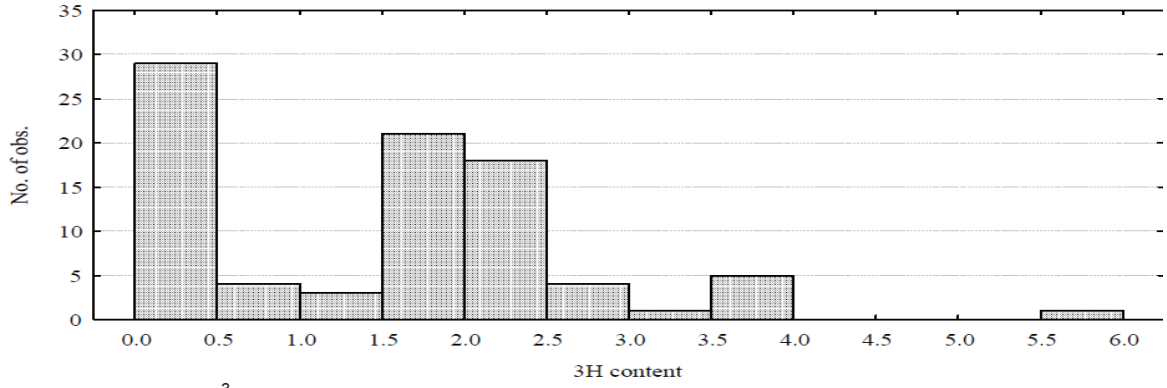

Figure 6-15: *Range of ^3H content of groundwater in Borena (Adopted from OWWDSE, 2006)*

6.9. GROUNDWATER RECHARGE ESTIMATION

Groundwater recharge is an important component of the water balance and evaluation of groundwater resources largely depends on it (Freeze and Cherry, 1979). Thus quantification of the rate of natural groundwater recharge is a basic prerequisite for efficient groundwater resources management, i.e. for developing an effective water shade management strategy that will ensure the protection of groundwater resources not only from climate change, but also from other stresses. However, accurate spatial and temporal characterization of groundwater recharge can be difficult due to its dependence on a multitude of hydro-metrological elements such as rainfall, evapotranspiration, and hydrogeological heterogeneity (Lerner *et al*., 1990).

Groundwater recharge is affected by many parameters and complex processes which themselves are influenced by many factors. The key environmental factors controlling recharge are climate, soils and geology, vegetation and land use, topography, and depth to water table. Precipitation is affected by climatic factors such as wind and temperature, resulting in complex and dynamic distributions while the intensity and spatial distribution of precipitation influences the amount of recharge.

In arid and semiarid regions, application of water-balance and Darian method is more difficult than in humid regions because precipitation is frequently only slightly different from actual evapotranspiration; small errors in these two components thus cause large errors in recharge estimates. Moreover, the extreme temporal variability of semi-arid climates magnifies the error unless otherwise long time series monitoring are conducted to assess mean annual recharge rate. Hence, indirect, physical approaches, such as water balance and Darcy flux measurements were found the least successful whereas methods using tracers (such as Cl, ^{3}H, and ^{36}Cl) have been found to be the most successful. Of the tracer techniques available, Cl-mass balance techniques appear to be the simplest, least expensive, and most widely used for recharge estimation (Sophocleous, 2004). Although there are multiple uncertainties in using CMB for recharge quantification, it was the only method applied in this research as the other methods may relatively produce the most uncertainties.

From previous works OWWDSE had attempted to quantify the groundwater recharge amount. This study used water balance, rainfall-recharge relationship, and Kirchner formula and chloride mass balance methods. The results obtained from these methods were 54, 59, 69 and 39mm/yr respectively. The CMB method used 700mm/yr annual rainfall representing the highland regions and 2 to 3mg/l mean rainfall chloride content representing East African rainfall. EGS (2000) had also estimated groundwater recharge rate between 10 and 40mm/yr using well-mixed model (aquifer porosity and saturated aquifer thickness). However, most of the data used were outside of this study boundary.

6.9.1. Chloride Mass Balance Method (CMB)

Chloride, one of the most common elements in groundwater, which only precipitates at very high concentrations, has been recognized as an ideal conservative tracer of water-cycle processes (Huang, 2010). Environmental tracers such as chloride (Cl) are produced naturally in the Earth's atmosphere and are used to estimate recharge rates (Allison and Hughes, 1978; Phillips, 1994). Chloride is deposited as dry and as wet (dissolved in rainwater) fallout. Most plants do not take up chloride; therefore, it is concentrated in the soil in proportion to the actual evapotranspiration. Chloride in the soil can hence be used as an indicator of evaporative enrichment and groundwater recharge. The availability of longer runs of data of rainfall chemistry is necessary in order to apply the CMB technique in estimating recharge with limited uncertainties. In this project, however, only one month mean rainfall concentration was used which could not represent for variable climatic changes.

According to Allison *et al*., 1985, 1994, Edmunds *et al*. 1988: it was assumed that the only source of chloride is from the soil surface, either by rainfall or dry deposition, and that there is no contribution of chloride from weathering of geological materials. The recharge rate is, hence, given by:

$$P * Cl_p + D = R * Cl_{gw}$$

Where P is mean annual rainfall in mm/yr, Cl_p is the mean chloride concentration of rainfall in mg/l, D is dry deposition, R is the mean annual recharge rate and Cl_{gw} is the mean chloride concentration in groundwater.

From the above equations the annual groundwater recharge can be rewritten as:

$$R = \frac{P * Cl_p + D}{Cl_{gw}}$$

However, in the research area there is no any monitored data for Cl concentration fallout as dry deposition. The dry deposition fallout is, therefore, considered to be zero. The unsaturated soil thickness in most area is thick and hence the Cl content reaches equilibrium until reaches groundwater table. This means that the concentration of Cl from dry deposition fallout is insignificant relative to the depth of water table. Hence, the above equation is reduced to:

$$R = \frac{P * Cl_p}{Cl_{gw}}$$

It can be well noticed that in semi-arid environs like the present research area, where evapotransipiration is much higher than precipitation, higher Cl concentration is expected in groundwater than in precipitation and can thus underestimate the annual groundwater recharge. further more, there is variable thickness of sediments and lacustrine deposits. In periods of intense flooding, the waters are retained in this deposit for a while, producing a concentration of salts (mainly chlorides) by evaporation, which may have hydrochemical implications when they are dissolved by rainfall and runoff waters (Cerón, 1997). The Chloride which remained in sediment is leached out to the groundwater. Therefore, the applicability of CMB may underestimate the recharge of the area unless otherwise selective wells at thin sediment deposit are used. Accordingly, very shallow and open hand dug wells in thick sediment containing concentrated Cl were discarded and only the Cl content from medium well depths, hand-dug wells and springs which fall in subgroup 1 and 2 were used. Because, the water which belong to these subgroups have not under gone longer water-rock interactions and therefore, little or no input of chloride ion expected from the soil or rocks. From subgroup 2, some wells with very high chloride content had also been removed.

In general, for the applicability of CMB the following assumptions have been made in selected water sources (deep wells, hand-dug wells and springs);

- ✓ Chloride mass flux into the system has not changed over time
- ✓ Bulk wet is the only inputs of chloride to the system; Chloride from dry fall is negligible
- ✓ Chloride is conservative in the system
- ✓ No external surface water or groundwater input occurs in to the system
- ✓ The system is at steady state
- ✓ No runoff from the system occurs; the runoff remains in lower flat lands of the area

6.9.1.1. Rainwater Chloride

One month rainfall water (mid September to mid October, 2011) was collected from Mega and Yabello stations. The mean rainwater chloride concentration in the area is 0.91mg/l and has zero standard deviations and has a low detection limit.

6.9.1.2. Groundwater Chloride

The total water samples show very high standard deviations in groundwater chloride content. This variability of chloride concentration signifies the availability of other chloride sources apart from atmospheric fallout (Table 6.2). Therefore, chloride concentrations of water samples categorized under subgroup 1 and some manually selected water samples from subgroup 2 were used for the recharge estimation (Annex 7 and Figure 6.16).

Table 6-2*: Statistical description of Cl concentration in mg/l in the study area*

Minimum	Maximum	Harmonic mean	Average	SD
8.64 (Gof-Gedo)	2330 (Sarite)	47.5	212.8	368.3

To estimate the groundwater recharge rate by CMB, harmonic mean of chloride content in groundwater should be used, (Eriksson, 1985). The Harmonic mean of the Cl_{gw} is calculated as in formula of:

$$\text{Harmonic mean} = \frac{N}{\Sigma_{i=1}^{n}(1/Cl_{gw})}$$

Where N is number of data used, Cl_{gw} is groundwater chloride content in mg/l in each respective sample.

The number of data used is 27 (see Annex 7) and thus the harmonic mean for this data is 19.2mg/l. Hence the estimated recharge using CMB is 28mm/year, which is 4.74% of the annual mean rainfall (590.8mm/yr) of the area (Table 6.3).

Table 6-3*: Estimated groundwater recharge rate for the study area*

Harmean Cl_{gw}	Cl_p	Annual Rainfall	Groundwater Recharge
19.2mg/l	0.91mg/l	590.8mm/yr	28mm/yr

Given that input chloride concentrations can vary significantly from site to site within a region of investigation, it is unsurprising that CMB estimations are site specific. Groundwater recharge rate varies therefore, from 11.37mm/yr to 62.23mm/yr, which is 1.92% to 10.5% of the annual rainfall (Annex 7).

Attempt had also been made to estimate spatial variations of groundwater recharge using mean annual rainfall and harmonic mean of Cl concentrations in groundwater between each respective rainfall contour intervals (Iysohyetal contour) (Table 6.4 and Figure 6.17). The amount of recharge rate estimated shows variations mainly with topography, groundwater Cl content and annual rainfall amounts. The northwestern (Mermero), northeastern (Yabello) and eastern (Mega) sectors get highest recharge rates where as the southwestern sectors get the lowest. The recharge rates estimated at each spot for different sources of groundwater verifies the above results that show higher recharge near Yabello, Megado, Mega, and Mermero localities (Figure 6.16). Here, however, the amount of recharge varies with in small spatial variation that reflects variations of Cl content in groundwater with variable topography, geology, and climates.

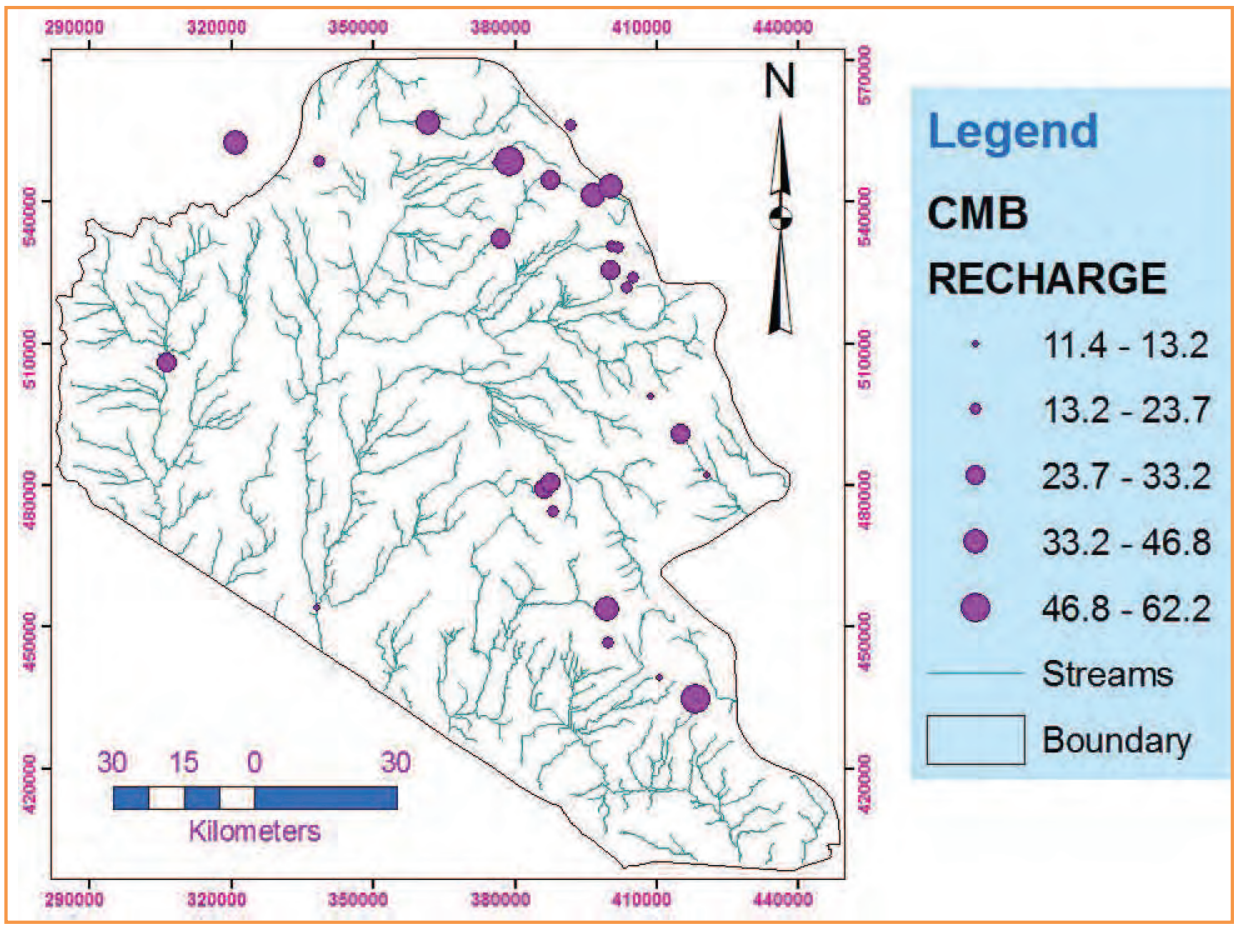

Figure 6-16*: Spatial distribution map of groundwater recharge amount estimated from CMB method*

Table 6-4*: Mean annual rainfall and groundwater recharge rate between rainfall iysohyetal contour intervals*

P Range (mm/yr)	**P**(mean)(mm/yr)	Cl_p (mg/l)	Harmean Cl_{gw}(mg/l)	P^*Cl_p	**R (mm/yr)**
<450	450	0.91	75.8	409.5	**5.4**
450-500	475	0.91	75.8	432.25	**5.7**
500-550	525	0.91	26.21	477.75	**18.23**
550-600	575	0.91	18.99	523.25	**27.55**
600-650	625	0.91	18.22	568.75	**31.22**
>650	650	0.91	17.95	591.5	**32.96**

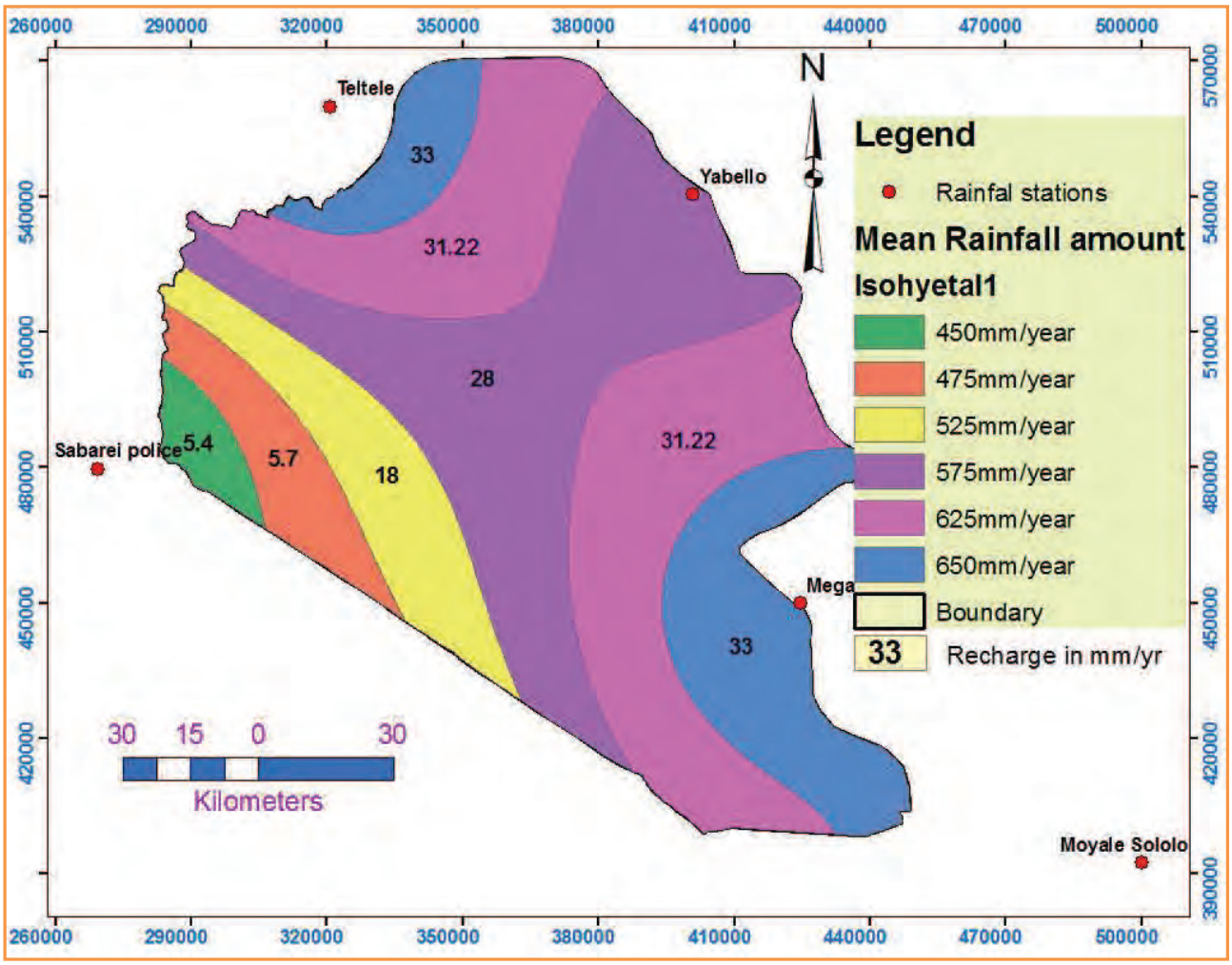

Figure 6-17*: Spatial variation of annual groundwater recharge rate estimated from CMB method and mean rainfall amount between each respective Iysohyetal contour intervals.*

7. CONCLUSION AND RECOMMENDATION

7.1. CONCLUSION

The Borena groundwater chemical composition in general varies over a wide range and broadly distributed rather than forming distinct clusters. It is characterized by different water facies even within few kilometer intervals. However, three main water types can be distinguished depending on their position on a Piper diagram. These are Ca-Mg-HCO_3, Na-HCO_3 and Ca-Mg-SO_4-Cl/Na-Cl/SO_4 water types. Generally Ca-Mg-HCO_3 type waters occur in areas of recharge (generally topographically higher areas) and Na-Cl/Na-SO_4 type waters in discharging rift (i.e. the lower lying areas). The intermediate water types are a result of hydrogeochemical processes that occur between the two end members of Ca-Mg-HCO_3 and Na-Cl/Na-SO_4.

From HCA three major groups based on their TDS value and ten subgroups based on visual examination were selected. In each subgroup distinct hydrgeochemical processes were clearly observed. It shows groundwater evolutions and flow directions from the highland escarpments to the lowland plains and rift sector.

About 71.3% of calcite has positive indices which are slightly over saturated with calcite, particularly for those samples categorized in subgroup 1. SI of anhydrite and halite are all negative, which indicates under saturation with respect to groundwater during flow processes.

The dissolution of minerals like olivine, pyroxenes, plagioclase, anhydrite, halite and dissolution of CO_2 gases are required to derive the observed natural groundwater chemistry in the area. In most cases, this dissolution is balanced by the precipitation and/or weathering of calcite minerals, and clay minerals like Ca-montmorilonite, chalcedony, illite, and K-micas. Cation exchange reactions, particularly in Sarite lower plains, were also controls to a lesser extent the chemical composition of groundwater. Furthermore, from the correlations of Oxygen-18 isotopic composition and chloride content intensive evaporation and dissolution and/or sediment leaching can be distinguished as salinity sources.

The isotopic composition of Oxygen-18 and Deuterium in groundwater varies from -5.08$^0/_{00}$ to 0.08$^0/_{00}$ and from -29$^0/_{00}$ to -2.4$^0/_{00}$ respectively. The mean composition is -2.93$^0/_{00}$ for Oxygen-18 and -13.9$^0/_{00}$ for Deuterium. Some isotope compositions were plot on a LMWL indicating a predominantly meteoric source. Most of the isotopic compositions were deviated from the LMWL in a direction indicative of fractionation due to possible strong evaporation. In this work the altitude effect on $\delta^{18}O$ composition shows a depletion of -0.1$^0/_{00}$ per 100m elevation rise. The analysis result of environmental isotope in general identifies three recharge mechanisms. These are direct precipitation recharge, regional groundwater recharge and/or fast selective recharge from intensive rainfall and flash floods recharge mechanisms. These mechanisms were observed in higher altitude recharge areas, in middle plain sector; particularly at Gelchet well field and along the axial Ririba rift and lower plain sectors respectively.

The hydrogeochemical and environmental isotope analysis clearly indicates that the regional groundwater flow direction are from the elevated basement rocks near Elwaya, Yabello, Utalo, Gololcha via the middle plain sectors of Gelchet to the main north-south trending Ririba fault, from the elevated middle east of the study area (Arbale/Sayole area) to Megado/Biliko lower plains and from the southeastern extreme (Shanacha locality) to west direction and then returns to south following the replica of surface flows. Based on the current available data, the flow directions from northwest elevated volcanic rocks (Mermero area) seems vertical deep circulation in vertically fractured basalt aquifer instead of directly flowing to Ririba valley. But this needs further investigation for verification.

The groundwater recharge rate estimated for the sub-basin using chloride mass balance method is 28mm/yr. The amount of recharge rate estimated shows variations mainly with topography, groundwater chloride content and annual rainfall amounts. The northern (Mermero), northeastern (Yabello) and eastern (Mega) parts of the area get highest where as the southwestern and southern sectors get the lowest recharge rates.

7.2. RECOMMENDATION

Based on the result of current investigation the following recommendations are made:

- In the Northwestern and Western sector of the study area, similar hydrgeochemical processes is observed from HCA. The water types are dominated by Na-Ca-HCO_3 and Na-HCO_3 and represent intermediate rock-water interactions and water in the process of moving. However, as this cluster falls dominantly in recharge area, such facies might indicate deep groundwater circulation or slow groundwater flow that is associated with less permeability of the aquifer, as most of the basalt in which this subgroup falls is tertiary middle (Teltele) and upper basalt. However, in this work no water sample obtained for environmental analysis from this part as the available wells were not functioning at the time of sample collection. For this sector, hence, environmental isotope analysis should be conducted to verify and supplement the hydrochemical result.

- The chloride concentrations vary seasonally or annually depending upon the intensity of the moisture flux due to the incident rainfall and evapotranspiration. The availability of longer runs of data of rainfall chemistry as well as Cl concentration fallout as dry deposition is necessary in order to apply the CMB technique to estimate the groundwater recharge with limited uncertainties. Therefore, monitoring of rainfall and fallout as dry deposition chloride chemistry for a long time in this lowland is very crucial.

- To see the sustainability of groundwater some secondary tritium data were used in this work. However, most of them are falls in crystalline terrain bordering the study area and thus cannot give realistic interpretation on sustainability of groundwater in the study area. Therefore, sampling groundwater for tritium content analysis is highly recommended.

REFERENCES

Addis Hailu (2011). Groundwater-Surface water interaction and recharge estimation using hydrogeochemistry and isotope hydrology; Blue Nile Basin, Ethiopia. University of Addis Ababa, Addis Ababa, Ethiopia, Unpublished MSc Thesis.

Adams S., Titus R., Pietersen K., Tredoux G., Harris C. (2001). Hydrochemical characteristics of aquifers near Sutherland in the Western Karoo, South Africa. Journal of hydrology, vol. 241, pp 91–103.

Adomako D., Gibrilla A., Akiti T., Fianko R., Maloszewski P. (2011). Hydrogeochemical evolution and groundwater flow in the Densu River Basin. Journal of Water Resource and Protection, Ghana, Vol. 3, PP 548-561.

Alema Tesfaye (2009). Steady-state groundwater flow and contaminant transport modeling of Akaki welfield and its surrounding catchment, Addis ababa, Ethiopia. International Institute For geo-information Scienc and earth observation, the Netherlands, unpublished MSc thesis.

Ali M. Subyani (2004). Use of chloride-mass balance and environmental isotopes for evaluation of groundwater recharge in the alluvial aquifer. Journal of environmental geology, Wadi Tharad, Western Saudi Arabia, Vol. 46, PP 741-749.

Andarge Yitbarek (2009). Hydrogeological and hydrochemical framework of complex volcanic system in the Upper Awash River basin, Central Ethiopia: with special emphasis on inter-basins groundwater transfer between Blue Nile and Awash rivers. University of Poitiers, Unpublished PhD Thesis.

Anderson, M. P. & Woessner, W. W. (1992). Applied groundwater modeling: Simulation of flow and advective transport. San Diego Academic Press

Andrew S. Wilson (2005). Hydrogeology, conceptual model and groundwater flow within alluvial aquifers of the Tenthill and Mama Catchments, Lockyer Valley, Queensland. University of Technology, Queensland, MSc thesis.

Appelo C.A.J. and Postma D. (2005). Geochemistry, groundwater and pollution (second edition), Amsterdam, the Netherlands, pp.649.

Appelo C. A. J. and Postma D. (1992). Geochemistry, Groundwater and Pollution. Lyngby,Amsterdam

Athanael R. (2008). Groundwater recharge assessment in the Makutupora basin, Dodma Tanzania. International Institute for Geo-information Science and Earth Observation, the Netherlands, MSc thesis.

Bizune Bekele (2011). Hydro chemical and isotopic characteristics of the groundwater system of Alleydege Plain. University of Addis Ababa, Addis Ababa, Ethiopia, Unpublished MSc Thesis.

Clark I. D. and Fritz P. (1997). Environmental isotopes in hydrogeology. Lewis Publishers,New York.

Cerón J.C., Jimenez-Espinosa R.Pulido-Bosch A. (2000). Numerical analysis of hydrogeochemical data: a case study (Alto Guadalentin, southeast Spain). Journal of geochemstiry Vol. 15 pp 1053-1067.

Coppock L.D. (1994). Synthesis of pastoral research, development and change in the Borena plateau of southern Ethiopia, the Borena Plateau of southern Ethiopia.

Cüneyt Güler, Geoffrey D. Thyne · John E., McCray A. Keith Turner (2002). Evaluation of the graphical and multivariate statistical methods used for classification of water chemistry data. Journal of Hydrogeology, Vol. 10, pp 455–474.

Dana J. D. (1995). Manual of Mineralogy (20th edition). Pp. 598.

Demilie M., Wohnlich S., Wisotzky F., Gizaw B. (2007). Groundwater recharge, flow and hydrogeochemical evolution in a complex volcanic aquifer system, central Ethiopia. Journal of Hydrogeology, V.15, PP 1169–1181

EGS (Ethiopian Institute of Geological survey) (2004, 1999 & 1991). A report on regional geological mapping of the Yabello, Sololo and Hagere-Mariam area. Unpublished Report, Addis Ababa, Ethiopia.

EGS (Ethiopian Institute of Geological survey) (2000). A report on hydrogeological and isotope hydrological investigation in part of Genale-Dawa basin. Unpublished report, Addis Ababa, Ethiopia.

Fetter C.W. (2001). Applied Hydrogeology (fourth edition). Prentice-Hall, Inc. Upper Saddle River, New Jersey, PP. 598.

Fetter C.W. (1994). Applied Hydrogeology (third edition). Prentice-Hall, Inc. Upper Saddle River, New Jersey, PP. 654.

Freeze A. R. and Cherry J. A. (1979). Groundwater. Prentice-Hall, Inc.

Getachew Hadush, (2008).Groundwater contribution and recharge estimation in the uppers Blue Nile flows, Ethiopia. International Institute for Geo-information Science and Earth Observation, the Netherlands, Unpublished MSc Thesis.

Gibson J.J., Edwards T.W.D., Bursey G.G (1993). Estimating evaporation using stable Isotopes: quantitative results and sensitivity analysis for two catchments in northern Canada in: 9th Symposium/workshop on Northern Res. Basin, Canada-august 1992 .Nordic hydrology, Vol. 24, PP 79-94.

Güler S. C. (2003). Hydrologic and geologic factors controlling surface and groundwater chemistry in Indian Wells-Owens Valley area, southeastern California, USA. Journal of Hydrology pp. 1-22

Hem J.D. (1989). The study and interpretation of the chemical characteristics of natural water (3rd edition). USGS Water-Supply Paper 2254, US Geological Survey, pp. 263.

Hounslow, A.W. (1995). Water quality data analysis and interpretation, Boca Ratonj etc: CRC Lewis.

Huang T., Pang Z. (2010). estimating groundwater recharge following land-use change using chloride mass balance of soil profiles: a case study at Guyuan and Xifeng in the Loess Plateau of China. Journal of Hydrogeology.

Lerner D.N., Issar A.S. and Simmers I. (1990). Groundwater recharge: A guide to understanding in estimating natural recharge. International contribution to Hydrogeology, Vol. 8, pp 345.

Kohfahl C., Sprenger C., Jose Benavente Herrera J.B., Meyer H., Chaco´n F., Pekdeger A., (2008). Recharge sources and hydrogeochemical evolution of

groundwater in semiarid and karstic environments a field study in the Granada Basin (Southern Spain). Applied Geochemistry, Vol. 23, PP 846–862

Kovalevsky V. S., Kruseman G.P., Rushton K.R. (2004). Groundwater studies an international guides for hydrogeological investigations, Series on groundwater no 3, UNESCO, PP.430

MAB CONSULT–Consulting Hydrogeologists and Engineers (2009). A report on groundwater potential zone mapping using GIS and Remote sensing - moyale-teltele sub basin - dire, arero, yabelo and teltele woredas, borena zone of oromia regional state. Unpublished Report.

Mazor E. (2004). Chemical and Isotopic groundwater hydrology (third edition). Weizmann Institute of Science Rehovot, Israel; Marcel dekker, Inc. pp 453.

MoWR (Ministry of Water Resources) (2005). A report on Genale Dawa River Basin Master Plan Study Project. Unpublished report, Addis Ababa, Ethiopia.

MoWR (2002). Ethiopian Guideline Specification for Drinking Water Quality. Ministry of Water Resource, Addis Ababa.

Nwankwoala, H.O., Udom, G.J., 2011. Hydrochemical facies and ionic ratios of groundwater in Port Harcourt, southern Nigeria. Research Journal of Chemical Sciences, 1(3):87- 101.

OWWDSE (Oromia Water Works Design and Supervision Enterprise) (2011). A report on Borena groundwater potential assessment project in the south and southwest of Yabello town volcanic plains. Unpublished report, Addis Ababa, Ethiopia.

OWWDSE (Oromia Water Works Design and Supervision Enterprise) (2006). A report on geology for Borena groundwater potential assessment project in the south and southwest of Yabello town volcanic plains. Unpublished report, Addis Ababa, Ethiopia.

Pang H., He Y., Zhang Z., Lu A., Gu J. (2004). The origin of summer monsoon rainfall at New Delhi by deuterium excess. Journal of Hydrology and earth system Sciences, China, Vol. 8, PP 115-118.

Pierre P. D., Plummer L.N. (2005). Geochemistry and the understanding of ground-water systems. Journal of Hydrogeology, Vol.13, pp 263–287

Rwebugisa R. A. (2008). Groundwater recharge assessment in The Makutupora, Dodoma Tanzania. International Institute For geo-information Science and Earth Observation, the Netherlands, Unpublished MSc Thesis.

Seifu Kebede, Travi Y., Tamiru alemayehu, Tenalem Ayenew (2005). Groundwater recharge, circulation and geochemical evolution in the source region of Blue Nile river, Ethiopia. Journal of applied geochemistry, vol. 20, pp 1658-1676.

Seifu Kebede (2004). Environmental isotope and geochemistry in groundwater and lake hydrology, cases from Blue Nile basin and main Ethiopian rift, Ethiopia. University of Avignon, PhD Thesis.

Shaw. E.M., Beven K.J., Chappell N.A., Lamb R. (2011). Hydrology in practice (Fourth edition), pp.543.

Sophocleous M., (2004). Groundwater recharge, in Groundwater, [Eds. Luis Silveira, Stefan Wohnlich, and Eduardo J. Usunoff], in Encyclopedia of Life Support

Systems (EOLSS), Developed under the Auspices of the UNESCO, Eolss Publishers, Oxford, UK, [http://www.eolss.net]

Stevens H.H., John Gr., ficke F., Smoot G.F. (1978). Water temperature-influential factors, field measurement, and data presentation, chapter D1, USGS Science for changing World.

Stimson J., Frape S., Drimmie R., Rudolph D. (2001). Isotopic and geochemical evidence of regional-scale anisotropy and interconnectivity of an alluvial fan system, Cochabamba valley, Bolivia. Journal of applied geochemistry vol.16, pp 1097-1114.

Tilahun Azagegn (2008). Hydrogeochemical characterization of aquifer systems in upper awash basin and adjacent Abay plateau using geochemical modeling and isotope hydrology. University of Addis Ababa, Addis Ababa, Ethiopia, Unpublished MSc Thesis.

World Health Organization (2004). Guide Lines for Drinking Water Quality (Third edition).Volume.1, recommendations. Pp. 515.

Zagana E., Obeidat M., Kuells Ch. and Udluft P., (2007). Chloride, hydrochemical and isotope methods of groundwater recharge estimation in eastern Mediterranean areas, a case study in Jordan. Journal of hydrological processes, Vol. 21, pp 2112-2123

APPENDICES

Annex 1: *Mean monthly rain fall in and near the project area*

Stations	Country	Jan	Feb	Mar	Apr	May	Jun	Jul	Aug	Sep	Oct	Nov	Dec	Annual
Yabello	Ethiopia	24.8	30.5	61	144	100.5	12.2	8.2	12.1	30.1	95	49.6	15	583
Mega	Ethiopia	23.6	43.3	75.3	158.8	93.9	30.6	34.1	21.9	20	92.7	66.7	27	688
Taltele	Ethiopia	38.4	37.1	88.2	156.5	101	35.4	17.7	10.6	37.2	97.6	59	27.3	706
Moyalle	Ethiopia	13.7	21.7	43.9	150.4	92.2	14.7	7.4	7	14.9	98.9	84.6	27.3	576.8
North Horr	Kenya	13	4	27	40	11	0	3	6	0	10	40	26	180
Moyale Sololo	Kenya	16	20	58	264	69	8	8	9	8	111	126	27	724
Sabarei police	Kenya	26	27	79	67	40	5	7	4	2	20	66	53	396

Annex 2: *Environmental Isotope of Rainfall data (both original and secondary data)*

Sample Id	Locality	Sample Source	$\delta^{18}O$	$\delta^{2}H$	LMWL	d-excess
BR-RF1	Yabello	Original	-3.11	-10.76	-10.23	11.36
BR-RF2	Mega	Original	-3.68	-18.48	-14.3	7.72
BR-RF3	Yabello	Original	-0.7	-2	6.89	3
BR-RF5	Mega	Original	-4.39	-23.72	-19.38	7.57
Eth 81	Hidilola	Secondary	-3.36	-10.6	-12.02	13.32
Eth 84	Hidilola	Secondary	-3.18	-10	-10.74	12.64
Eth 90	Hidilola	Secondary	0.32	14	14.18	11.72
Eth 96	Hidilola	Secondary	-2.42	-6.2	-5.33	11.03
Eth 86	Mega	Secondary	-1.88	1.6	-1.49	14.99
Eth 88	Mega	Secondary	-2.86	-9	-8.46	11.36
Eth 91	Mega	Secondary	-6.2	-37.2	-32.24	6.94
Eth 97	Mega	Secondary	-3.19	-7.5	-10.81	15.21
Eth 79	Moyale	Secondary	-4.22	-17.8	-18.15	12.25
Eth 82	Moyale	Secondary	3.94	27.7	39.95	-0.35
Eth 92	Moyale	Secondary	-1.04	5.7	4.5	13.1
Eth 95	Moyale	Secondary	3.82	31.8	39.1	4.6
Eth 78	Negele	Secondary	-4.16	-10.6	-17.72	19.02
Eth 85	Negele	Secondary	-1.57	1.4	0.72	12.58
Eth 89	Negele	Secondary	-3.82	-13.6	-15.3	13.6
Eth 80	yabello	Secondary	0.56	17.1	15.89	13.11
Eth 83	yabello	Secondary	1	5.5	19.02	-1.62
Eth 87	yabello	Secondary	-1.91	7.2	-1.7	20.8

Annex 3: *Analyzed Environmental Isotope data and on field measured physico-chemical data, (*) represent the data source is BGWPA report of OWWDSE (2011), the other are original data analyzed for this work.*

Sample Id	Easting (m)	Northing(m)	Elevation(m a.s.l.)	Depth(m)	PH	EH(mv/l)	EC(µs/cm)	TDS(mg/l)	T(^{0}C)	δ^{18}O(0/00)	δ^2H(0/00)	D-excess	^{3}T(TU)	Sampling date
BR-BH1(GW1)	360826	505258	1118	185	6.65	21	1124	676	24.5	-3.47	-20.63	7.1		5/9/2011
BR-BH2	339581	463165	1739	232	7.65	-37	1865	1116	24.5	-1.7	-8.94	4.69		6/9/2011
BR-BH3	371540	501553	1150	172.25	7.2	36	1610	943		-3.41	-19.6	7.69		7/9/2011
BR-BH4(BTW10)	338417	505453	949	161	6.5	31	745	446	34.3	0.08	-2.4	-3		7/9/2011
BR-BH5(BTW7)	361304	509658	1137	213	6.39	36	1060	633	33.5	-3.42	-18.97	8.35		7/9/2011
BR-BH6	379120	520197	1197	132	6.82	11	1010	604	30.9	-3.74	-17.89	12.06		7/9/2011
BR-7a	378487	533487	1270		6.2	49	809	485	30.9	-3.5	-16.3	11.68		7/9/2011
BR-BH7	377047	532085	1245	69	6.25	49	737	441	29.8	-3.49	-16.51	11.38		7/9/2011
BR-BH8	346964	545325	992	216	6.54	27	813	487	36	-2.7	-15.08	6.55		8/9/2011
BR-BH9	350065	566262	922	125	7.33	-22	2400	1474	37.7	-3.01	-15.52	8.55		8/9/2011
BR-BH10	361667	556788	1038	89	6.45	32	972	583	29.9	-2.81	-12.03	10.45		8/9/2011
BR-BH11	404143	539599	1624	67	6.27	42	1952	1171	26	-3.6	-15.5	13.27		9/9/2011
BR-BH12	378708	548522	1379		6.54	30	712	427	26.4	-2.52	-8.64	11.51		8/9/2011
BR-BH13	395181	541249	1915		6.27	42	615	369	26	-3.29	-13.46	12.89		9/9/2011
BR-BH14	418353	434964	1487	47	6.5	31	312	188.5	22.9	-5.08	-29	11.66		10/9/2011
BR-BH15(BTW4A)	407196	416266	785	214	6.73	17	1674	1005	31.5	-2.78	-7.19	15.06		10/9/2011
BR-BH16	418497	444596	1569		6.79	14	1031	619	25.5	-2.99	-16.48	7.41		10/9/2011
BR-BH17	424085	448742	1711	47.2	6.93	7	748	450	24	-2.84	-15.23	7.51		11/9/2011
BR-BH18	423996	448723	1699	48	6.66	21	1475	887	22.2	-2.38	-11.06	7.97		11/9/2011
BR-BH19	420379	482683	1472	35	6.7	18	2500	1499	27.5	-3.31	-17.1	9.41		11/9/2011
BR-BH20	338052	523061	1069	162	7.14		672	414	25	-0.79	-4.51	1.83		19/12/2011
BR-BH21	402823	467061	1538	75						-3.94	-17.01	14.48		20/12/2011
BR-BH22*	412154	416043	789	131						-2.28	-5.41	12.83	-0.25	
BR-BH23*	338000	454149	739	134						-2.46	-10.63	9.05	0.1	
BR-BH24*	398972	516763	1304	150						-3.84	-14.26	16.46	0.4	
BR-BH25*	389294	520566	1246	160.74						-2.84	-12.63	10.09		
BR-HDW1	343419	466417	735		6.8	15	7270	4400	29.4	-1.97	-12.92	2.81		6/9/2011
BR-HDW2	356156	471948	781		6.7	20	4830	2950	29.4	-1.79	-13.88	0.46		6/9/2011
BR-SP1	387546	544392	1576		6.72		335	200	24.8	-3.67	-15.67	13.68		9/9/2011
BR-SP2	417295	433446	1180		7.12	-5	2040	1222	22.7	-2.94	-15.67	7.87		10/9/2011
BR-SP3	425431	447100	1580		6.74	18	1220	733	23.4	-3.33	-14.58	12.04		10/9/2011
BR-SP4	399530	453659	2214		7.6		114	70.6	20.7	-4.19	-13.12	20.41		20/12/2011
BR-RF1	400826	540334	1740		7.47		39	23.8	26.2	-3.11	-10.76	14.1		7/11/2011
BR-RF2	424488	449720	1800		7.4		39	24	24	-3.68	-18.48	10.96		7/11/2011
BR-RF3	400826	540334	1740		7.7		28.2	16.89	24.5	-0.7	-2	3.62		7/11/2011
BR-RF5	424488	449720	1800							-4.39	-23.72	11.43		20/12/2011

Annex 4: *Hydrochemical data of water samples in Borena low lands (**) represent the original data generated in this research and for others the data source is the BGWPA report of OWWDSE (2011), units in mg/l unless indicated)*

No	Location	Sample ID	Easting(m)	Northing (m)	Altitude(m)	W. Depth (m)	pH	T (^{0}C)	EC(µs/cm)	TDS	Na	K	Ca	Mg	F	Cl	HCO3	NO3	SO4
1	Gelchet	BR-BH1(GW1)	360826	505258	1118	185	7.95		1236	860	150	12.5	104.9	7.82	1.72	103.6	180.6	16.7	346.8
2	Goray	BR-BH2	339581	463165	811	232	7.5	36.6	1990	1250	325	5.7	81.44	1.08	7.8	155.5	29.3	3.36	550
3	Gobso	BR-BH3	371540	501553	1150	172.25	7.95	30.1	1753	1230	164	14.4	125.2	47.5	1.58	190.09	140.3	10.4	410
4	Liso/Ririba	BR-BH4(BTW10)	338417	505453	949	161	7.66		802	516	114	9.5	39.5	10.2	1.55	66.9	251.1	43.9	25.56
5	Gelechet	BR-BH5 (BTW7)	361304	509658	1137	213	7.25	32.8	1544	1056	160	14	96.8	31.1	1.88	198.6	188.89	1.8	302.5
6	Wayam Kala	BR-BH6	379120	520197	1197		7.5	33.4	1042	712	114	7.7	72.2	22.14	0.05	55.8	218.9	0.3	216.4
7	Adegelchet	BR-BH7	377047	532085	1245		7.8	29.7	720	448	60	4.7	60.9	25.38	0.95	18.24	351.36	1.99	38
8	Sarite/Giwesa	BR-BH8	346964	545325	992	216	7.89	28	860	490	166	3.4	29.1	4.9	1.96	42.24	459.7	0.44	0.8
9	Birindar	BR-BH9	350065	566262	882		7.34	30.2	5180	3492	1080	14.8	154.7	28.6	1.21	1200	418.09	0.44	801
10	Bule Bishan Dhaanan	BR-BH10	361667	556788	1038	89	7.78	29	1052	634	124	5.1	61.7	37.8	1.44	11.5	576.82	10.2	39
11	Olla Bersa/Kella	BR-BH11	404143	539599	1624		7.02	24.3	1170	790	69	4.4	123.5	38.9	1.85	148.8	187.39	44.55	256
12	Elwaya	BR-BH12	378708	548522	1379		7.4	26.2	721	415	56	5.3	83.79	24.3	0.07	9.6	468.48	0.3	0.534
13	Obda**	BR-BH13	395181	541249	1915		7		528	317	77.7	18.3	280	78	0.62	109.2	263	174	4.09
14	Gof Gedo	BR-BH14	418263	434758	1483		7.04	22.1	400	248	16	4.5	34.4	20.52	0.22	8.64	240.1	0.5	6.67
15	Megado/Alabor	BR-BH15 (BTW4A)	407108	416060	785	214	7.8	31.9	1855	1239	186	27	88.2	95.04	0.98	83.5	796.42	21.2	155.5
16	Romso village	BR-BH16	418497	444586	1569		7.6	24.8	1125	727	72	19	118.19	38.3	0.87	69.1	409.92	1.78	131.16
17	Mega Town	BR-BH17	424085	448742	1711	47.2	7.35	22.8	740	446	29	6.2	61.74	48.6	0.28	59.5	337.78	3.8	18.8
18	Did Mega	BR-BH18	425998	445672	1540		7.9	23.4	1418	960	35	7.1	88.2	135.4	0.95	150.7	538.75	0.214	124
19	Dubluk Town	BR-BH19	420112	482697	1476	35	7.96	23.3	1861	1186	200	35.5	74.97	56.16	1.45	263.04	383.6	5.2	168
20	Horbate/Ambo	BR-BH20	338052	523061	1069	162	7.5	33.8	996	616	84	14.5	81.9	41.25	0.95	85.56	460.18	0.1	21.09
21	Gololcha	BR-BH21	402823	467061	1538	75	7.9	22.3	1831	1398	100	7.5	194	91.8	1	111.36	210.82	2.39	654
22	Biliko	BR-BH22	412154	416043	789	131	8.47	31.6	1578	1003	170	28.5	66.15	90.72	0.4	63.36	620.74	20.5	160
23	Goray/Melka Sadeka	BR-BH23	338000	454149	739		8.03	34.9	733	464	84	9.8	40.6	16.7	0.83	41.28	254.7	12.15	82.77
24	Harewayu	BR-BH24	398972	516763	1304		8.15	24.6	1769	1376	156	8.2	164.1	48.6	2.8	76.8	168.36	2.2	671.8
25	Utalo	BR-BH25	389294	520566	1246	160.74	8.39	32.1	617	410	98	3	16.8	2.7	0.47	91.2	53.68	4.19	109.47
26	Dubluk area	BR-BH26 (DUTW-1)	425179	477832	1452	83	7.68	24.5	3240	2324	276	45.5	282.2	81	0.85	576	278.16	16	534
27	Dubluk Town	BR-BH27 (DUTW-2)	419909	482966	1467	60	7.8	25.1	2630	1704	274	36.5	145.5	86.9	0	610.6	480.19	0.22	202.9
28	Gobso	BR-BH28 (BTW-3)	369372	504302	1132	202	7.7	29.2	1159	650	106	10.9	61.41	22.14	0.82	120.96	147.57	7.2	146.3
29	Sarite	BR-BH29 (BTW6A)	345844	527739	966	108	6.93	30.7	4800	3438	650	41	392	48.6	2	1088	276.7	0.66	860.6
30	Sarite	BR-BH30 (BTW6B)	346062	527765	965	294	7.35	34.2	8210	6210	930	79	704	77.8	1.78	2330	175.68	0.5	1002.7
31	Dillo	BR-BH31 (BTW8)	352697	491178	995	215	7.01	37	2100	1365	206	24	177.64	95.37	0.37	107.12	1152.9	3.68	121.86
32	Gelechet	BR-BH32 (GPW2)	362521	507901	1136	204	7.54		1187	768	125	11	82.84	33.74	0.51	105.05	417.61	22.63	174.7
33	Gelechet	BR-BH33 (GW5)	358825	504597	1112	154	7.45		1151	766	132	10.9	60.8	20.52	0.85	106.95	212.65	8.67	248.82
34	Gelechet	BR-BH34 (GW4)	361707	505679	1125	187	7.47		1266	884	126	12.5	83.6	27.36	0.64	109.79	192.15	8.3	341.04
35	Maheir/Furole	BR-BH35	396126	421963	805	210	7.2	34.3	6550	5429	640	80	123.5	734.4	0.55	341.8	3132.96	0.585	1428.3
36	Dubluk Town	BR-BH36	420073	482723	1472	20	7.4	24.9	1254	784	110	26	80.26	46.98	0.82	90.2	491.9	9.62	62.8
37	Borama/Gesu	BR-BH37	401121	535238	1746		7.1	23.8	2780	1656	200	2.3	220	117.2	3.28	604.8	406.9	0.1	134
38	Medhacho	BR-BH38	420413	459077	1569		7.54	25.1	1734	1268	119	12.2	211.7	37.8	1.45	111.36	237.17	0.26	512
39	Anga Arsole	BR-BH39	428684	461190	1474		7.92	24.8	1388	800	234	12.9	30.9	16.2	1.85	150.7	439.2	5.95	68
40	Dembela Bedena	BR-BH40	415127	490919	1542		7.58	25.5	435	272	11.5	18	45.86	19.98	0.2	16.2	228.38	6.1	7.72
41	Ego	BR-BH41	428520	485091	1455	76	8.48	25.2	1550	930	150	29	136.7	24.8	0.6	211.2	283.04	19.63	165
42	Ego	BR-BH42	433721	482285	1416	61	7.84	24	1503	899	152	25	97	37.8	1.75	207.36	360.1	30.26	106
43	Anole	BR-BH43	442268	475284	1377		7.99	23.7	3450	2313	420	46.5	264.6	65.88	1.79	710.4	286.94	27.8	534
44	Angaa Arsole	BR-BH44	429444	460938	1466		8.57	23.7	1171	685	200	16	29.11	11.9	1.55	153.6	189.34	0.25	149.52
45	Birindar	BR-BH45	346344	567057	922		8	41.4	2860	1887	520	17.5	35.3	15.1	6.15	220.8	421.6	0.9	730
46	Chari Arburo	BR-BH46	391665	556156	1549	70	7.56	25.2	1283	840	109	7.1	112.9	32.4	2.5	29.76	292.8	0.41	310
47	Gesu	BR-BH47	399057	537973	1824	60	7.44	23.2	1006	570	68	5.4	101.4	32.4	1.87	131.5	278.16	17.2	58
48	Romso/Didibe	BR-BH48	415808	436192	1490	74	6.7	23.3	1815	1162	103	31	149.9	119.9	0.61	59.5	969.17	0.7	186.9
49	Gotu Tute	BR-BH49	306254	505927	937		7.81	28.9	918	597	145	7.8	50.96	12.65	0.94	19.2	561.2	1	2.14

No	Location	Sample ID	Easting(m)	Northing (m)	Altitude(m)	W. Depth (m)	pH	T (^{0}C)	EC(µs/cm)	TDS	Na	K	Ca	Mg	F	Cl	HCO3	NO3	SO4
50	Cheri Turura	BR-BH50	443048	419387	1326	35	7.09	24.6	2450	1600	136	5	263.9	99	0.36	537.6	325.5	20.5	188.9
51	Did Melle- Melbana	BR-BH51	435391	421252	1403		7.06	25.3	2070	1469	114	32	227.5	118.25	0.92	140.16	813.74	0.9	416.52
52	Melbana-Girriftu	BR-BH52	434101	431696	1394	72	6.93	25.6	2460	1809	124	26.5	327.6	128.7	0.93	141.12	1046.64	0.25	432.02
53	Horbate/Dawa	BR-BH53	324139	528775	1140		8.6	24.7	653	424	160	1.3	2.65	1.08	1.17	76.8	228.38	0.2	15.2
54	Melbana	BR-BH54	442726	430402	1352		7.61	26.4	2240	1562	116	33.5	191.1	115.6	0.54	249.6	510.69	7.76	340.4
55	Silala	BR-BH55	452256	430934	1305		7.57	25.7	2110	1350	178	39.5	109.2	97.9	1.82	259.2	485.44	11.22	340.4
56	Melbana/silala	BR-BH56	454202	431112	1301		7.57	24.9	1903	1220	194	37	118.3	64.9	1.32	197.8	477.02	5.11	232.29
57	Nekayo/Mermero	BR-BH57	305786	513683	965		7.56	31.4	914	580	124	9.4	51.9	15.66	3.1	56.7	434.9	0.3	26.17
58	Shanacha	BR-BH58	439353	411265	1198		6.87	25.7	1035	680	54	2.1	109.2	47.3	1.94	118.08	328.3	3.48	89.45
59	Dhaka Kala	BR-BH59	320975	552429	1436		7.44	29.7	653	418	88	3.8	57.2	10.26	0.32	13.23	392.8	6.47	1.07
60	Dololo Makala	BR-BH60	429636	441835	1458		6.33	27.4	1747	1196	34	11.5	308	58.3	0.29	69.9	926	6.66	128
61	Dilo	BR-BHM61 (WDW2)	351284	495846	1101	215	7.4		1286	835	134	11.3	109.4	18.4	1.5	110.2	244	43.8	183.7
62	Dambala Dara	BR-BHM62(WDW1)	343976	490986	960	171.4	7.79		806	526	120	10	45.6	9.2	1.8	60.6	263.9	37.3	50.4
63	Gelchet	BR-BHM63(GW2)	362519	506349	1130		7.47		1285	880	156	13.5	83.6	27.6	1.5	117.2	174.2	9.11	370.3
64	Goray Crater	BR-HDW1	343304	466191	735		7.8	29	5210	3794	870	82	116.4	120.4	2.55	600.96	684.66	17.61	1079
65	Dillo Crater	BR-HDW2	356220	471573	775		8.32	29.5	5800	4158	900	59.5	83.8	241.4	3.1	850.56	690.03	5.47	1100
66	Elwaya	BR-HDW3	375912	548302	1276		7.07	24.4	792	512	42	8.4	83.8	34.6	2.75	44.16	404.1	31.56	32.1
67	Dubluk Town	BR-HDW4	420549	482197	1463		7.54	20.1	474	302	36	21	35.28	10.8	0.8	44.16	111.26	14.5	48
68	Dubluk Town	BR-HDW5	420501	481774	1453		7.47	22.3	2270	1488	200	61	154.35	58.86	1.02	356.16	363.07	39	194
69	Nyaaru	BR-HDW6	396611	541206	1810		7.36	19.6	514	290	24	10.8	58.2	22.7	1.15	12.5	307.44	0.25	3
No	Hobok	BR-HDW7	306861	483561	822		8.59	28.3	847	540	168	14.4	11.5	3.8	1.17	75.8	320.13	4.9	30.7
70	Arbale/Sayole	BR-HDW8	383545	464667	1059		7.08	27.9	729	468	59	4.5	70.6	17.3	1.63	53.8	225.46	0.3	96.12
71	Arbale/Hulluko	BR-HDW9	383090	465285	1037		7.01	28.4	884	575	74	11	78.5	22.1	2.02	63.36	257.66	6.03	104.13
72	Medhacho Crater	BR-HDW10	417811	461164	1481		7.89	18.5	2680	1649	405	34.5	111.1	37.3	0.57	433.9	175.68	11.03	480.6
73	Kobale	BR-HDW11	397828	540078	1801		7.52	21.7	1101	720	52	58.5	109.2	52.25	1.98	95.04	538.75	0.72	29.9
74	Dharito	BR-HDW12	401786	530290	1755		7.42	24.6	459	304	31.5	5.7	50.16	11.88	0.68	31.2	165.6	2.7	41.65
75	Fallee	BR-HDW13	408739	498642	1610		6.75	21.7	397	250	38	8.6	37.8	4.9	0.37	40.6	159.9	0.8	1.5
76	Fallee	BR-HDW14	406870	502998	1563		7.41	22.3	630	416	39	6.5	74.8	17.8	1.09	57.65	260.96	1.01	24
77	Moyate	BR-HDW15	405056	523933	1674		6.69	21.2	455	281	24.5	10	52.8	13.5	0.57	26.46	238.5	0.2	0.8
78	Harewayu	BR-HDW16	403655	521689	1495		6.53	21.2	467	306	27.5	13	61.6	8.64	0.36	26.46	241.3	0.4	5.61
79	Sunkana/Sarite	BR-HDW17	338474	548500	1380		7.18	22.4	600	352	60	3.1	55.4	18.4	0.04	24.6	350.75	0.3	0.53
80	Dhokole	BR-HDW18	388094	474292	1674		6.73	21	452	274	33.5	9.1	41.36	12.42	1.45	33.1	173.97	0.11	28.6
81	Megado crater	BR-HDW19	412606	431062	733		7.1		9840	7536	1280	300	208	515.16	0.88	1286.9	3733.2	0.9	1269.6
82	Areri	BR-SP1	387546	544392	1576		7.48	23.3	346	210	27	2.6	35.28	12.42	3	16.32	181.5	0.11	4.5
83	Megado	BR-SP2	417295	433446	1225		7.6	22.9	2250	1480	118	31	22.05	218.2	0.2	56.6	1150.7	2.22	223.2
84	Mega Town	BR-SP3	425317	446907	1596		7.48	21.8	1374	879	52	7.6	101.4	87.5	0.45	149.8	459.69	26.2	98
85	Gololcha/Chorressa	BR-SP4	399530	453659	2214		7.2	19.4	144	80	12.5	1.4	12.35	3.24	0	13.44	46.85	3.5	9.08
86	Arbale	BR-SP5	399580	446563	1302		7.9	40.1	438	260	21.5	2.4	49.4	14	0.75	29.76	158.1	0.64	34
87	Gobso/Bule Dhela	BR-SP6	387650	480489	1750		7.34	24.1	240	146	20	1.7	22.93	6.48	1.16	20.16	96.6	0.7	10.81
88	Maagole	BR-SP7	386330	479034	1958		7.18	24.6	231	130	23	1.6	17.6	8.1	3.2	16.32	90.8	0.33	13.1
89	Gololcha/Harkiso Dambiti	BR-SP8	399790	455433	1818		8.1	18.6	692	414	33	6	88.2	18.9	0.63	78.72	187.4	2.45	72
90	Yaatu/Harewayu	BR-SP9	400331	525416	1777		7.33	24.5	257	164	17.5	4.1	30.8	5.4	0	20.79	109.4	0.96	9.08
91	Dharito	BR-SP10	400605	530501	1706		7.15	24.9	299	165	21.5	2.6	36.1	4.86	1.16	22.7	123.46	0.2	12.28
92	Gerbi/Yabello	BR-SP11	400170	543066	1838		6.84	22.8	207	124	18.5	1.6	20.24	5.4	0.33	13.23	106.6	0.64	0.53
93	Saakee/Megado	BR-SP12	410499	439266	1269		7.8	27	819	496	78	15.5	37.8	40.5	1.31	47.3	322.7	0.3	93.45
94	Megado crater	BR-SP13	413258	431648	1756		7.18		11680	8826	1900	375	240	349.9	1.35	1694	3623.4	0.8	1692
95	Yabelo**	BR-RF1	400826	540334	1740		5.58		49	26	0.6	1.3	2.76	1.66	0.55	0.91	23.06	1	3.9
96	Mega**	BR-RF2	424488	449720	1800		5.89		68	38	0.5	3	4.6	2.21	0.58	0.91	38.43	0.85	3.71
97	yabello**	BR-RF4	404143	539599	1624		5.5		20	12	0.3	0.1	1.84	1.1	0.44	0.91	10.25	0.65	0.29
98	Mega**	BR-RF5	424488	449720	1800		5.89		23.4	14.1	0.3	0.2	2.82	0.56		0.91	9.76	0.11	0.19

Annex 5: *Water Type total data set in research area*

Sample ID	Water Type	Sample ID	Water Type	Sample ID	Water Type
BR-BH1(GW1)	Na-Ca-SO4	BR-BH34 (GW4)	Na-Ca-SO4	BR-HDW4	Na-Ca-HCO3-Cl
BR-BH2	Na-SO4	BR-BH35	Mg-HCO3-SO4	BR-HDW5	Na-Ca-Cl-HCO3
BR-BH3	Na-Ca-Mg-SO4-Cl	BR-BH36	Na-Ca-HCO3	BR-HDW6	Ca-Mg-HCO3
BR-BH4(BTW10)	Na-Ca-HCO3-Cl	BR-BH37	Ca-Mg-Cl	BR-HDW7	Na-HCO3-Cl
BR-BH5 (BTW7)	Na-Ca-SO4-Cl	BR-BH38	Ca-SO4	BR-HDW8	Ca-Na-HCO3
BR-BH6	Na-Ca-SO4-HCO3	BR-BH39	Na-HCO3	BR-HDW9	Ca-Na-HCO3
BR-BH7	Ca-Na-Mg-HCO3	BR-BH40	Ca-Mg-HCO3	BR-HDW10	Na-Cl-SO4
BR-BH8	Na-HCO3	BR-BH41	Na-Ca-Cl-HCO3	BR-HDW11	Ca-Mg-HCO3
BR-BH9	Na-Cl-SO4	BR-BH42	Na-Ca-HCO3-Cl	BR-HDW12	Ca-Na-HCO3
BR-BH10	Na-Mg-Ca-HCO3	BR-BH43	Na-Ca-Cl-SO4	BR-HDW13	Ca-Na-HCO3-Cl
BR-BH11	Ca-SO4	BR-BH44	Na-Cl-SO4-HCO3	BR-HDW14	Ca-HCO3
BR-BH12	Ca-Mg-HCO3	BR-BH45	Na-SO4	BR-HDW15	Ca-HCO3
BR-BH13	Ca-Mg-HCO3	BR-BH46	Ca-Na-SO4-HCO3	BR-HDW16	Ca-Na-HCO3
BR-BH14	Ca-Mg-HCO3	BR-BH47	Ca-Na-HCO3-Cl	BR-HDW17	Ca-Na-HCO3
BR-BH15 (BTW4A)	Na-Mg-HCO3	BR-BH48	Mg-Ca-HCO3	BR-HDW18	Ca-Na-HCO3
BR-BH16	Ca-Mg-HCO3	BR-BH49	Na-Ca-HCO3	BR-HDW19	Na-Mg-HCO3
BR-BH17	Mg-HCO3	BR-BH50	Ca-Mg-HCO3	BR-SP1	Ca-Na-HCO3
BR-BH18	Mg-HCO3	BR-BH51	Ca-Mg-HCO3-SO4	BR-SP2	Mg-HCO3
BR-BH19	Na-HCO3	BR-BH52	Ca-Mg-HCO3-SO4	BR-SP3	Mg-Ca-HCO3-Cl
BR-BH20	Ca-Mg-HCO3	BR-BH53	Na-HCO3-Cl	BR-SP4	Ca-Na-HCO3
BR-BH21	Ca-Mg-SO4	BR-BH54	Ca-Mg-Na-HCO3-SO4-Cl	BR-SP5	Ca-HCO3
BR-BH22	Na-Mg-HCO3	BR-BH55	Mg-Na-Ca-HCO3-Cl-SO4	BR-SP6	Ca-Na-HCO3
BR-BH23	Na-HCO3	BR-BH56	Na-Ca-Mg-HCO3-Cl-SO4	BR-SP7	Na-Ca-HCO3
BR-BH24	Ca-Mg-HCO3	BR-BH57	Na-Ca-HCO3	BR-SP8	Ca-HCO3-Cl
BR-BH25	Na-Cl-SO4	BR-BH58	Ca-Mg-Na-HCO3-Cl	BR-SP9	Ca-Na-HCO3
BR-BH26 (DUTW-1)	Ca-Na-Cl	BR-BH59	Na-Ca-HCO3	BR-SP10	Ca-Na-HCO3
BR-BH27 (DUTW-2)	Na-Ca-Mg-Cl-HCO3	BR-BH60	Ca-Mg-HCO3	BR-SP11	Ca-Na-HCO3
BR-BH28 (BTW-3)	Na-Cl-SO4	BR-BHM61 (WDW2)	Na-Ca-HCO3-SO4	BR-SP12	Na-Mg-HCO3
BR-BH29 (BTW6A)	Na-Ca-Cl-SO4	BR-BHM62(WDW1)	Na-HCO3	BR-SP13	Na-HCO3-Cl
BR-BH30 (BTW6B)	Na-Ca-Cl	BR-BHM63(GW2)	Na-Ca-HCO3	BR-RF1	Ca-Mg-HCO3
BR-BH31 (BTW8)	Na-Ca-Mg-HCO3	BR-HDW1	Na-SO4-Cl	BR-RF2	Ca-Mg-HCO3
BR-BH32 (GPW2)	Na-Ca-HCO3-SO4	BR-HDW2	Na-Mg-Cl-SO4	BR-RF4	Ca-Mg-HCO3
BR-BH33 (GW5)	Na-Ca-SO4	BR-HDW3	Ca-Mg-HCO3	BR-RF5	Ca-Mg-HCO3

Annex 6: *Simulated Saturation Index of common minerals*

Sample Id	X	Y	Z	$SI_{Anhydrite}$ ($CaSO_4$)	$SI_{Aragonite}$ ($CaCO_3$)	$SI_{Calcite}$ ($CaCO_3$)	$SI_{Dolomite}$ (CaMg(CO3)2)	$SI_{Fluorite}$ (CaF2)	SI_{Gypsum} (CaSO4:2H2O)	SI_{Halite} (NaCl)	Sample Id	X	Y	Z	$SI_{Anhydrite}$ ($CaSO_4$)	$SI_{Aragonite}$ ($CaCO_3$)	$SI_{Calcite}$ ($CaCO_3$)	$SI_{Dolomite}$ (CaMg(CO3)2)	$SI_{Fluorite}$ (CaF2)	SI_{Gypsum} (CaSO4:2H2O)	SI_{Halite} (NaCl)
BH31	352697	491178	995	-1.65	0.66	0.8	1.79	-1.94	-1.49	-6.33	BR-BH55	452256	430934	1305	-1.41	0.49	0.63	1.56	-0.61	-1.19	-5.97
BH1	360826	505258	1118	-1.29	0.39	0.53	0.22	-0.45	-1.05	-6.41	BR-BH56	454202	431112	1301	-1.49	0.53	0.68	1.44	-0.78	-1.27	-6.04
BH10	361667	556788	1038	-2.39	0.68	0.83	1.84	-0.092	-2.18	-7.45	BR-BH57	305786	513683	965	-2.55	0.34	0.48	0.86	-0.29	-2.36	-6.76
BH11	404143	539599	1624	-1.36	-0.37	-0.23	-0.62	-0.39	-1.14	-6.6	BR-BH58	439353	411265	1198	-1.82	-0.26	-0.12	-0.24	-0.39	-1.61	-6.8
BR-BH12	378708	548522	1379	-4.07	0.36	0.5	0.84	-3.31	-3.85	-7.86	BR-BH59	320975	552429	1436	-3.86	0.23	0.37	0.4	-2.16	-3.66	-7.53
Br-BH13	395181	541249	1915	-2.94	0.03	0.17	0.08	-1.01	-2.7	-6.7	BR-BH6	379120	520197	1197	-1.55	0.1	0.24	0.39	-3.81	-1.37	-6.81
Br-BH14	418263	434758	1483	-3.24	-0.67	-0.52	-0.95	-2.57	-3.01	-8.42	BR-BH60	429636	441835	1458	-1.41	0.02	0.16	-0.02	-1.74	-1.2	-7.27
Br-BH15	407108	416060	785	-1.8	0.94	1.08	2.61	-1.3	-1.61	-6.45	BR-BH7	377047	532085	1245	-2.33	0.54	0.68	1.39	-1.23	-2.13	-7.56
Br-BH16	418497	444586	1569	-1.64	0.56	0.7	1.27	-1.05	-1.42	-6.91	BR-BH8	346964	545325	992	-4.28	0.41	0.55	0.72	-0.86	-4.07	-6.4
Br-BH17	424085	448742	1711	-2.68	-0.01	0.13	0.48	-2.23	-2.45	-7.35	BR-BH9	350065	566262	882	-1.05	0.27	0.41	0.47	-0.98	-0.85	-4.59
Br-BH18	425998	445672	1540	-1.91	0.78	0.92	2.37	-1.22	-1.68	-6.9	BR-BH61	351284	495846	1101	-1.52	0.03	0.18	-0.14	-0.53	-1.29	-6.43
Br-BH19	420112	482697	1476	-1.78	0.63	0.77	1.75	-0.84	-1.55	-5.9	BR-BH62	343976	490986	960	-2.33	0.15	0.29	0.17	-0.66	-2.09	-6.71
Br-BH2	339581	463165	811	-1.2	-0.79	-0.65	-2.77	0.49	-1.04	-5.95	BR-BH63	362519	506349	1130	-1.37	-0.21	-0.06	-0.32	-0.7	-1.13	-6.34
Br-BH20	338052	523061	1069	-2.52	0.52	0.66	1.47	-1.21	-2.34	-6.76	BR-HDW1	343304	466191	735	-1.1	0.76	0.9	2.19	-0.53	-0.9	-4.98
Br-BH21	402823	467061	1538	-0.93	0.61	0.76	1.5	-86	-0.7	-6.58	BR-HDW10	417811	461164	1481	-1.25	0.24	0.39	0.57	-1.48	-1.01	-5.38
Br-BH22	412154	416043	789	-1.91	1.37	1.51	3.6	-2.21	-1.72	-6.61	BR-HDW11	397828	540078	1801	-2.32	0.53	0.68	1.35	-0.33	-2.09	-6.91
Br-BH23	338000	454149	739	-2.12	0.51	0.65	1.36	-1.57	-1.95	-7.07	BR-HDW12	401786	530290	1755	-2.3	-0.27	-0.12	-0.53	-1.46	-2.08	-7.58
Br-BH24	398972	516763	1304	-0.94	0.71	0.86	1.52	-0.03	0.72	-6.55	BR-HDW13	408739	498642	1610	-3.81	-1.08	-0.93	-2.44	-2.03	-3.57	-7.36
Br-BH25	389294	520566	1246	-2.31	-0.17	-0.03	-0.44	-2.36	-2.12	-6.64	BR-HDW14	406870	502998	1563	-2.43	0.03	0.18	0.05	-0.89	-2.2	-7.22
Br-BH26	425179	477832	1452	-0.91	0.68	0.83	1.45	-0.9	-0.69	-5.46	BR-HDW15	405056	523933	1674	-3.99	-0.85	-0.7	-1.7	-1.54	-3.76	-7.75
Br-BH27	419909	482966	1467	-1.53	0.82	0.96	2.06		-1.31	-5.42	BR-HDW16	403655	521689	1495	-3.09	-0.94	-0.8	-2.15	-1.87	-2.85	-7.7
Br-BH28	369372	504302	1132	-1.78	0.03	0.17	0.28	-1.38	-1.57	-6.5	BR-HDW17	338474	548500	1380	-4.2	-0.19	-0.04	-0.24	-3.89	-3.97	-7.4
Br-BH29	345844	527739	966	-0.65	0.09	0.23	-0.05	-0.16	-0.46	-4.85	BR-HDW18	388094	474292	1674	-2.53	-1.06	-0.91	-2.05	-0.83	-2.3	-7.51
Br-BH3	371540	501553	1150	-1.2	0.46	0.6	1.16	-0.66	-1	-6.14	BR-HDW19	412606	431062	733	-1.07	0.78	0.93	2.55	-1.4	-0.84	-4.51
Br-BH30	346062	527765	965	-0.47	0.54	0.68	0.83	-0.16	-0.29	-4.41	BR-HDW2	356220	471573	775	-1.3	1.13	1.27	3.39	-0.61	-1.1	-4.82
Br-BH32	362521	507901	1136	-0.167	0.27	0.42	0.74	-1.61	-1.43	-6.48	BR-HDW3	375912	548302	1276	-2.33	-0.08	0.07	0.09	-0.14	-2.11	-7.33
BR-BH33	358825	504597	1112	-1.62	-0.24	-0.09	-0.37	-1.28	-1.38	-6.44	BR-HDW4	420549	482197	1463	-2.38	-0.53	-0.39	-1.01	-1.42	-2.14	-7.35
BR-BH34	361707	505679	1125	-1.39	-0.15	-0.01	-0.22	-1.42	-1.16	-6.46	BR-HDW5	420501	481774	1453	-1.48	0.39	0.54	0.98	-0.86	-1.25	-5.78
BR-BH35	396126	421963	805	-1.24	0.79	0.93	3.08	-2.33	-1.07	-5.41	BR-HDW6	396611	541206	1810	-3.42	-0.08	0.07	0.01	-0.91	-3.18	-8.09
BR-BH36	420073	482723	1472	-2.11	0.29	0.43	0.98	-1.27	-1.89	-6.61	BR-HDW7	306861	483561	822	-3.1	0.53	0.67	1.27	-1.74	-2.9	-6.48
BR-BH37	401121	535238	1746	-1.57	0.22	0.37	0.8	0.2	-1.35	-5.56	BR-HDW8	383545	464667	1059	-1.86	-0.38	-0.19	-0.61	-0.67	-1.66	-7.09
BR-BH38	420413	459077	1569	-0.93	0.42	0.56	0.72	-0.46	-0.71	-6.51	BR-HDW9	383090	465285	1037	-1.82	-0.31	-0.16	-0.5	-0.47	-1.61	-6.93
BR-BH39	428684	461190	1474	-2.42	0.35	0.49	1.05	-0.93	-2.2	-6.05	BR-RF1	400826	540334	1740	-4.32	-4.14	-3.99	-7.92	-2.66	-4.08	-10
BR-BH4	338417	505453	949	-2.67	-0.05	0.09	-0.11	-0.83	-2.43	-6.69	BR-RF2	424488	449720	1800	-4.14	-3.4	-3.25	-6.54	-2.41	-3.91	-10.85
BR-BH40	415127	490919	1542	-3.07	0.01	0.16	0.31	-2.58	-2.85	-8.3	BR-RF4	404143	539599	1624	-5.59	-4.72	-4.57	-9.09	-3.01	-5.36	-11.06
BR-BH41	428520	485091	1455	-1.52	1.3	1.45	2.51	-1.34	-1.3	-6.12	BR-RF5	424488	449720	1800	-5.59	-4.17	-4.02	-8.46		-5.35	-11.06
BR-BH42	433721	482285	1416	-1.83	0.63	0.78	1.48	-0.53	-1.61	-6.11	BR-SP1	387546	544392	1576	-3.37	-0.31	-0.16	-0.45	-0.28	-3.14	-7.91
BR-BH43	442268	475284	1377	-0.95	-0.95	1.09	1.91	-0.27	-0.73	-5.19	BR-SP10	400605	530501	1706	-2.88	-0.75	-0.61	-1.74	-1.08	-2.66	-7.87
BR-BH44	429444	460938	1466	-2.11	-0.61	0.75	1.45	-1.09	-1.88	-6.11	BR-SP11	400170	543066	1838	-4.45	-1.38	-1.23	-2.72	-2.36	-4.22	-8.15
BR-BH45	346344	567057	922	-1.52	0.47	0.6	1.27	-0.25	-1.39	-5.63	BR-SP12	410499	439266	1269	-2.18	0.24	0.38	1.16	-1.17	-1.97	-7.03
BR-BH46	391665	556156	1549	-1.31	0.32	0.47	0.74	-0.18	-1.09	-7.1	BR-SP13	413258	431648	1756	-0.9	0.89	1.03	2.52	-0.93	-0.67	-4.23
BR-BH47	399057	537973	1824	-2.01	0.18	0.33	0.49	-0.38	1.79	-6.61	BR-SP2	417295	433446	1225	-2.36	0.13	0.28	1.88	-3.3	-2.13	-6.81
BR-BH48	415808	436192	1490	-1.56	0.03	0.18	0.59	-1.4	-1.33	-6.84	BR-SP3	425317	446907	1596	-1.9	0.36	0.51	1.27	-1.72	-1.66	-6.72
BR-BH49	306254	505927	937	-3.66	0.65	0.79	1.38	-1.31	-3.45	-7.15	BR-SP4	399530	453659	2214	-3.4	-1.62	-1.47	-3.25		-3.16	-8.3
BR-BH5	361304	509658	1137	-1.36	-0.14	0	-0.08	-0.6	-1.18	-6.13	BR-SP5	399580	446563	1302	-2.32	0.39	0.53	0.99	-1.56	-2.18	-7.79
BR-BH50	443048	419387	1326	-1.34	0.21	0.35	0.62	-1.63	-1.12	-5.78	BR-SP6	387650	480489	1750	-3.11	-0.86	-0.72	-1.65	-1.25	-2.88	-7.94
BR-BH51	435391	421252	1403	-1.09	0.48	0.62	1.31	-0.94	-0.87	-6.44	BR-SP7	386330	479034	1958	-3.13	-1.15	-1.01	-2.02	-0.49	-2.91	-7.97
BR-BH52	434101	431696	1394	-0.98	0.59	0.73	1.42	-0.82	-0.76	-6.42	BR-SP8	399790	455433	1818	-1.92	0.56	0.71	1.02	-1.27	-1.68	-7.15
BR-BH53	324139	528775	1140	-3.99	-0.24	-0.1	-0.23	-2.28	-3.77	-6.48	BR-SP9	400331	525416	1777	-3.07	-0.69	-0.55	-1.51		-2.85	-7.99
BR-BH54	442726	430402	1352	-1.22	0.79	0.93	2	-1.46	-1	-6.18											

Annex 7: *Chloride concentration in groundwater and Annual recharge estimated for each spot. Cl_{gw} is Chloride in groundwater (mg/l), Cl_p is Chloride concentration in precipitation (mg/l) and P is annual precipitation (mm/year)*

Sample Id	X	Y	Z	Cl_{gw}	Cl_p	p	$Cl_p * P$	$(Cl_p * P)/Cl_{gw}$
BR-BHE14	418263	434758	1483	8.64	0.91	590.8	537.63	62.23
BR-SPE4	399530	453659	2214	13.44	0.91	590.8	537.63	40
BR-SPM5	399580	446563	1302	29.76	0.91	590.8	537.63	18.07
BR-HDWE4	420549	482197	1463	44.16	0.91	590.8	537.63	12.17
BR-BHE40	415127	490919	1542	16.2	0.91	590.8	537.63	33.19
BR-HDWE6	396611	541206	1810	12.5	0.91	590.8	537.63	43.01
BR-SPE6	387650	480489	1750	20.16	0.91	590.8	537.63	26.67
BR-SPE7	386330	479034	1958	16.32	0.91	590.8	537.63	32.94
BR-SPE9	400331	525416	1777	20.79	0.91	590.8	537.63	25.86
BR-SPE10	400605	530501	1706	22.7	0.91	590.8	537.63	23.68
BR-HDWE12	401786	530290	1755	31.2	0.91	590.8	537.63	17.23
BR-HDWE13	408739	498642	1610	40.6	0.91	590.8	537.63	13.24
BR-HDWE15	405056	523933	1674	26.46	0.91	590.8	537.63	20.32
BR-HDWE16	403655	521689	1495	26.46	0.91	590.8	537.63	20.32
BR-SP11	400170	543066	1838	13.23	0.91	590.8	537.63	40.64
BR-HDWE18	388094	474292	1674	33.1	0.91	590.8	537.63	16.24
BR-BHM10	361667	556788	1038	11.5	0.91	590.8	537.63	46.75
BR-BHM12	378708	548522	1379	9.6	0.91	590.8	537.63	56
BR-SPE1	387546	544392	1576	16.32	0.91	590.8	537.63	32.94
BR-BHR23	338000	454149	739	41.28	0.91	590.8	537.63	13.02
BR-HDWM3	375912	548302	1276	44.16	0.91	590.8	537.63	12.17
BR-BHR49	306254	505927	937	19.2	0.91	590.8	537.63	28
BR-HDWE17	338474	548500	1380	24.6	0.91	590.8	537.63	21.85
BR-BH59	320975	552429	1436	13.23	0.91	590.8	537.63	40.64
BR-SPM12	410499	439266	1269	47.3	0.91	590.8	537.63	11.37
BR-BHM7	377047	532085	1245	18.24	0.91	590.8	537.63	29.48
BR-BH46	391665	556156	1549	29.76	0.91	590.8	537.63	18.07

Annex 8: *Carbon 14 date of groundwater from eastern crystalline terrain bordering the study area (adopted from OWWDSE, 2006)*

Locality name	E	N	d18O	dD	TU	14C	d13C	Age- Person Model
UDET	39.24	4.75	-3.2	-13	1.7	112	-6.7	Modern
WACHILE	39.06	4.54	-1.6	-7.6		91.1	-4.3	Modern
Y ABELO	38.13	4.88	-3.4	-13		90.1		Modern
DUBLUK	38.28	4.36	-2.9	-13	1.1	109	-10.9	Modern
MEGA	38.31	4.05	-3.2	-14	0.4	74.8		
MELBENA	38.48	3.89	-4.0	-12		37	-0.4	
HIDILOLA	38.57	3.69	-4.4	-11	1.6	113	-13.1	Modern
BOKULBOMA	38.67	3.86	-2.6	-14	0	57.3	-3.8	
EGDER	38.86	3.91	-2.9	-11	0	55.2	-8.1	
TUKA	38.86	3.60	-3.8	-19	1.5	102	-12.7	Modern
ELGOF	39.06	3.85	-3.0	-16	0.1	70.4	2.8	
EL KALU	39.18	3.77	-2.5	-15		72.2	-8.7	
NEGELE	39.58	5.31	-1.9	-6.5	0.9	91	-5.7	
CHILANKO	40.00	4.20	-2.7	-14	1.9	103	-12.9	Modern
YABELO	38.10	4.91	-3.5	-12		95.6	-11.9	Modern
MEGA	38.32	4.04	-3.3	-12		77.4	-10	

Annex 9: *Mean climatic conditions at stations in and near the project area*

Stations	Jan	Feb	Mar	Apr	May	Jun	Jul	Aug	Sep	Nov	Oct	Dec	Annual
Mean monthly rainfall (mm)													
Yabello	24.8	30.5	61	144	100.5	12.2	8.2	12.1	30.1	95	49.6	15	583
Mega	23.6	43.3	75.3	158.8	93.9	30.6	34.1	21.9	20	92.7	66.7	27	688
Teltele	38.4	37.1	88.2	156.5	101	35.4	17.7	10.6	37.2	97.6	59	27.3	706
Mean monthly Temp (^{0}c)													
Yabello	20.2	20.9	21.2	20.3	19.5	18.7	18.1	18.7	19.8	19.7	19.5	19.5	19.7
Mega	20.7	21.1	20.6	19.7	18.4	16.7	16.2	16.8	18.3	18.9	19.1	19.7	18.9
Teltele	23.4	24.7	24.1	22.5	21.9	21.7	21.7	22.3	22.9	22.7	22.6	22.6	22.8
Wind Speed (km)													
Yabello	2	2.1	2.2	1.9	1.5	1.4	1.4	1.5	1.7	1.8	2	2	1.8
Mega	3.1	3	3	3	2.9	2.9	3.3	3.4	3.4	3.3	3.3	3.5	3.2
Relative Humidity (%)													
Yabello	53.5	52.7	59.8	72.4	75.6	71.8	71.4	67	63.9	70.2	65.5	56.2	65
Mega	55.9	58.8	68.5	82	86.2	84.7	81.7	78.4	73.5	78.5	77.1	66.9	74.4
Sunshine Duration (Hr)													
Yabello	8.6	8.8	8.3	6.5	6.2	4.4	3.4	4.1	6	5.7	6.9	8.8	6.5
Mega	9.7	8.4	7.4	5.8	5.2	4.1	3.9	5.3	5.7	5.6	6	7.8	6.2

Annex 10: ***A)*** *Graph showing depth of wells, depth to Water strike and Static water level profiles in Borena volcanic plains and* ***B)*** *Thickness of Aquifer horizons; adopted from OWWDSE, 2011*

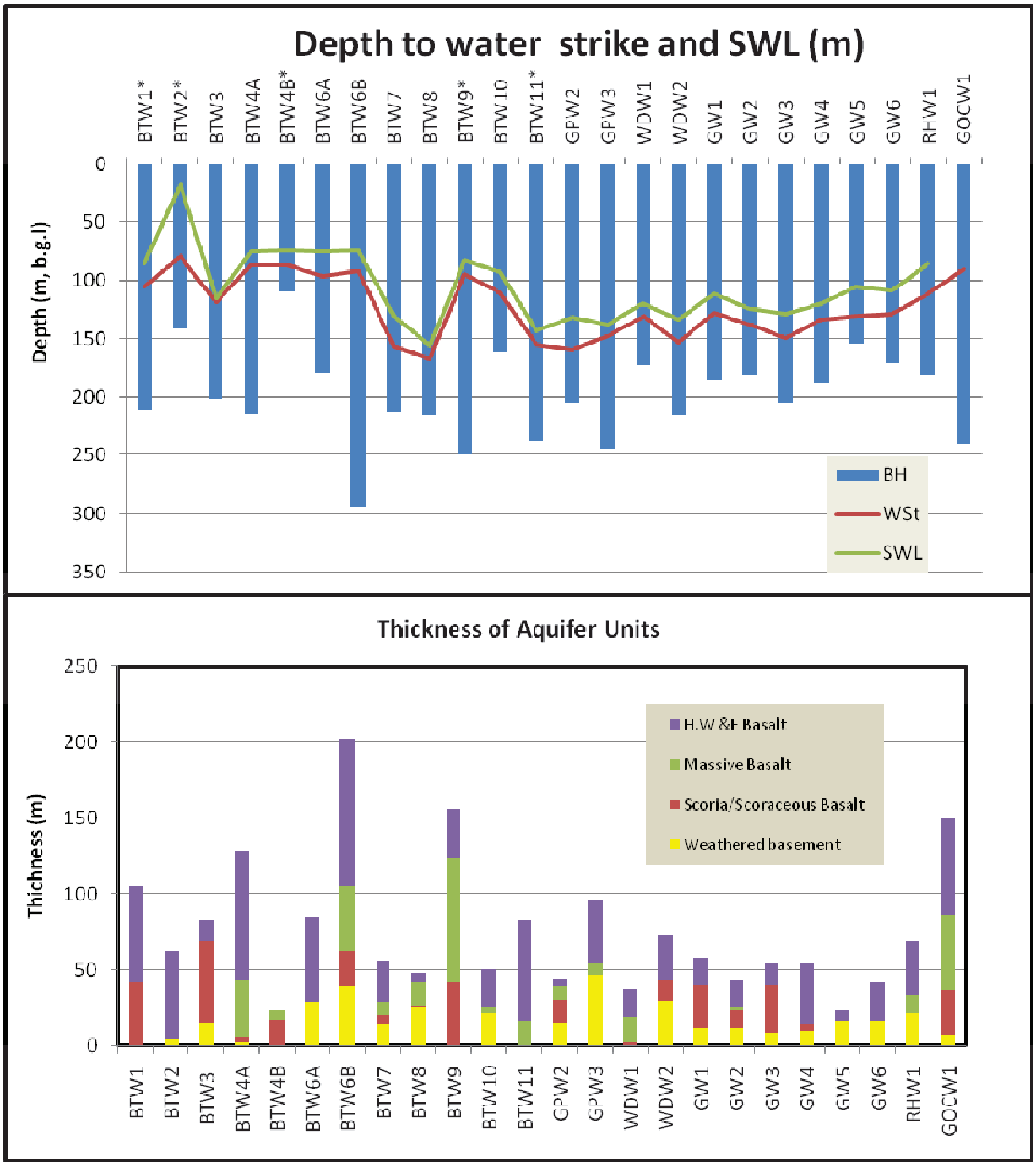

Annex 11: *Lithological log of some representative wells in volcanic plains*

BR-BH5 (BTW7) Well Log; Gelchet

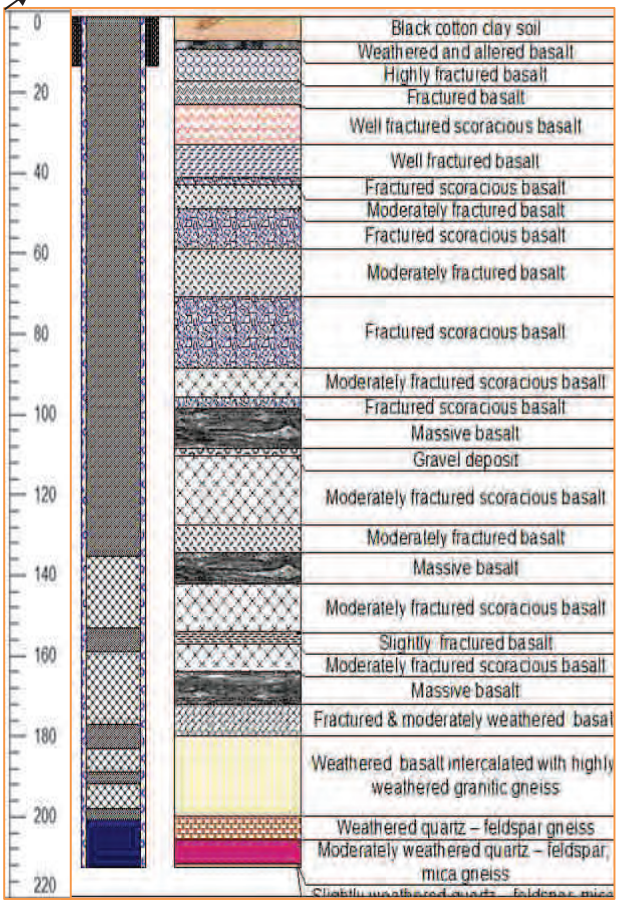

BR-BH30 (BTW6) Well Log; Sarite

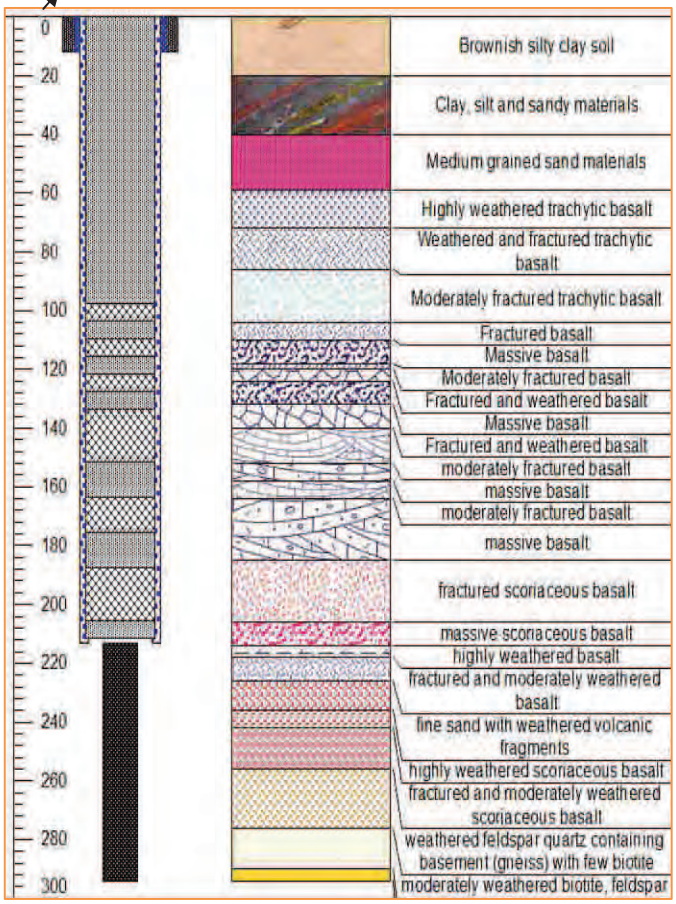

BR-BH15 (BTW4) well log; Megado

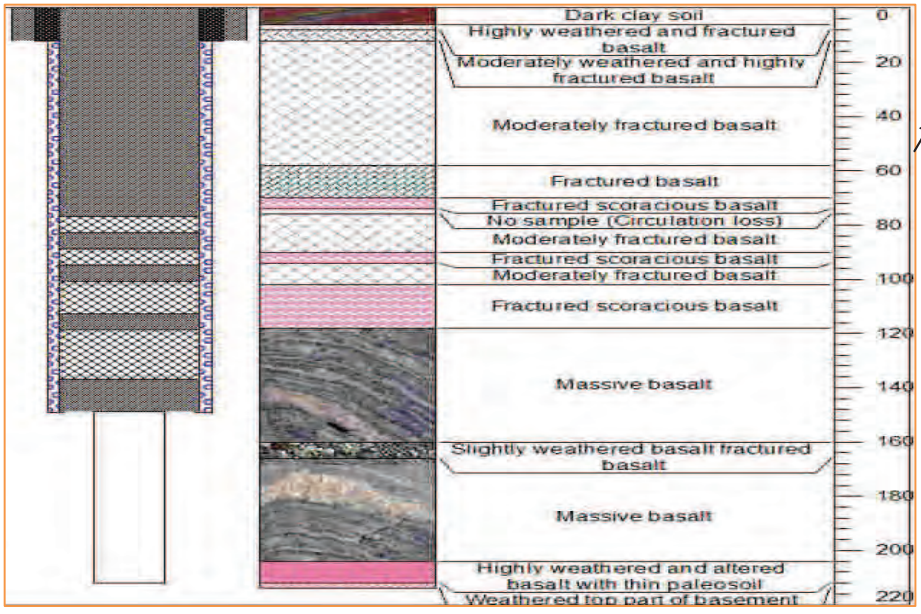

Annex 12: *Plates*